NTNU – Trondheim
Norwegian University of
Science and Technology

Analytical and Numerical Modeling of Paraffin Wax in Pipelines

Marte Stubsjøen

Petroleum Geoscience and Engineering
Submission date: June 2013
Supervisor: Jon Steinar Gudmundsson, IPT

Norwegian University of Science and Technology
Department of Petroleum Engineering and Applied Geophysics

Preface

The presented master thesis is a result of the compulsory subject *TPG 4905 Petroleum production, master thesis* conducted at the Department of Petroleum Engineering and Applied Geophysics at the Norwegian University of Science and Technology (NTNU) in the spring of 2012 . The study of the numerical wax deposit model was initiated by Siljuberg (2012), taken one step further by the writer (Stubsjøen, 2013) and is finally fulfilled with the current work.

I want to thank my supervisor Jon Steinar Gudmundsson for his kind support throughout the semester, Erlend Våtevik for always fixing whatever computer trouble I would meet, and Ole Martin Brende for being available whenever I would need him.

Abstract

Paraffin wax deposition, or the settling of solid wax particles on pipelines and equipment, is an extensive problem encountered in oil production and transportation. Flowing through subsea pipelines, oil and condensate are subject to cooling. If the temperature of a supersaturated crude oil mixture drops below the solubility limit of wax, known as the wax appearance temperature (WAT), solid paraffin start to appear in solution. Assuming temperatures below the WAT and a radial heat flux from the fluid to the surroundings, paraffin will precipitate, adhere to the inner pipe wall and gradually accumulate. The result is an undesirable layer of paraffin wax on the inner pipe wall causing flow restrictions, reduced production and a need for remediation.

In the current thesis, the applicability of five effective thermal conductivity models for determination of the effective thermal conductivity of paraffin wax deposits have been evaluated. Based on the structure of the deposit, the Effective Medium Theory is found applicable. The influence of the deposit on the thermal conditions in the pipeline has been examined, and the temperature at the deposit surface is found to increase with an increasing wax deposit thickness. The increased temperature at the oil/deposit interface reduces the radial temperature gradient in the pipeline, being the thermal driving force for deposition. The result is a reduced growth rate of the wax layer with time and a need for dynamic simulations to avoid over prediction of the wax deposit thickness.

The most important part of the presented work, is the implementation of an analytical and a numerical model facilitating wax deposit predictions. Simulations have been conducted on a typical subsea pipeline and the results have been compared. The analytical model, with its assumption of thermodynamic equilibrium between the solubility of wax and the actual wax concentration at ever point in the pipeline, has shown to yield a significantly higher amount of wax to be expected, compared to the results obtained by the numerical model, taking the precipitation kinetics of wax into account.

Sammendrag

Avsetning av parafiner i forbindelse med produksjon og transport av olje er et utbredt problem i petroleumsindustrien. Når olje og kondensater strømmer gjennom undervannsrørledninger fra reservoaret til produksjonsfasilitetene, utsettes fluidet for kjøling. Dersom temperaturen i rørledningen faller under løselighetsgrensa for voks, vil utfelling av parafiner i fast form inntreffe. Med temperaturer i røret under voksutfellingsgrensa og en radiell varmestrømning fra fluidet til omgivelsene, vil parafiner felles ut av råoljen og avsettes på den indre rørveggen. Resultatet er et uønsket lag av parafiner som skaper restriksjoner for strømning eller, i verste fall, blokkerer røret fullstendig med redusert produksjon eller produksjonsstans som følge.

Fem modeller som beregner den effektive termiske ledningsevnen til to-komponent systemer har blitt undersøkt i den presenterte oppgaven for å kunne modellere den termiske ledningsevnen til voksavsetningen. Basert på avsetningens struktur er "the Effective Medium Theory" funnet anvendbar og blitt implementert i de senere voksavsetningsmodellene. Voksavsetningens innflytelse på de termiske forholdende i rørledningen har blitt undersøkt, og en økende tykkelse av vokslaget er funnet å gi en økt temperatur på overflaten av voksavsetningen. Som en konsekvens av den økte temperaturen på voksavsetningsens overflate, vil den radielle temperaturgradienten, kjent som den termiske drivkraften for avsetning, avta med en økende vokstykkelsen. Resultatet er en avtagende vekstrate med tid og en påkrevd dynamisk modellering dersom en overestimering av vokslagets tykkelse skal unngås.

Undersøkelsene ovenfor leder frem til oppgavens hovedformål; en implementasjon av en analytisk og en numerisk voksavsetningsmodell med en påfølgende sammenligning av simuleringsresultater. Den analytiske modellen baserer seg på termodynamisk likevekt der det antas at vokskonsentrasjonen følger løseligheten i ethvert punkt i rørledningen, mens den numeriske modellen inkluderer en "precipitation rate constant" som tar hensyn til avviket mellom løselighet og faktisk konsentrasjon som kan oppstå ved turbulent strømning. Basert på litteraturstudiet og prinsippet beskrevet, var den analytiske modellen forventet å gi en større voksavsetningstykkelse enn de numeriske simuleringene. Dette ble bekreftet ved en sammenligning av de analytiske og numeriske resultatene. For de simulerte forholdene ga den analytiske modellen etter et døgn en maksimal voksavsetningstykkelse som var 3.1 mm høyere enn den numeriske modellen og etter en uke var forskjell på 15.8 mm.

Contents

List of Figures

List of Tables

Nomenclature

Table 1: Latin and greek symbols applied.

Latin	**Symbols**	**Unit**
A_i	Solid/liquid interface area	m^2
A_{lm}	Logarithmic mean area	m^2
$A_{lm,\ deposit}$	Logarithmic mean area of the deposit	m^2
$A_{lm,\ pipe}$	Logarithmic mean area of the pipe	m^2
A_p	Surface area of nucleus	m^2
A_{wi}	Area of inner pipe wall	m^2
A_{wo}	Area of outer pipe wall	m^2
A_j^C	Coefficient for numerical concentration calculations	s^{-1}
A_j^T	Coefficient for numerical temperature calculations	s^{-1}
B_j^C	Coefficient for numerical concentration calculations	s^{-1}
B_j^T	Coefficient for numerical temperature calculations	s^{-1}
C	Concentration of wax dissolved in solution	wt-%
C_b	Concentration of wax in the bulk flow	wt-%
C_j^C	Coefficient for numerical concentration calculations	s^{-1}
C_j^T	Coefficient for numerical temperature calculations	s^{-1}
C_p	Spesific heat capacity of oil	J/(kg.K)
C_{wall}	Concentration of wax in the near-wall region	wt-%
C_{WAT}	Maximum concentration of wax in oil	wt-%
C_1	Eddy viscosity correlation constant	-
C_2	Eddy viscosity correlation constan	-
d	Inner pipe diameter	m
d_p	Diameter of nucleus	m
D_{AB}	Binary diffusion coefficient of solute A in solvent B	m^2/s
D_{wo}	Binary diffusion coefficient of wax in oil	m^2/s
$\frac{dC}{dr}$	Concentration gradient	wt-%/m
$\frac{dm}{dt}$	Mass deposit rate of wax in oil at liquid/solid interface	kg/s
$\frac{dT}{dr}$	Temperature gradient	K/m
$\frac{dV_z^+}{dy^+}$	Temperature gradient	K/m
D_{eff}	Effective binary diffusion coefficient	m^2/s
D_j^C	Coefficient for numerical concentration calculations	s^{-1}
D_j^T	Coefficient for numerical temperature calculations	s^{-1}
E_A	Activation energy	J/mol
f	Friction factor	-

F_w	Weight fraction of wax in deposit	-
G	Growth rate of precipitated wax particles	m/s
h_i	Inner convective heat transfer coefficient	$W/(m^2K)$
h_o	Outer convective heat transfer coefficient	$W/(m^2K)$
J''	Mass flux	$kg/(s.m^2)$
k	Thermal conductivity	(W/m.K)
k_d	Mass transfer rate from bulk to individual nucleus surface	W/(m.K)
k_{dep}	Thermal conductivity of paraffin wax deposit	W/(m.K)
k_e	Effective thermal conductivity	W/(m.K)
k_f	Thermal conductivity of fluid	W/(m.K)
k_M	Inner convective mass transfer coefficient	m/s
k_{oil}	Thermal conductivity of oil	W/(m.K)
k_{pipe}	Thermal conductivity of the pipe	W/(m.K)
k_r	Precipitation rate constant	s^{-1}
$k_{r,cloud}$	Precipitation rate constant at cloud point	s^{-1}
k_{wax}	Thermal conducitivity of wax	W/(m.K)
L	Length of pipeline	m
$\dot{m}$	Mass flow rate	kg/s
n_i	Number of steps in lateral direction	-
n_j	Number of steps in radial direction	-
q	Rate of heat transfer	W
q''	Heat flux	W/m^2
Q	Flow rate	m^3/s
r	Radial coordinate at distance of interest	m
r_{dep}	Effective flow radius	m
r_i	Inner pipe radius	m
r_o	Outer pipe radius	m
R	Total heat resistance	$(m^2K)/W$
R_{dep}	Heat resistance of Deposit	$(m^2K)/W$
R_i	Inner heat resistance	$(m^2K)/W$
R_o	Outer heat resistance	$(m^2K)/W$
R_{pipe}	Heat resistance of pipe	$(m^2K)/W$
T	Temperature	K
T_b	Average bulk flow temperature	K
T_{cloud}	Temperature at cloud point, equals WAT	K
T_{dep}	Temperature at deposit surface	K
T_i	Inlet temperature	K
T_{sea}	Ambient temperature	K

T_{wi}	Temperature at inner pipe wall	K
T_{wo}	Temperature at outer pipe wall	K
$T_w{}^+$	Dimensionless wall temperature	K
T_∞	Fluid temperature	K
U	Overall heat transfer coefficient	$W/(m^2K)$
u	Average fluid flow velocity	m/s
u_τ	Friction velocity	m/s
u_z	Fluid velocity in lateral direction	m/s
v	Volume fraction	-
V_a	Molecular volume	cm^3/mol
V_z	Axial velocity	m/s
V_z^+	Dimensionless turbulent velocity	-
y	Distance from inner pipe wall	m
y_τ	Friction distance	m
y_z^+	Dimensionless distance from inner pipe wall	-
z	Axial distance	m

Greek	**Symbols**	**Unit**
α_T	Thermal diffusivity	m^2/s
α_{tot}	Total thermal diffusivity	m^2/s
β	Constant for heat of fusion crystallization	-
Δr	Grid size in radial direction	m
Δr_{wall}	Wall thickness	m
δ	Deposit thickness	m
ε	Eddy diffusivity	m^2/s
ε_h	Turbulent heat diffusivity	m^2/s
ε_m	Turbulent mass diffusivity	m^2/s
γ	Dimensionless function of molar volume	-
μ_{cloud}	Dynamic viscosity of oil at WAT	Pa.s
μ_{oil}	Dynamic viscosity of oil	Pa.s
ν_{oil}	Kinematic viscosity of oil	m^2/s
ρ_{oil}	Density of oil	kg/m^3
ρ_{wax}	Density of wax	kg/m^3
ρ_n	Number density of nucleus	$1/m^3$
τ_w	Wall shear stress	Pa

Table 2: Dimensionless Numbers.

Symbol	**Number**	**Definition**
Re	Reynolds Number	$\frac{ud}{\nu}$
Pr	Prandtl Number	$\frac{c_p \mu}{k} = \frac{\nu}{\alpha}$
$\mathrm{Pr_T}$	Turbulent Analogy to the Prandtl Number	$\frac{\varepsilon}{\varepsilon_h}$
Nu	Nusselt Number	$\frac{hd}{k_f}$
Sc	Schmidt Number	$\frac{\nu}{D_{AB}}$
$\mathrm{Sc_T}$	Turbulent Analogy to the Schmidt Number	$\frac{\varepsilon}{\varepsilon_m}$
Sh	Sherwood Number	$\frac{k_M d}{D_{wo}}$
Sh_p	Sherwood Number for Micro Particles	$\frac{k_d d_p}{D_{wo}}$

Table 3: Acronyms and Abbreviations.

Abbreviation	**Description**
CPM	Cross Polar Microscopy
DSC	Differential Scanning Calorimetry
FTIR	Fourier Transform Infrared Spectoscopy
HRD	Heat Resistance Distribution
HTGC	High Temperature Gas Chromatography
MATLAB	Matrix Laboratory
NMR	Nuclear Magnetic Resoncance
OPEX	Operational Expenditure
WAT	Wax Apperance Temperature
WPC	Wax Precipitation Curve

1 Introduction

As oil production is moving further offshore to colder regions and greater depths, the oil industry is facing increasing challenges in the area of flow assurance. One of the problems arising when tempting to ensure an economically feasible flow of hydrocarbons from the reservoir well bore to the treatment facilities, is the deposition of high molecular weight paraffins at the inner pipe wall, a topic to be presented below.

1.1 The Problem of Wax Deposition

The solubility of paraffins, interchangeably referred to as wax or paraffin wax, is temperature dependent, decreasing with decreasing temperature. At typical reservoir conditions[1], the wax molecules are kept dissolved in the oil. Flowing through the subsea pipeline resting on the ocean floor, the waxy crude looses heat to the colder surroundings and a radial temperature gradient over the cross-sectional area of the pipe is established.

If the temperature of a supersaturated wax-oil mixture drops below the wax appearance temperature (WAT), also known as the cloud point, solid wax molecules start to appear in solution. Assuming the existence of a radial temperature gradient, the precipitated wax will deposit on the inner pipe wall, causing flow restrictions or, in worst case, plugs the pipeline entirely. The result is a need for intervention and a possible shut-down of production (Huang, 2011).

1.2 Field Development

In 2012, there were more than 8500 km subsea export pipelines and 3000 km subsea infield flow lines at the Norwegian continental shelf. Out of these, almost 1000 km of the export lines were oil flowing and a substantial fraction of the produced and transported fluids were oils and gas condensates containing paraffin waxes (Rønningsen, 2012). On a global basis, waxy crudes have been estimated to represent about 20% of the petroleum reserves produced and pipelined, making prediction of wax deposits a relevant area for the petroleum industry (Frigaard et al., 2007).

Deposition of wax is recognized as a complex process involving a number of disciplines, among those flow dynamics, fluid chemistry, precipitation kinetics (crystal growth) and thermodynamics (Rønningsen, 2012). Currently there is no good method available for detection of wax deposits in oil flowing pipelines; When the pressure drop in a pipeline system has increased noticeably, the problem is already

[1]Typical off-shore reservoir conditions are temperatures between 70-150°C and pressure in the range of 55-100 MPa (Singh et al., 2000).

severe (Schulkes, 2013). Without any satisfying methods for detection available, mathematical modeling is a valid option for wax deposit prediction and what is applied in the industry.

Running wax deposit simulations, the aim is to be able to predict whether deposition should be expected or not, where in the pipeline accumulation of paraffin wax might occur and how fast the potential situation will progress. The simulators are meant to serve as a tool to support project decisions related to wax deposition, including planning of thermal insulation, pigging intervals and other remediation techniques to be applied.

Handling of wax deposits is an expensive affaire, adding significant costs to the operational expenditure (OPEX). Addressing the problem of deposition at an early stage of a field development project, may reduce the overall cost of the field. Applying insulation to prevent deposit formation in the first place may reducing or avoide loss of system capacity and the use of expensive chemical injection (Leontaritis et al., 2003).

1.3 Current Work

The aim of the current work, is to implement an analytical and a numerical model for prediction of paraffin wax deposits on the wall of a typical subsea oil flowing pipeline. If the applicability of the models is not be limited to flow loops, where the temperature at the pipe wall can be kept artificially constant, calculations of a varying wall temperature throughout the pipeline is required.

To gain knowledge and insight into the phenomena of heat and mass transfer, a theoretical study will have to be conducted. The aim of the study is to be able to mathematically derive and construct the wax deposit models and implement the results in the chosen computer language. Assuming a successfully implementation of the models, the final objective is to run simulations for comparison of the predicted wax deposit thicknesses when the same fluid under the same flow conditions has been applied. This will allow for quantification of the deviation between the results obtained by the two models that will occur, if any.

2 Modeling

A simulator is a mathematical model or computer code imitating a real-world system (O'Hagan, 2006). The aim of a simulator is to be able to predict the responses of a system over time. To execute the simulations, a mathematical model based upon the physical processes of the system in question will have to be developed. The model represents the system to be examined and the simulations imitates what takes place within the system.

2.1 Model Classifications

A simulator can be built as a probabilistic or a deterministic model. In a probabilistic model, randomness is present and the outcome is a probability distribution (O'Hagan, 2006). A probabilistic model provides a structured approach to account for uncertainty and is frequently applied in the area of economy. A deterministic model produces the same output values every time, if given the same input, and can be regarded a mathematical function taking in a vector $\mathbf{x}$ (input values) resulting in an output vector $y = f(\mathbf{x})$ (O'Hagan, 2006).

Simulators can be further divided into static and dynamic models. In a static model, the conditions of a system does not change with time, that is, steady state is assumed. In a dynamic model, on the other hand, the evolving behavior of a system is described. The changes in conditions, accounted for in a dynamic model, results in a more complex and computational expensive model (O'Hagan, 2006). As a result, the calculations of a dynamic model will have to be iterative, that is, at each time step the dynamic model takes in the current state vector as parts of its input and produces an updated vector to be used in the next step.

Since there is no randomness involved in the modeled wax deposition process, the analytical and numerical wax deposit models are both deterministic. As the static models are less computational expensive than the dynamic models, static simulations are preferred if the situation allows for it. The need for dynamic simulations in the current work will be evaluated in Chapter 9.

2.2 Uncertainty in Modeling

In every model there is uncertainty regarding how close the outcome of the simulations are to the actual real-world values. This uncertainty is related to the accuracy of the input values and the correctness of the model, that is, if the mathematical model is a valid description of the actual conditions of the system (O'Hagan, 2006).

One way to gain knowledge about the uncertainty of a model, is to perform a sensitivity analysis. The idea of a sensitivity analysis is to characterize how the

simulation outputs responds to a change in the input values (Kennedy and O'Hagan, 2001). Identifying which inputs the result is relatively sensitive, or insensitive, to provides knowledge about which inputs one should pay extra close attention to. For the purpose of uncertainty reduction, a sensitivity analysis on the implemented wax deposit models will be recommended as part of a future work.

2.3 Programing Language

The wax deposit models have been implemented in MATLAB. MATLAB is an acronym for Matrix Laboratory and a software widely used among engineers and scientist in industry and academia (MathWorks, 2013). The program can be used for development of algorithms, creation of models, numerical calculations and visualization.

The main advantage of using MATLAB, compared to spreadsheets or traditional programming languages, is the tools and built-in math functions (MathWorks, 2013). The language was found suitable for the current work because of its flexibility and ease of use.

3 Transport Phenomena

The overall behavior of paraffin wax in pipelines can be described theoretically by heat, mass and momentum equations. As the transport phenomena can be characterized by the same type of general equation, the processes are often considered as one discipline (Geankoplis, 2003). Momentum transfer, or fluid mechanics is divided into two branches; fluid statics and fluid dynamics. The former is dealing with fluids at rest, whilst the latter applies to fluids in motion. In the current thesis, fluid dynamics is utilized when calculating the temperature and concentration profiles of the numerical solution. The main focus will, however, be at the principles of heat and mass transfer as these are the governing mechanisms.

3.1 General Equation

The general transport equation describes the rate of transfer for any of the three transport processes and can be written as (Geankoplis, 2003):

$$\text{Rate of Transfer} = \frac{\text{Driving Force}}{\text{Resistance}} \tag{3.1}$$

or mathematically:

$$\Psi_z = -\delta \frac{d\Gamma}{dz} \tag{3.2}$$

where Ψ_z (amount of property/s.m^2) is the flux of the property defined as amount of property being transferred per unit time per unit cross-sectional area perpendicular to the z direction of flow, δ (m^2/s) is a proportionality constant termed diffusivity, Γ (property/m^3) is the concentration of property, and z (m) is the distance in the transport direction.

Integrating and rearranging Equation (3.2), results in a general expression for the flux of the property is obtained:

$$\Psi_z \int_{z_1}^{z_2} dz = -\delta \int_{\Gamma_1}^{\Gamma_2} d\Gamma \tag{3.3}$$

$$\Psi_z = \frac{\delta(\Gamma_1 - \Gamma_2)}{z_2 - z_1} \tag{3.4}$$

The transport equation is in heat and mass transfer known as Fourier's law and Fick's law, respectively, and will be presented in the succeeding chapters.

3.2 Dimensionless Numbers

A dimensionless number is a quantity with no physical dimension associated with it. It is widely used in mathematics and physics and also familiar from everyday life (counting). Dimensionless numbers are often expressed as ratios of non-dimensionless quantities, as are the case in the current thesis. When two or more processes can be expressed by dimensionless equations of the same form, they are referred to as analogous (Incropera et al., 2011).

Two pair of analog dimensionless numbers have been applied in the current work. The Prandtl number in heat transfer is analog to the Schmidt number in mass transfer, and the Nusselt number in heat transfer to the Sherwood number in mass transfer. Additionally, the Reynolds number (Re) from momentum transfer has been used.

3.3 Flow Regimes

Fluid flow can be divided into two flow regimes; laminar and turbulent flow. In the laminar flow regime, the movement of the fluid is highly ordered and streamlines at which the fluid particles move along can be identified. Under turbulent flow conditions, the fluid movement is highly irregular and velocity fluctuations characterizes the flow. The fluctuations in turbulent flow affects the transfer processes, increasing the rate of transfer in the fluid (White, 2008).

3.3.1 Reynolds Number

The Reynolds number (Re) is a dimensionless quantity expressing the ratio of inertia to viscous forces, defined as (White, 2008):

$$Re = \frac{\rho u d}{\mu} = \frac{u d}{\nu} \tag{3.5}$$

where ρ (kg/m^3) is the fluid density, u (m/s) is the fluid velocity, d (m) is the inner pipe diameter, μ (kg/m.s) is the dynamic viscosity and ν (m^2/s) is the kinematic viscosity. The kinematic viscosity, defined as (White, 2008):

$$\nu = \frac{\rho}{\mu} \tag{3.6}$$

where ρ (kg/m^3) is the fluid density and μ (kg/m.s) the dynamic viscosity as above. The kinematic viscosity is a transport property in momentum transfer, also referred to as diffusivity of momentum.

The flow regime in which one are operating in is determined by the value of the Reynolds number. When the Reynolds number is very low, the effects of inertia

are negligible and the fluid motion is viscous (creep). Moderate Reynolds number indicates laminar flow, whilst high Reynolds numbers implies turbulent conditions (White, 2008).

In a cylinder, the transition zone between laminar and turbulent flow is found around the critical Reynolds number $\mathrm{Re}_{d,crit} \approx 2300$ (White, 2008). Below the critical Reynolds number the flow is laminar and above a breakdown of the laminar motion causes the flow to become turbulent (White, 2008). Under normal operative conditions, the flow in oil flowing pipelines, as investigated in the current thesis, will be turbulent.

4 Heat Transfer

Heat transfer, or heat, is defined as *thermal energy in transit due to a spatial temperature difference*. There are three basic mechanisms of heat transfer; thermal conduction, thermal convection and thermal radiation (Incropera et al., 2012). In the current thesis, thermal conduction and thermal convection are the ones of interest and to be applied in the temperature profile calculations.

4.1 Conduction

Heat transfer by conduction is a result of heat being conducted through a material by the transfer of energy of motion between adjacent molecules. As higher molecular energies are associated with higher temperatures, energy transfer by conduction will, in the presence of a temperature gradient, occur in the direction of a decreasing temperature (Incropera et al., 2011). This spontaneous heat flow continues to take place until an equilibrium temperature has been reached. Examples of heat transfer by conduction known from everyday life are heat transfer through walls and freezing of the ground during winter.

The physical mechanisms of conduction varies depending on the state of the material. In a gas, molecules are in continuous random motion, exchanging energy when colliding, transporting kinetic energy by molecule movement from high-temperature regions to regions with lower temperature. Similarly, in a liquid, high energy molecules collides with lower energy molecules, resulting in heat transfer from regions with high temperatures to regions with low temperatures.

In solids, heat transfer by conduction can occur by two mechanisms. In all solids, heat is conducted by the transmission of vibration between adjacent atoms. Additionally in metallic solids, the conduction occurs by free electrons moving through the metal lattice (Geankoplis, aarstall).

4.1.1 Governing Equation

The rate at which heat is transferred by conduction is governed by Fourier's law (Incropera et al., 2011):

$$q'' = -k\frac{dT}{dx} \tag{4.1}$$

where q″ (W/m^2) is the heat flux due to conduction, defined as the rate of heat transfer per unit area, k (W/m.K) is the thermal conductivity and $\frac{dT}{dx}$ (K/m) is the temperature gradient, or temperature difference dT (K) across a layer of thickness dx (m).

Thermal conductivity is a material characteristic providing an indication of the rate at which energy is transferred (Incropera et al., 2012). The values for a solid varies greatly, from very high values for metals to very low values for insulating materials. The conductive heat flux increases with an increasing thermal conductivity, as seen from Equation (4.1). The minus sign in Fourier's law is a result of the direction of energy transport being from higher to lower energy levels.

4.1.2 Conduction Through Cylinders

When a fluid holding a higher temperature than the surroundings is flowing through a cylinder, heat is transferred through the walls. Expressing the heat flux as heat transfer, q (W), per unit area, A (m), Fourier's law in radial coordinates is written as (Geankoplis, 2003):

$$\frac{q}{A} = -k\frac{dT}{dr} \tag{4.2}$$

where k (W/m.K) is the thermal conductivity of the cylinder, dT (K) is the temperature difference between the inside and outside of the cylinder and dr (m) is the thickness of the wall. The interface area at which heat transfer occurs is given as:

$$A = 2\pi rL \tag{4.3}$$

where r (m) is the radial coordinate and L (m) the length of the cylinder.

Considering a cylinder of length L (m), with an inside radius r_1 (m) at a temperature T_1 (K), and an outer radius r_2 (m) with a temperature T_2 (K), then substituting Equation (10.11) into Equation (4.2), the following expression is obtained:

$$\frac{q}{2\pi rL}\int_{r_1}^{r_2}\frac{dr}{r} = -k\int_{T_1}^{T_2}dT \tag{4.4}$$

which integrated and rearranged can be expressed as:

$$q = k\frac{2\pi L}{ln(r_2/r_1)}(T_1 - T_2) \tag{4.5}$$

Multiplying the numerator and denominator by (r_2-r_1), an equation expressing the radial heat flux through the wall of the cylinder is obtained:

$$q = \frac{T_1 - T_2}{(r_2 - r_1)/(kA_{lm})} = \frac{T_1 - T_2}{R} \tag{4.6}$$

where A_{lm} (m^2) is the log mean area of the pipe and R (m^2K/W) is the thermal resistance, expressed as:

$$A_{lm} = \frac{(2\pi L r_2) - (2\pi L r_1)}{ln(2\pi L r_2 / 2\pi L r_1)} = \frac{A_2 - A_1}{ln(A_2/A_1)} \tag{4.7}$$

$$R = \frac{r_2 - r_1}{k A_{lm}} = \frac{ln(r_2/r_1)}{2\pi k L} \tag{4.8}$$

where the variables are as presented.

4.1.3 Conduction Through Multiple Layers

Assuming a radial heat flux in the system and layer of paraffin wax on the inner pipe wall, there will be heat flow through multiple layers in series in the pipeline. Two concentric layers will, in such a case, have to be taken into consideration when performing the heat flux calculations.

Since the rate of heat transfer is identical across each layer, the radial heat flow in the pipe can be expressed as (Geankoplis, 2003):

$$q = \frac{T_{dep} - T_{wi}}{(r_{dep} - r_{wi})/(k_{dep} A_{lm,dep})} = \frac{T_{wi} - T_{wo}}{(r_{wo} - r_{wi})/(k_{pipe} A_{lm,pipe})} \tag{4.9}$$

where T_{dep} (K) is the interface temperature between oil and deposit, T_{wi} (K) is the temperature at the inner pipe wall, T_{wo} (K) is the temperature at the outer pipe wall, r_{dep} (m) is the radius measured from the centerline of the pipe to the deposit interface, or the effective flow radius, r_{wi} (m) is the inner pipe radius, r_{wo} (m) is the outer pipe radius, k_{dep} (W/m.K) is the thermal conductivity of the deposit and k_{pipe} (W/m.K) is the thermal conductivity of the pipe. The log mean area of the deposit and the log mean area of the pipe, $A_{lm,dep}$ (m^2) and $A_{lm,pipe}$ (m^2), respectively, are given as:

$$A_{lm,dep} = \frac{A_{wi} - A_{dep}}{ln(A_{wi}/A_{dep})} \tag{4.10}$$

$$A_{lm,pipe} = \frac{A_{wo} - A_{wi}}{ln(A_{wo}/A_{wi})} \tag{4.11}$$

with the interface areas at which heat transfer occurs expressed as:

$$A_{dep} = 2\pi r_{dep} L \tag{4.12}$$

$$A_{wi} = 2\pi r_{wi} L \tag{4.13}$$

$$A_{wo} = 2\pi r_{wo} L \tag{4.14}$$

From Equation (4.9), the temperature differences across the deposit and the pipe wall can be found:

$$\Delta T_{dep} = q\frac{(k_{dep}A_{lm,dep})}{r_{dep} - r_{wi}} \tag{4.15}$$

$$\Delta T_{wall} = q\frac{(k_{pipe}A_{lm,pipe})}{r_{wi} - r_{wo}} \tag{4.16}$$

Adding Equation (4.15) and Equation (4.16), the internal temperature drops out and the final equation to be implemented in the wax deposit models can be written as:

$$q = \frac{T_{dep} - T_{wo}}{(r_{wi} - r_{dep})/(k_{dep}A_{lm,dep}) + (r_{wo} - r_{wi})/(k_{pipe}A_{lm,pipe})} \tag{4.17}$$

$$q = \frac{T_{dep} - T_{wo}}{R_{dep} + R_{pipe}} = \frac{T_{dep} - T_{wo}}{\sum R} \tag{4.18}$$

where T_{dep} (K) is the temperature at the surface of the deposit, T_{wo} (K) is the outer wall temperature, R_{dep} (m^2K/W) is the thermal resistance of the deposit, R_{pipe} (m^2K/W) is the thermal resistance of the pipe and $\sum R$ (m^2K/W) is the sum of the resistances in a series, or the total resistance towards heat flow.

4.2 Dimensionless Numbers in Heat Transfer

In the heat transfer calculations, the Nusselt number (Nu), the Prandtl number (Pr) and the Reynolds number are the necessary quantities to determine the convective heat transfer coefficient, the eddy diffusivity and the flow regime, the former being variables presented below.

4.2.1 Nusselt Number

The Nusselt number is defined as the ratio of convective to conductive heat transfer normal to the surface at which heat transfer occurs. The quantity equals a dimensionless temperature gradient at the surface of the body, and provides a measure of the convective heat transfer at the surface.

For a fluid flowing through a cylinder, the Nusselt number is defined as (Incropera et al., 2011):

$$Nu = \frac{hd}{k_f} \tag{4.19}$$

where h ($W/m^2.K$) is the convective heat transfer coefficient, d (m) is the inner pipe diameter and k_f (W/m.K) is the thermal conductivity of the fluid.

By the means of empirical correlations, the Nusselt number will be used to determine the convective heat transfer coefficient. The applicable correlations are presented in Appendix B.

4.2.2 Prandtl Number

The Prandtl number provides a measure of the relative effectiveness of energy transport by diffusion. It is defined as the ratio of kinematic viscosity to thermal diffusivity (Incropera et al., 2012):

$$Pr = \frac{C_p \mu}{k_f} = \frac{\nu}{\alpha_T} \tag{4.20}$$

where C_p (J/K.kg) is the specific heat capacity of the fluid, μ (Pa.s) is the dynamic viscosity, k_f (W/m.K) is the thermal conductivity, ν (m^2/s) is the kinematic viscosity and α_T (m^2/s) is the thermal diffusivity.

The Prandtl number will be applied in the eddy diffusivity calculations and in the empirical Nusselt number correlations.

4.3 Fourier's Law in the Turbulent Flow Regime

Fourier's law, as written in Equation (4.1), is valid in the laminar flow regime only. By the use of semi-empirical correlations, the applicability of the fundamental law of transfer can be extended to the turbulent flow regime. Based on the concept of heat transfer coefficients, Fourier's law, including contribution from turbulent flow, can be written as (Gudmundsson, 2012):

$$q'' = -(\alpha_T + \varepsilon_h)\frac{dT}{dr} \tag{4.21}$$

where α_T (m^2/s) is the thermal diffusivity, ε_h (m^2/s) is the turbulent, or eddy, heat diffusivity, and $\frac{dT}{dr}$ (K/m) is the radial temperature gradient.

The eddy diffusivity for heat transfer is defined by Prandtl mixing length theory (Geankoplis, 2003):

$$\frac{\varepsilon_h}{\alpha_T} = \frac{Pr}{Pr_T}\frac{\varepsilon}{\nu} \tag{4.22}$$

where ε_h (m^2/s) is the turbulent heat diffusivity, α_T (m^2/s) is the turbulent thermal diffusivity, Pr and Pr_T are the dimensionless Prandtl number and turbulent Prandtl number, respectively, ε (m^2/s) is the eddy diffusivity and ν (m^2/s) is the kinematic viscosity.

The turbulent analogy of the Prandtl number expresses the ratio of thermal turbulent diffusivity to molecular thermal diffusivity as (Geankoplis, 2003):

$$Pr_T = \frac{\varepsilon}{\varepsilon_h} \tag{4.23}$$

The momentum diffusivity, ε (m^2/s), is determined by Van Driest's equation (Van Driest, 1956):

$$\frac{\varepsilon}{\nu} = (C_1 y^+)^2 \left[1 - \exp\left(\frac{-y^+}{C_2}\right)\right]^2 \left|\frac{dV_z^+}{dy^+}\right| \tag{4.24}$$

where C_1 and C_2 are dimensionless eddy viscosity correlation constants, y^+ is the dimensionless wall normal distance and V_z^+ is the dimensionless velocity determined by:

$$V_z^+ = \begin{cases} y^+ & y^+ \leq 5 \\ 5 \ln y^+ - 3.05 & 5 < y^+ < 30 \\ 2.5 \ln y^+ + 5.5 & y^+ \geq 30 \end{cases} \tag{4.25}$$

where $y^+ = \frac{y}{\nu}\sqrt{\frac{\tau_w}{\rho}} = \left(1 - \frac{r}{R}\right)\frac{Re}{2}\sqrt{\frac{f}{8}}$, $f = \frac{0.305}{Re^{0.25}}$, $C_1 = 0.4$ and $C_2 = 26$ (Lee, 2008).

4.4 Convection

In thermal convection, heat transfer occurs by bulk motion and mixing of macroscopic elements of warmer and cooler portions of a fluid (Geankoplis, 2003). Heat transfer by convection often involves an energy exchange between a solid surface and a fluid, as are the case with oil flowing through the pipeline.

4.4.1 Governing Equation

The rate of heat transfer by convection is given by Newton's law of cooling (Incropera et al., 2011):

$$q'' = h(T_s - T_\infty) \tag{4.26}$$

where q" (W/m^2) is the convective heat flux, T_s (K) is the temperature of the surface, T_∞ (K) is the temperature of the fluid and h ($W/m^2.K$) is the convective heat-transfer coefficient.

The convective heat flux is proportional to the difference between the surface temperature and the fluid temperature, as can be seen from Equation (4.26). If heat is transferred from the fluid to the surface ($T_\infty > T_s$), the heat flux is positive. If the situation is reversed ($T_\infty < T_s$), the heat flux is negative.

The convective boundaries for a situation with radial heat flux from the outside to the inside of a cylinder is illustrated in Figure 4.1.

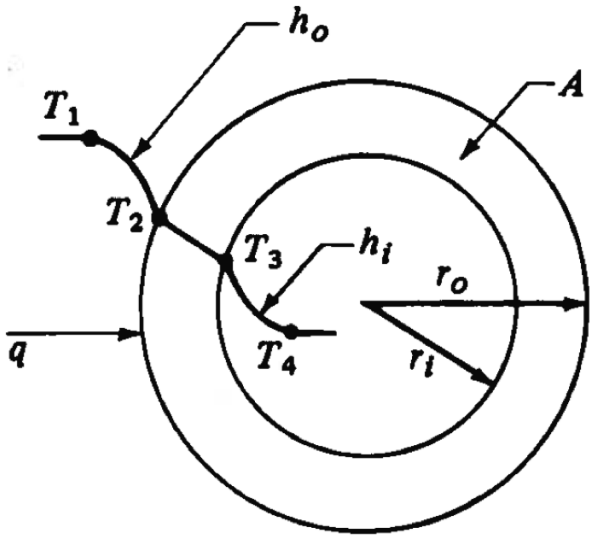

Figure 4.1: Radial heat flow from the outside to the inside of a pipe with convective boundaries and temperature nodes of interest (Geankoplis, 2003).

4.4.2 Convective Heat Transfer Coefficient

Calculating the convective heat flux by Newton's law of cooling requires the convective heat transfer coefficient, h (W/m^2.K), to be known. The quantity is a function of fluid properties, flow velocity, temperature differences and system geometry, giving an indication of the rate at which heat transfer by convection will occur (Geankoplis, 2003).

To determine the convective heat transfer coefficient in the current work, the definition of the Nusselt number and an empirical correlation found suitable for the flow conditions and system geometry is applied.

4.5 Heat Transfer in Oil Flowing Pipelines

In the wax deposit modeling, the temperature at the solid/liquid interface must be known. Before first deposition, the inner pipe wall constitutes the solid/liquid interface. When a layer of deposit is formed, the deposit surface is the interface in question. To perform the calculations, Fourier's law of conduction and Newton's law of cooling will have to be combined.

The combined heat transfer is often expressed in terms of an overall heat transfer coefficient (Geankoplis, aarstall):

$$q = UA\Delta T_{overall} \tag{4.27}$$

where q (W) is the rate of heat transfer, U (W/m^2.K) is the overall heat transfer coefficient, A (m^2) is the interface area at which heat transfer occurs and $\Delta T_{overall}$ (K) is the temperature difference between the average bulk flow temperature and the ambient temperature.

For radial heat flux a cylinder [...], Equation (4.6) and Equation (4.26) can be combined to:

$$q = h_i A_w i(T_1 - T_2) = \frac{T_2 - T_3}{(r_2 - r_1)/(k_A A_{lm,A})} = h_o A_{wo}(T_3 - T_4) \tag{4.28}$$

where h_i (W/m^2.K) is the inner convective heat transfer coefficient, A_i (m^2) is the inner pipe wall (solid/liquid interface area), T_1 (K) is the average bulk flow temperature, T_2 (K) and T_3 (K) are the temperatures at the inner and outer pipe wall, respectively, r_2 (m) is the outer pipe radius, r_1 (m) is the inner pipe radius, k_A (W/m.K) is the conductive heat transfer coefficient of the pipe, $A_{lm,A}$ (m^2) is the log mean area of the pipe, h_o (w/m^{2}K) is the outer heat transfer coefficient, A_o (m^2) is the outer pipe wall area and T_4 (K) is the ambient temperature.

For an oil flowing pipeline with an existing layer of deposit, Equation (4.28) can be written as:

$$\begin{aligned} q = h_i A_{dep}(T_b - T_{dep}) &= \frac{T_{dep} - T_{wi}}{(r_{wi} - r_{dep})/(k_{dep} A_{lm,dep})} \\ &= \frac{T_{wi} - T_{wo}}{(r_{wo} - r_{wi})/(k_{pipe} A_{lm,pipe})} = h_o A_{wo}(T_{wo} - T_{sea}) \end{aligned} \tag{4.29}$$

where h_i (W/m^2.K) is the inner convective heat transfer coefficient, A_{dep} (m^2) is the surface area of the deposit, T_b (K) is the average bulk flow temperature, T_{dep} (K) is the temperature at the oil/deposit interface, T_{wi} (K) is the temperature at the inner pipe wall, r_{wi} (m) is the inner pipe radius, r_{dep} (m) is the effective flow radius, k_{dep} (W/m.K) is the thermal conductivity of the deposit, $A_{lm,dep}$ (m^2) is the log mean area of the deposit, k_{pipe} (W/m.K) is the thermal conductivity of the pipe, T_{wo} (K) is the temperature at the outer pipe wall, h_o (W/m^{2}K) is the outer convective heat transfer coefficient, A_{wo} (m^2) is the outer pipe wall area, T_{wo} (m) is the temperature at the outer pipe wall and T_{sea} is the ambient sea temperature.

The log mean areas of the deposit and the pipe are found by Equation (4.10) and Equation (4.11), respectively. If there is no deposit in the pipe line, the second term in Equation (4.29) falls out.

5 Mass Transfer

Mass transfer is defined as *mass in transit as the result of a species concentration difference in a mixture* (Incropera et al., 2011). Just as a temperature difference in a media inevitably results in heat transfer, a difference in concentration of chemical species in a mixture leads to transfer of mass. The current chapter presents the theoretical foundation necessary for the understanding of the wax deposition process.

5.1 Diffusion

Mass transfer due to random molecular motion is known as diffusion. Diffusion of mass is analogue to the situation with heat transfer by conduction, but unlike conduction heat transfer, diffusion of a species always involves the movement of molecules or atoms from one region to another.

5.1.1 Governing Equation

The rate of mass diffusion, or mass flux, in a binary mixture of chemical species A and B is given by Fick's law (Incropera et al., 2011):

$$J'' = -D_{AB}\frac{dC}{dr} \tag{5.1}$$

where J'' (kg/s.m^2) is the mass flux or amount of solute A in solvent B transferred by diffusion per unit time and per unit area perpendicular to the direction of transfer, D_{AB} (m^2/s) is a binary diffusion coefficient, also known as the mass diffusivity, and $\frac{dC}{dr}$ (kg/m^4) is the radial concentration gradient. The minus sign in the equation reflects that mass diffusion occurs in the direction of decreasing concentration.

The diffusion coefficient, D_{AB} (m^2/s), provides an indication of the rate at which species A is transferred through species B by the diffusion process. The binary diffusion coefficient is analogue to the kinematic viscosity in momentum transfer and the thermal conductivity coefficient in heat transfer, that is, they represents the proportionality constant, δ, in Equation (3.1). A correlation for calculation of the diffusion coefficient for calculation of wax transfer in oil, D_{wo} (m^2/s) will be presented in Appendix C.

5.2 Dimensionless Numbers in Mass Transfer

The dimensionless numbers applied in the mass transfer calculations, are the Schmidt number (Sc) and the Sherwood number (Sh).

5.2.1 Schmidt Number

The Schmidt number equals is defined as the ratio of kinematic viscosity to mass diffusivity and provides a measure of the relative effectiveness of mass transport by diffusion (Incropera et al., 2011):

$$Sc = \frac{\nu}{D_{AB}} \tag{5.2}$$

where ν (m^2/s) is the kinematic viscosity and D_{AB} (m^2/s) is the binary diffusion coefficient. The Schmidt number will be used in the calculations of the turbulent mass diffusivities as presented below.

5.2.2 Sherwood Number

The Sherwood number equals a dimensionless concentration gradient at the surface of a body. It provides a measure of the convection mass transfer occurring at the surface and is defined as (Incropera et al., 2011):

$$Sh = \frac{k_M d}{D_{wo}} \tag{5.3}$$

where k_M (m/s) is the mass transfer coefficient, d (m) is the inner pipe diameter and D_{AB} (m^2/s) is the binary diffusion coefficient. The Sherwood number will be used to determine the mass transfer coefficient in the numerical modeling.

5.3 Fick's Law in the Turbulent Flow Regime

Fick's law, as defined by Equation (5.1), is only valid in the laminar flow regime. Semi-empirical correlations can again be applied to extend the area of validity to the turbulent flow regime. With the contribution from turbulent flow included, Fick's law is written as (Geankoplis, 2003):

$$J'' = -(D_{AB} + \varepsilon_m)\frac{dC}{dr} \tag{5.4}$$

where D_{AB} (m^2/s) is the binary diffusion coefficient, ε_m (m^2/s) is the turbulent mass diffusivity and $\frac{dC}{dr}$ (kg/m^4) is the concentration gradient in the mixture.

The turbulent, or eddy, mass diffusivity is defined by Prandtl mixing length theory (Geankoplis, 2003):

$$\frac{\varepsilon_m}{D_{AB}} = \frac{Sc}{Sc_T}\frac{\varepsilon}{\nu} \tag{5.5}$$

where ε_m (m^2/s) is the turbulent mass diffusivity, D_{AB} (m^2/s) is the binary diffusion coefficient, Sc is the Schmidt number, Sc_T is the turbulent analogy to the Schmidt

number, ε (m^2/s) is the eddy diffusivity and ν (m^2/s) is the kinematic viscosity.

The turbulent analogy to the Schmidt number expresses the ratio of turbulent mass diffusivity to molecular mass diffusivity:

$$Sc_T = \frac{\varepsilon}{\varepsilon_m} \tag{5.6}$$

where ε (m^2/s) is the momentum diffusivity and ε_m (m^2/s) the turbulent mass diffusivity. The momentum diffusivity is given by Equation (4.24).

6 Paraffin Wax

Crude oil is a mixture of a range of hydrocarbons including paraffins, aromatics, naphtens, resins and asphaltens (Venkatesan, 2004). One of the problems associated with hydrocarbon production, is the precipitation of paraffin molecules when the oil is cooled leading to deposition. The current chapter introduces the chemistry and physics behind wax deposition and presents methods to deal with the challenge in the field.

6.1 Chemistry of Wax

Paraffin wax is a reference to linear chain alkanes (n-paraffins) containing more than 16 carbon atoms (Leontaritis et al., 2003). The general chemical formula of paraffins is C_nH_{2n+2}. Depending on the chemical composition, paraffins might be in either a gaseous, liquid or solid phase under ambient conditions. Paraffins with less than four carbon atoms (C_1-C_4) will be at a gaseous state, paraffins with five to sixteen carbon atoms (C_5-C_{16}) at a liquid state, and the series of C_{16}-C_{70+}, causing the encountered wax deposition problems, will be in a solid state (Leontaritis et al., 2003).

The carbon number distribution of paraffins in crude oils varies from one fluid to another. Most of the paraffins found in crudes are in the range from C_{18}-C_{65} (Ekweribe et al., 2008). To determine the exact wax composition, a laboratory analysis will have to be conducted for each fluid in question. One method widely used is the High Temperature Gas Chromatography (HTGC). The molecular weight distribution of the hydrocarbons is then characterized as a function of the carbon number, that is, the weight percent of all hydrocarbons with a certain carbon number is identified (Singh et al., 2011).

6.2 Wax Appearance

Wax separation in hydrocarbon containing systems is mainly driven by thermodynamic interaction. Because waxy crystals are incompressible and liquid hydrocarbons only slightly compressible, a change in pressure induces little or no wax appearance. Thus, a pressure drop at dynamic or static conditions has almost no effect on wax precipitation. The separation of the heaviest components, is rather a result of heat loss (cooling) from the liquid to the surroundings (Leonaritis et al., 2003; Villazon and Civan, 2009).

The wax appearance temperature, is defined at the point where 0.02 mole percent of the wax particles has precipitated out of solution, creating a binary mixture of oil and wax (Singh et al., 2011). Since the solubility of wax is decreasing with

decreasing temperature, a lower cloud point will result in a later occurrence of wax in solution, favorable for the situation.

The location of the WAT separates one region containing oil in a liquid phase and waxy crystals in a solid phase, and another region in which the wax has not precipitated out of solution yet (Villazon and Civan, 2009). The wax appearance boundary where the flow is single phase above it and multiphase below, is in other words inferred from the temperature profile.

There are several existing methods to determine the WAT, among those the Cross Polar Microscopy (CPM) and the Differential Scanning Calorimetry (DSC). Modeling of wax precipitation and subsequent deposition is found to be highly sensitive towards the WAT prediction ability (Villazon and Civan, 2009). Because of the importance of the parameter, it is recommended to make use of two independent techniques to obtain a sufficient degree of accuracy when determining the WAT (Venkatesan and Fogler, 2004; Venkatesan and Creek, 2010).

6.3 Deposit Formation

When oil in the near-wall region is cooled below the WAT, it starts to gel at the pipeline wall. The deposition, or gelation, is a result of flocculation of orthorhombic wax crystallites appearing in the fluid during cooling; the precipitated wax crystals are forming a network. The gel deposited does not consist of pure solidified paraffins, but is rather a wax-oil mixture containing a large fraction of oil trapped in a 3-D network of wax crystals (Singh et al., 2000).

The process of wax deposition can be described by the following four steps (Huang, 2011)[2]:

1. Formation of an incipient layer of deposit on the cold pipe wall surface.
2. Radial mass flux of paraffin molecules from the bulk fluid toward the oil/deposit interface (A).
3. Radial flux of paraffin molecules from the surface of the deposit into the deposit layer (B).
4. Precipitation of paraffin molecules inside the deposit resulting in an increased solid wax content.

The growth rate of the deposit is determined by the difference in radial flux from the bulk to the oil/deposit interface (flux A) and the flux from the interface and into the deposit (flux B) as illustrated in Figure 6.1.

[2]The five steps of wax deposition originally proposed by Singh et al. (2000) have been summarized into four major steps (Huang ,2011).

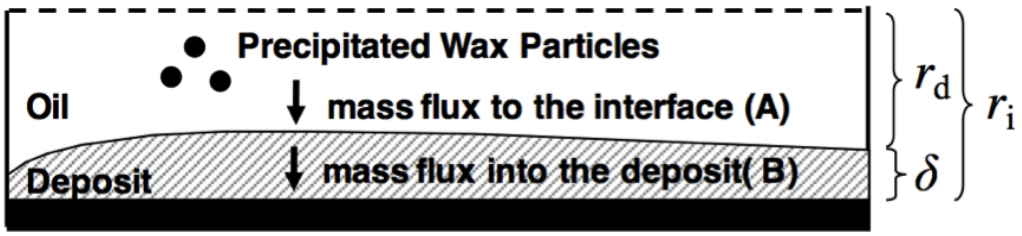

Figure 6.1: An illustration of the principles of wax deposition by molecular diffusion. The stippled line represents the centerline of the pipe and the thicker line the pipe wall (Huang, 2011).

The driving force for deposition is the radial concentration gradient causing a mass flux of wax molecules towards the inner pipe wall (Venkatesan, 2004). As the concentration gradient is inferred from the temperature gradient, the temperature profile in the pipeline is required when performing wax deposit simulations. The radial concentration gradient is referred to as the mass driving force for wax deposition and the temperature radial gradient, ordifference, is referred to as the thermal driving force (Huang, 2011).

6.4 Wax Handling

To avoid wax crystallization or to remove already existing deposits, various tools of chemical and mechanical nature can be applied. To inhibit the formation of deposit or to modify the WAT, paraffin inhibitors or dispersants can be used, preventing agglomeration and deposition. For remediation of deposits already formed, the use of hot solvents is a possible solution.

Examples of mechanical methods applied, are pipeline electrical heating and pigging (mechanical scrapping), the latter being one of the most frequently used remediation techniques in the field (Benall et al., 2008; Lee, 2008; Huang, 2011; Singh et al., 2011). Paraffin wax deposition can also be prevented by insulation of the pipelines, either by using external insulating coating or pipe-in-pipe systems (Leontartis et al., 2003; Schulkes, 2013; Stokkenes, 2013).

7 Literature

The literature study introduces the possible mechanisms behind paraffin wax deposition and presents the theoretical foundation of the analytical and numerical models, important for understanding of the presented results from the simulations in later chapters.

7.1 Wax Deposition Mechanisms

Calculation of the radial mass transport of wax molecules in the viscous sub-layer is considered one of the most important factors in the prediction of wax deposition (Lee, 2008). A comprehensive study of the mechanisms responsible for wax deposition was conducted by Burger et al. (1981), a work that has been a widely cited reference since. Burger et al. (1981) identified four possible mechanisms responsible for wax deposition: Molecular diffusion, Brownian diffusion, shear dispersion and gravitational settling (Burger et al., 1981).

In the early 2000s, Azevedo and Teixeira (2003) did a review of the modeling of wax deposition mechanisms. Molecular diffusion of paraffins, as described by Burger et al. (1981), was acknowledged as the dominant mechanism responsible for paraffin wax deposition. It was argued that experimental evidence suggests that gravity settling and shear dispersion do not contribute significantly in the process. However, not enough experimental evidence was found to exclude the possibility of Brownian diffusion taking part (Azevedo and Teixeira, 2003).

A paper of more recent date states that the overall consensus in the field is that molecular diffusion in the viscous sub-layer is the dominant mechanism of wax deposition (Singh et al., 2011). Rønningsen (2012) is somewhat more careful in his formulation, using the term *fairly well-established* when commenting upon molecular diffusion as an important factor in control of the amount of wax molecules available for deposition in the pipeline.

7.2 Wax Deposition Modeling

A number of mathematical models have been developed for the purpose of wax deposit prediction. Among those are the models presented, representing two different approaches towards wax deposit modeling in terms of mathematics and fundamental assumptions.

7.2.1 Analytical Model

In the analytical model, the mass rate of wax transfer is calculated by Fick's law. The radial flux of wax molecules is computed with the assumption of thermodynamic equilibrium in the mass transfer boundary layer, that is, the wax concentration is, in other words, assumed to follow the solubility at every point in the pipeline (Azevedo and Teixeira, 2003; Lee, 2008; Aiyejina et al., 2011).

The assumption of thermodynamic equilibrium in the viscous sub-layer is found to be valid in the laminar flow regime only. Under turbulent flow conditions, as encountered in oil flowing pipelines, the concentration field is found to be correlated to the temperature field and must, in order to obtain correct modeling, be taken into consideration (Venkatesan and Fogler, 2004).

When the difference in solubility and actual wax concentration in the boundary layer is significant, the analytical model is expected to result in an over prediction of wax deposits. The situation situation arises in turbulent flow, when the precipitation kinetics of wax molecules in the boundary layer is slow (Venkatesan and Fogler, 2004; Lee, 2008; Huang, 2011).

The analytical model assumes a constant weight fraction of wax in deposit during the deposition process. This is a simplification of the situation, as the process of deposition is described by a radial flux of wax molecules from the bulk to the oil/deposit interface followed by a flux of molecules from the interface and into the deposit where further precipitation of paraffin wax occurs (Singh et al., 2000). An interesting study, however outside the scope of the current work, is an evaluation of the growing wax content in the deposit and its consequences for deposit thickness prediction and selection of remediation techniques.

7.2.2 Numerical Model

The implemented numerical model has been stepwise developed from a general mathematical model describing the process of wax deposition (Singh et al., 2001). Based on the balance of energy and mass, a set of equations to calculate the growth rate and aging of wax deposits was derived. To calculate the mass flux of wax molecules, the convective mass transfer coefficient obtained from the laminar Sherwood number was applied.

The model was found to successfully predict the results of wax deposition under laminar flow conditions, but to over estimate the deposit thickness in the turbulent flow regime (Lee, 2008). The over prediction is explained by a neglect of precipitation of wax molecules in the oil phase, physically correct under laminar flow conditions, but an important feature in the turbulent flow regime where the rate of cooling is relatively slow (Huang, 2011).

A refinement of the model was presented by Venkatesan and Fogler (2004). The basic equations derived by Singh et al. (2001) was applied to calculate the growth rate of the deposit, but with the convective mass transfer rate estimated by the Sherwood number and an experimentally obtained solubility curve (Lee, 2008). The model showed to under predict the deposit thickness, a finding believed to be a result of supersaturated wax molecules in solution without sufficient time to precipitate that was not accounted for (Huang, 2011).

Based on the same equations, Lee (2008) developed a wax deposition model applicable in both the laminar and the turbulent flow regime. The finite difference method (FDM) was applied on a coupled set of heat and mass transfer equations and a precipitation rate constant was included to account for precipitation kinetics of the wax molecules. The correct results was explained by the impact of precipitation kinetics on the diffusion mass flux in the boundary layer, reducing the diffusive mass transfer rate of wax molecules significantly (Lee, 2008). The model has been acknowledge as a correct correlation of the phenomena of heat and mass transfer that *provides a robust and rigorous way of predicting wax deposition* in both flow regimes (Aiyejina et al., 2011).

8 Effective Thermal Conductivity of Two Component Systems

Correct wax deposition modeling requires correct modeling of the effective thermal conductivity of the wax deposit. Since the gel layer at the pipeline wall is a two component system composed of paraffin wax and oil, computational models to determine the effective thermal conductivity of a heterogenous material has been investigated

8.1 Thermal Conductivity

The effective thermal conductivity of heterogeneous materials is strongly affected by its composition and structure. Several methods to determine the property exists. Some includes the use of empirical parameters to account for variations in composition and structure, others make use of numerical techniques (Bunthebart and Jobman, 2008).

In many applications analytical models are preferred. The main advantage of an analytical model is the rapid and low cost calculations, and the independency of empirical correlations. Each of the analytical models presented have a physical basis and are producing results of reasonable accuracy, even with an unknown microstructure (Wang et al., 2006; Bunthebart and Jobman, 2008).

In the current work, the thermal conductivity of oil, wax, pipe and deposit are required. The thermal conductivity of oil, wax and pipe duplex steel, being the material of the pipe, are table values reported in Table 4. The effective thermal conductivity of the wax deposit will have to be calculated from one of the proposed models as it is a binary mixture of oil and wax.

Table 4: Thermal conductivity values of oil, paraffin wax and duplex steel to be applied in the wax deposit models (Gudmundsson, 2012; Mirazizi, 2012).

Substance	**Thermal Conductivity [W/m.K]**
Oil	0.10
Paraffin Wax	0.25
Duplex Steel	20

8.2 Stratified Models

The simplest analytical models are the Parallel model and the Series model. With the heat flow being in the vertical direction, the Parallel model assumes a distribution of the two components in distinct vertical layers. Mathematically, the model is expressed as (Wang et al., 2006):

$$k_e = v_1 k_1 + v_2 k_2 \tag{8.1}$$

where k_e (W/m.K) is the effective thermal conductivity of the material, k_1 (W/m.K) is the thermal conductivity of the first component, k_2 (W/m.K) is the thermal conductivity of the second component, and v_1 and v_2 are the volume fractions of the two components.

The Series model assumes a distribution of the two components in distinct horizontal layers, the heat flow still being in the vertical direction. The model is given as (Wang et al., 2006):

$$k_e = \left(\frac{v_1}{k_1} + \frac{v_2}{k_2} \right)^{-1} \tag{8.2}$$

with the thermal conductivities and volume fractions as declared above.

The volume fractions can further be expressed as (Awad and Muzychka, 2008):

$$v_2 = (1 - v_1) \tag{8.3}$$

where v_1 is the volume fraction of the first component and v_2 is the volume fraction of the second component.

8.3 Maxwell-Eucken Model

A conductivity formula suitable for two component systems consisting of a continuous and a dispersed phase was presented by Maxwell (1904) and further developed by Eucken (1940), resulting in the Maxwell-Eucken Model (Serpil and Servet, 2006). The model assumes the dispersion of small spheres of one substance within a continuous matrix of a different component. Based on the thermal conductivity of the components, two variations of the model exists.

8.3.1 Maxwell-Eucken 1

If the thermal conductivity of the continuous phase is higher than the thermal conductivity of the dispersed phase ($k_{cont} > k_{disp}$), the Maxwell-Eucken 1 (ME1) is applicable (Awad and Muzychka, 2008):

$$k_1 > k_2$$

$$k_e = \frac{k_1 v_1 + k_2 v_2 \frac{3k_1}{2k_1+k_2}}{v_1 + v_2 \frac{2k_1}{2k_1+k_2}} \tag{8.4}$$

where k_e (W/m.K) is the effective thermal conductivity of the material, k_1 and k_2 (W/m.K) are the thermal conductivity of the two components and v_1 and v_2 are the two volume fractions.

8.3.2 Maxwell-Eucken 2

In the reversed cases, if the thermal conductivity of the continuos phase is less than the thermal conductivity of the dispersed phase, ($k_{cont} < k_{disp}$), the Maxwell-Eucken 2 (ME2) is suitable (Awad and Muzychka, 2008):

$$k_1 < k_2$$

$$k_e = \frac{k_2 v_2 + k_1 v_1 \frac{3k_2}{2k_2+k_1}}{v_2 + v_1 \frac{2k_2}{2k_2+k_1}} \tag{8.5}$$

with the thermal conductivities and volume fractions as above.

8.4 Effective Medium Theory

The basic assumption of the Effective Medium Theory (EMT), is a total random distribution of the two components within a material (Wang et al., 2006). The model is well suited in situations where neither of the components are continuous or dispersed, but rather randomly distributed (Awad and Muzychka, 2008).

$$v_1 \frac{k_1 - k_e}{k_1 + 2k_e} + v_2 \frac{k_2 - k_e}{k_2 + 2k_e} = 0 \tag{8.6}$$

where the variables are as before.

Rearranging Equation (8.6), a quadratic equation suitable for implementation in the computer program is obtained:

$$2(v_1 + v_2)k_e^2 - (2v_1v_2 - v_1k_2 - v_2k_2 + 2v_2k_2)k_e - (v_1 + v_2)k_1k_2 = 0 \tag{8.7}$$

$$k_e = \frac{-b \pm \sqrt{b^2 - 4ac}}{2a} \tag{8.8}$$

where

$$a = 2(v_1 + v_2)$$

$$b = -(2v_1v_2 - v_1k_2 - v_2k_2 + 2v_2k_2)$$

$$c = -(v_1 + v_2)k_1k_2$$

If Equation (8.8) yields two results, the positive outcome ($k_e > 0$) is the value of the effective thermal conductivity to be used.

8.5 Evaluation of Model Applicability

The applicability of the five effective thermal conductivity models for the wax deposit have been evaluated on the basis of structure. The layer of deposit is made up of a large fraction of oil trapped in a 3-D network of wax crystals, hence, the criteria for using the Parallel and the Series models are not met, as those requires stratified deposition into distinct layers.

The conclusion is confirmed by the microscope observations of a typical wax-oil gel in Figure 8.1. The image reveals that the wax-oil gel does not deposit into stratified layers. Additionally, neither the oil (black) nor the wax crystals (white) appear as small spheres within a continuous matrix of the other component. Hence, the Maxwell-Eucken Models are ruled out for application in the current work.

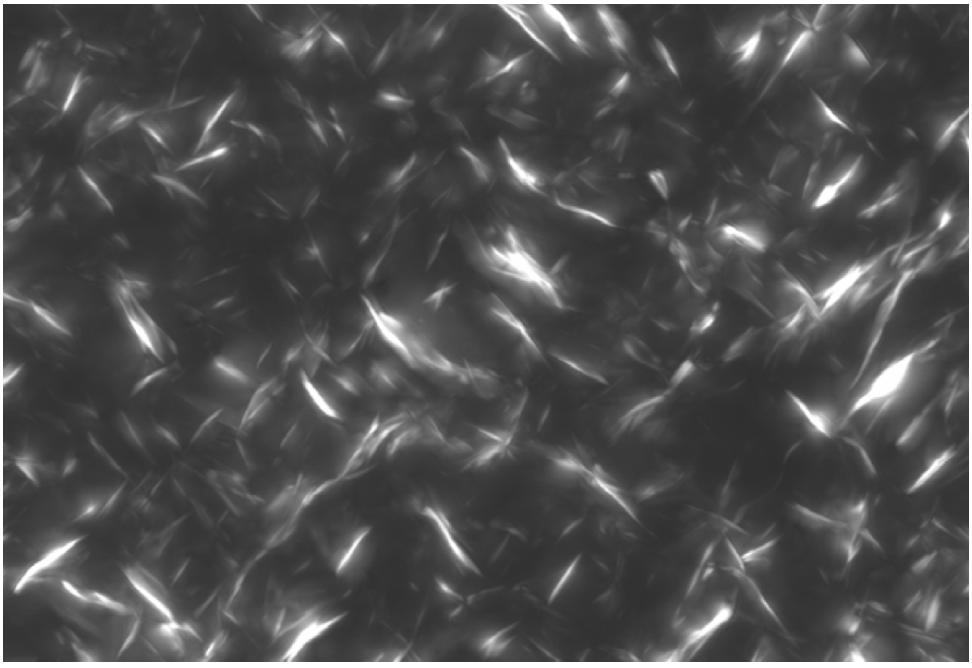

Figure 8.1: Microscope observations of a wax-oil gel (polarized light microscopy image). The oil is dark and the wax crystals are the bright (Venkatesan, 2004).

Instead, the averaging scheme of the Effective Medium Theory seems to be a reasonable model in the case of determining the effective thermal conductivity of the wax deposit with the assumption of a random distribution of the components. As a consequence, the EMT has been applied in the implemented wax deposit models. A schematic representation of the model structures are summarized in Figure G.1 in Appendix G.

8.6 Application of Models

To quantify the deviation, of source of error, that would arise if one of the former models were applied, the methods have been plotted as a function of wax. With the EMT as a base case, the deviation in percentage is found to range between -5.3% (Parallel model) and 11.1% (Series model). The graphs for the five effective thermal conductivity models are given in Figure 8.2 and the numerical values of the maximum deviation in Table 5.

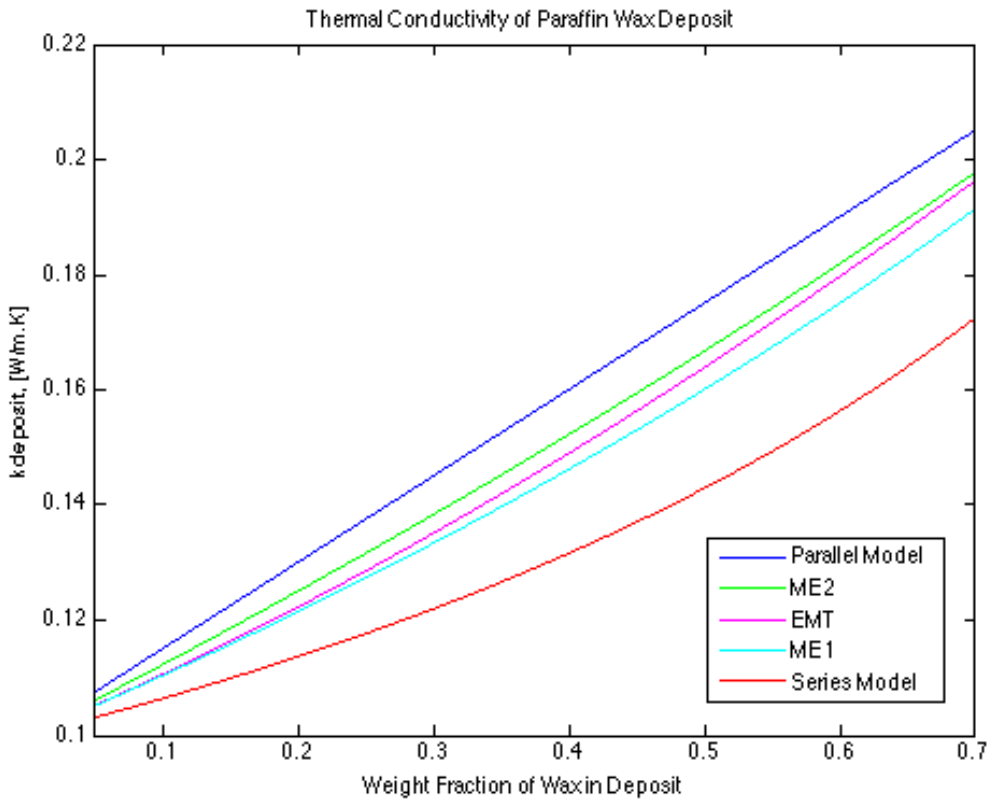

Figure 8.2: The five effective thermal conductivity models of two component systems plotted against weight fraction of wax in deposit. The EMT is found applicable for the wax deposit modeling.

Table 5: Comparison of the stratified models and the Maxwell-Eucken models to the EMT, displaying the maximum deviation in effective thermal conductivity that would occur if one of the former models were applied.

Model	**Maximum Deviation** [%]
Parallel	-5.3
Maxwell-Eucken 2	-1.6
Maxwell-Eucken 1	2.5
Series	11.1

9 Interface Temperatures

To establish the radial concentration gradient in the pipeline, being the mass driving force for deposition, the temperature conditions in the system must be known. In the current chapter, the influence of a layer of deposit on the thermal conditions in the pipeline is examined. The aim is to see how the temperature at the deposit surface changes with a layer of deposit and to evaluate if dynamic modeling of the wax deposit process will be necessary or not.

9.1 Thermal Resistance for Conduction and Convection

Resistance is defined as *the ratio of a driving potential to the corresponding transfer rate.* In case of thermal resistance, it is a measure of a substance's resistance towards heat flow (Incorpera and DeWitt, aarstall).

The thermal resistance for conduction heat transfer and convection heat transfer are given by different expressions. For conduction, the thermal resistance is derived from Fourier's law and, in radial coordinates, given as (Geankoplis, 2003):

$$R_{cond} \equiv \frac{T_s - T_\infty}{q} = \frac{r_2 - r_1}{kA_{lm}} \tag{9.1}$$

where R_{cond} (m^2K/W) is the thermal resistance for conduction, T_s (K) is the temperature of the surface, T_∞ (K) is the temperature of the fluid, q (W) is the heat transfer rate, r_1 (m) is the inner radius of the cylinder, r_2 (m) is the outer radius of the cylinder, k (W/m.K) is the thermal conductivity of the cylinder and A_{lm} is the log mean area of the cylinder.

From Newton's law of cooling, the thermal resistance for convection may be derived (Incropera et al., 2011):

$$R_{conv} \equiv \frac{T_s - T_\infty}{q} = \frac{1}{hA} \tag{9.2}$$

where T_s (K) is the temperature of the surface, T_∞ (K) is the temperature of the fluid, q (W) is the heat transfer rate, h ($W/m^2.K$) is the convective heat-transfer coefficient and A (m) is the area between surface and fluid.

Since the thermal resistances in a cylinder are in series (radial direction), a total heat resistance can be expressed as the sum of the individual heat resistances (Incropera et al., 2011):

$$R_{tot} = R_{in} + \sum_{i=1}^{m} R_{cond,i} + R_{out} + = \sum_{i=1}^{n} R_i \tag{9.3}$$

where R_{tot} (m^2K/W) is the total heat resistance, R_{in} (m^2K/W) is the inner convec-

tive heat resistance, $R_{cond,i}$ (m^2K/W) is the individual conductive heat resistances, R_{out} (m^2K/W) is the outer resistance, and $\sum R_i$ (m^2K/W) is the sum of the individual heat resistances. The index m is the total number of layers, and the index n the number of layers plus the convective heat resistances (n = m+2).

9.2 Situation in the Oil Pipeline

In an oil flowing pipeline, the conductive thermal resistance of the pipe is found as:

$$R_{pipe} = \frac{1}{(k_{pipe}\, A_{lm,\,pipe})/(r_{wi} - r_{wo})} \tag{9.4}$$

where R_{pipe} (m^2K/W) is the heat resistances of the pipe, k_{pipe} (W/m.K) is the thermal conductivity of the pipe, $A_{lm,pipe}$ (m^2) is the logarithmic mean area of the pipe, r_{wi} (m) is the inner wall radius and r_{wo} (m) is the outer wall radius. The conductive thermal resistance of a possible layer of wax deposit is given as:

$$R_{dep} = \frac{1}{(k_{dep}\, A_{lm,\,dep})/(r_{dep} - r_{wi})} \tag{9.5}$$

where R_{dep} (m^2K/W) is the individual heat resistance of the deposit, k_{dep} (W/m.K) is the thermal conductivity of the deposit, $A_{lm,dep}$ (m^2) is the logarithmic mean area, r_{dep} (m) is the effective flow radius measured from the central line of the interface pipe to the deposit interface and r_{wi} (m) is the inner wall radius. The logarithmic mean areas, A_{lm} (m^2) are calculated by Equation (4.11) and Equation (4.10), respectively.

The inner convective heat resistance is calculated as:

$$R_{in} = \frac{1}{h_i A_{in}} \tag{9.6}$$

where R_{in} (m^2K/W) is the inner heat resistance, h_i (W/m^2K) is the inner heat transfer coefficient, A_{in} (m^2) is the interface area between oil and clean pipe wall if no deposit is present or between oil and wax deposit if deposition has occurred.

The outer convective heat resistance is found as:

$$R_{out} = \frac{1}{h_o A_{wo}} \tag{9.7}$$

where R_{out} (m^2K/W) is the outer heat resistance, h_o (W/m^2K) is the outer heat transfer coefficients and A_{wo} (m^2) is the outer pipe wall area or the interface area between pipe and the surrounding sea water.

Expressing the heat flow in the system in terms of resistances, Equation (4.29) is written as (Geankoplis, 2003):

$$q = \frac{T_b - T_{sea}}{1/(h_i A_{dep}) + (r_{wi} - r_{dep})/(k_{dep} A_{lm,dep}) + (r_{wo} - r_{wi})/(k_{pipe} A_{lm,pipe}) + 1/h_o A_{wo}}$$

$$q = \frac{T_b - T_{sea}}{R_i + R_{dep} + R_{pipe} + R_o} = \frac{T_b - T_{sea}}{\sum R} \tag{9.8}$$

The contribution from the individual heat resistance to the total heat resistance is, in percentage, found as:

$$\text{contribution to heat resistance} = \frac{R'}{R_{tot}} \cdot 100\% \tag{9.9}$$

where R′ (m^2K/W) is the individual thermal resistance of interest and R_{tot} (m^2K/W) is the total thermal resistance.

9.3 Temperature Calculations

From Equation (4.28), expressing the radial heat flow in the system, the equations to calculate the temperature at the wax deposit surface, the inner pipe wall and the outer pipe wall can be derived. The temperature at the oil/deposit interface is found as

$$T_{dep} = T_{sub} + qR_i \tag{9.10}$$

where T_{dep} (K) is the temperature at the oil/deposit interface, T_sub (K) is the temperature in the near-wall region, q (W) is the radial heat flow and R_i (m^2K/W) is the inner heat resistance. If there is no wax deposit at the point of interest (clean pipe wall), the temperature at the inner pipe wall is given as:

$$T_{wi} = T_{sub} + qR_i \tag{9.11}$$

where T_{dep} (K) is the temperature at the oil/deposit interface, T_sub (K) is the temperature in the near-wall region, q (W) is the radial heat flow and R_i (m^2K/W) is the inner heat resistance. If a layer of deposit exists, the inner wall temperature is calculated as

$$T_{wi} = T_{dep} + qR_{dep} \tag{9.12}$$

T_{wi} (K) is the inner wall temperature, q (W) is the radial heat flow and R_{dep} (m^2K/W) is the individual heat resistance from the layer of deposit.

The outer wall temperature is in either case calculated as:

$$T_{wo} = T_{wi} + qR_{pipe} \tag{9.13}$$

T_{wo} (K) is the outer pipe wall temperature and R_{pipe} (m^2K/W) is the resistance of the pipe.

9.4 Influence of the Wax Deposit

To examine the influence of the wax deposit on the thermal conditions in the pipeline, the thickness of the deposit and the wax content have been evaluated separately. First, the deposit thickness has been varied with the assumption of a constant wax content in the deposit, then the deposit thickness has been kept constant and the wax content has been varied.

9.4.1 Influence of Deposit Thickness

When investigating the influence of the deposit thickness on the thermal situation in the pipeline, a deposit thickness ranging from 0-20 mm has been applied. This covers the situation from a clean pipe wall to, what is characterized as, a severe wax deposit buildup (Rønningsen, 2012).

Based on experiences from the Norwegian Continental Shelf, a wax fraction of 40 % in deposit has been applied (Rønningsen, 2012)[3]. The temperature in the near-wall region at the point of interest is set equal to 25 °C and the ambient sea temperature is assumed to hold 5°C (Rønningsen, 1992).

9.4.1.1 Results The wax deposit is found to add a layer of insulation to the system. With an increasing deposit thickness, the dominating heat resistance of the system changes from being the outer convective heat resistance (-72.92%) to the conductive heat resistance of the deposit (+75.54%). There is only a slight reduction in the contribution of the inner heat resistance and the contribution of the pipe as the deposit layer increases (-1.67% and -0.94%, respectively). The results are presented in Table 6.

As a consequence of the increasing thermal insulation, the temperature at the oil/deposit interface is found to increase as the layer of deposit grows. The temperatures at the inner and outer wall are simultaneously decreasing. The numerical values for the temperature changes of the simulated situation are given in Table

[3]The assumption of Rønningsen (2012) is based on experiences from the Norwegian Continental Shelf where knowledge about wax content has been acquired from samples of wax from back flow of a stuck foam pig in the pipeline between the Heimdal and Brae A platforms in the North Sea.

Table 6: Influence of the deposit thickness on the thermal resistance distribution in the pipeline. A constant wax fraction of 40% has been assumed.

	Heat Resistance Distribution [%]			
δ [mm]	$\frac{\mathbf{R_i}}{\mathbf{R}}$	$\frac{\mathbf{R_{dep}}}{\mathbf{R}}$	$\frac{\mathbf{R_{pipe}}}{\mathbf{R}}$	$\frac{\mathbf{R_o}}{\mathbf{R}}$
0	2.33	0	1.24	96.42
1	2.05	12.66	1.09	84.20
5	1.39	42.34	0.72	55.55
10	1.00	59.88	0.50	38.62
20	0.66	75.54	0.30	23.50
Difference [%]	- 1.67	75.54	- 0.94	- 72.92

Table 7: Influence of the deposit thickness on the temperature at the deposit surface, the inner pipe wall and an outer pipe wall. The temperature in the near-wall region is assumed to hold 25°C at the point of interest.

	Interface Temperatures [°C]		
δ [mm]	T_{dep}	T_{wi}	T_{wo}
0	-	24.53	24.28
1	24.59	22.01	21.80
5	24.73	16.17	16.03
10	24.82	12.74	12.64
20	24.89	9.70	9.64
Difference [%]	2.50	- 60.30	-60.46

7, shown an increase of 2.5% at the deposit surface and a decrease of -60.30% and -60.46% at the inner and outer pipe walls, respectively.

9.4.2 Influence of Wax Fraction

Examining the influence of the weight fraction of wax in deposit, the thickness of the layer has been kept constant at 20 mm. The investigated wax content ranges from 5-70%, being data reported from the field (Venkatesan, 2004; Lee, 2008). The temperature in the near-wall region at the point investigated is 25°C and the ambient temperature 5°C.

9.4.2.1 Results A layer of deposit with a higher wax content is found to create less resistance towards thermal flow than a layer of a corresponding thickness and a lower wax content. The contribution from the inner heat resistance and the resistance of the pipe are found to increase with 0.30% and 0.14%, respectively, whilst the contribution of the deposit layer is reduced with -11.29% and the outer resistance increased with 10.85% under the applied conditions when the wax content increases from 5 to 70 %. The numerical results for varying wax contents are given in Table 8, showing what is commented upon.

Table 8: Influence of the weight fraction of wax in deposit on the thermal resistance distribution in the pipeline. A deposit thickness of 20 mm has been applied.

	Heat Resistance Distribution [%]			
Wax [%]	$\frac{R_i}{R}$	$\frac{R_{dep}}{R}$	$\frac{R_{pipe}}{R}$	$\frac{R_o}{R}$
5	0.50	81.39	0.23	17.88
20	0.56	79.00	0.26	20.17
40	0.60	75.54	0.30	23.50
50	0.70	73.74	0.33	25.23
70	0.80	70.10	0.37	28.73
Difference [%]	0.30	-11.29	0.14	10.85

The temperature at the oil/deposit interface is lower with a high content of wax in the deposit, a finding caused by the thermal conductivity of wax being higher than the thermal conductivity of oil. A deposit with a higher wax fraction will cause less resistance towards heat flow than a layer of a corresponding thickness and a lower wax content. At the inner and outer pipe wall, the temperatures will be higher with a higher content of wax. The numerical values for the applied conditions are given in Table 9.

Table 9: Influence of the weight fraction of wax in deposit on the temperature at the deposit surface, the inner pipe wall and an outer pipe wall. The temperature in the near-wall region is assumed to hold 25°C at the point of interest.

	Interface Temperatures [°C]		
Wax [%]	T_{dep}	T_{wi}	T_{wo}
5	24.91	8.62	8.58
20	24.90	9.07	9.02
40	24.89	9.70	9.64
50	24.88	10.18	10.12
70	24.86	10.86	10.78
Difference [%]	-0.20	25.99	25.64

9.4.3 Discussion

With the assumption of a constant weight fraction of wax in the deposit, the insulating effect of the layer has shown to increase with an increasing thickness. Varying the wax content while keeping the deposit thickness constant, a higher wax fraction is found to cause less resistance towards heat flow than a layer of corresponding thickness with a lesser content of wax.

Assuming temperatures below the WAT and the existence of a radial temperature gradient in the pipeline, the deposit thickness and wax content are expected to increase with time, acting as opposing mechanisms when it comes to thermal resistance. Comparing the phenomena for the values of interest, the influence of the deposit thickness is found to be greater than the influence of the wax content. The percentage changes caused by an increased deposit thickness is given in the lower row of Table 10 and the percentage changes caused by the increased wax content in the last column, proving the deposit thickness to be the dominating factor.

The influence of the wax content in the deposit will not be further investigated in the current thesis. It is noted that the wax content will affect the thermal conditions in the pipeline, with a higher wax content causing the temperature at the deposit surface to be slightly lower than is the case with a lower wax content. Hence, an increased wax content in the deposit will cause a steeper thermal gradient, causing less reduction in the thermal driving force for deposition than were the case without aging. The consequences of an increasing wax content in the deposit is recommended investigated as part of a future work.

Independent of the amount of wax in deposit, the temperature at the oil/deposit interface will increase with a growing deposit thickness. The temperature at the deposit surface will be brought closer to the average bulk flow temperature with

Table 10: Deposit surface temperature with a varying deposit thickness and weight fraction of wax in the deposit. In the lower row, the percentage change caused by the increased deposit thickness is given, and in the column to the right the percentage change caused by the increasing wax content.

	Wax [%]					
δ [**mm**]	5	20	40	50	70	**Difference** [%]
1	24.61	24.60	24.59	24.58	24.57	-0.16
5	24.77	24.75	24.73	24.72	24.70	-0.28
10	24.85	24.84	24.82	24.80	24.78	- 0.28
20	24.91	24.90	24.89	24.88	24.86	-0.20
Difference [%]	1.55	1.51	1.48	1.43	1.35	

time, resulting in a lesser temperature gradient across the viscous sub-layer. A lower temperature gradient means a reduced thermal driving force for deposition. The result is a non-linear growth of the deposit thickness, where the mass rate of wax transfer is expected to be fast initially and to slow down as the thickness of the layer increases. To avoid over estimation of the final deposit thickness, the simulations will have to be dynamic.

10 Analytical Modeling

In the analytical model, Fick's law is applied to estimate the mass flux of wax with the assumption of thermodynamic equilibrium in the viscous sub-layer. In the current chapter, the mathematical model implemented in MATLAB is derived and the results from simulations performed on the Norne crude oil under real field is presented.

10.1 Application and Assumptions

The analytical wax deposition model is applicable for oil transporting pipelines. The governing equations, and hence the model, is valid in situations where the flow is non-reacting and there is no thermal energy generation in the fluid. The fluid mixture is assumed to be incompressible and the density consequently treated as constant. The density of wax is assumed equal to the density of oil, and the fluid mixture is treated as a Newtonian fluid, that is, the viscosity is considered independent of shear rate.

The maximum amount of wax dissolved in solution is determined by the wax appearance temperature and the solubility function. Above the wax appearance limit, the flow is single-phase (liquid only) and below it is a two phase mixture of liquid oil and solid wax. Zero water content and zero gas rate in the system is assumed.

The seawater surrounding the pipeline is assumed to hold a constant temperature of 5 °C (Rønningsen et al., 1992). The fluid flow is treated as one dimensional, with net flow of oil in the axial direction only, and the fluid velocity is assumed constant. Molecular diffusion from the near-wall region to the solid/liquid interface is considered as the sole mechanism for wax deposition, and the precipitated wax molecules in the viscous sub-layer are expected to deposit at the solid/liquid interface where the precipitation occurs. No shear-removal is included and there is no thermal insulation of the system.

The Effective Medium Theory model has been applied for the calculation of the effective thermal conductivity of the wax deposit, and the Dittus-Boelter correlation is found applicable to calculate the inner convective heat transfer coefficient. Thermodynamic equilibrium at every point in the pipeline has been assumed and the weight fraction of wax in deposit is assumed.

10.2 Flow Regions

Turbulent flow in a cylinder can be divided into three flow regions. Adjacent to the wall, there is a viscous sub-layer in which transfer processes are dominated by

diffusion. Next, there is a buffer layer, or transition zone, in which transfer by diffusion and turbulent mixing are comparable. In the center of the pipe, the flow is turbulent and the transport phenomena are dominated by turbulent mixing (White, 2008).

In operative oil flowing pipelines, turbulent diffusivities of temperature and chemical species are assumed to cause an uniform distribution of temperature and concentration over the cross-sectional area of the pipe (Aijeijna et al., 2011). Since the transport of wax is controlled by the prevailing gradients in the viscous sublayer, the thickness of the layer must be known to establish the temperature and concentration profiles in the near-wall region (Azevedo and Teixeira, 2003).

To determine the extension of the flow regions, von Kármán defined a dimensionless wall distance (Kay and Nedderman, 1985):

$$y^+ = \frac{y}{y_\tau} \tag{10.1}$$

where y^+ is the dimensionless wall distance, y (m) is the actual distance from the pipe wall and y_τ (m) is the friction distance found as:

$$y_\tau = \frac{\mu}{\tau_w \rho} \tag{10.2}$$

where μ (Pa.s) is the dynamic viscosity, ρ (kg/m^3) is the fluid density and τ_w (Pa) is the wall shear stress. The wall shear stress is given by (Incropera et al., 2011):

$$\tau_w = \mu \frac{du}{dy} = \frac{1}{2} f \rho u^2 \tag{10.3}$$

where $\frac{du}{dy}$ is the local velocity gradient, f is the friction factor, ρ (kg/m^3) is the fluid density and u (m/s) is the average flow velocity. The flow regions are divided into (Kay and Nedderman, 1985):

$y^+ \leq 5$	Viscous sub-layer
$5 < y^+ < 30$	Buffer layer
$y^+ \geq 30$	Turbulent core

10.3 Temperature Calculations

To establish the concentration gradient at the solid/liquid interface, the temperature in the viscous sub-layer and at the solid/liquid interface must be known. To determine those quantities, the average bulk flow temperature throughout the pipeline is required.

10.3.1 Average Bulk Flow Temperature

The average bulk flow temperature, or the lateral temperature profile, is calculated as (Gudmundsson, 2009):

$$T_b = T_{sea} + (T_i - T_{sea})exp\left(-\frac{U\pi d}{\dot{m}C_p}L\right) \tag{10.4}$$

where T_b (K) is the temperature of the bulk flow at the distance of interest, T_{sea} (K) is the ambient temperature, T_i (K) is the inlet temperature, U (W/m^2.K) is the overall heat transfer coefficient, d (m) is the inner pipe diameter, $\dot{m}$ (kg/s) is the mass flow rate, C_p (J/kg.K) is the heat capacity of oil and L (m) is the distance of interest.

10.3.2 Boundary Layer Temperature

For a subsea pipeline cooled from the outside, the following equations can be used to obtain the temperature profile (Kay and Nedderman, 1985):

$$T^+ = \begin{cases} {T_w}^+ + (Pr)y^+ & y^+ \leq 5 \\ {T_w}^+ - 5Pr + 5ln[0.2(Pr)y^+ + (1-Pr)] & 5 < y^+ < 30 \\ {T_w}^+ - 5Pr + 5ln[0.2(Pr)y^+ + (1-Pr)] - 2.5ln\frac{y^+}{30} & y^+ \geq 30 \end{cases} \tag{10.5}$$

where T_w^+ is the dimensionless wall temperature, Pr is the Prandtl number andy^+ is the dimensionless wall distance, given by:

$$y^+ = \frac{\rho u^* y}{\mu} \tag{10.6}$$

where ρ (kg/m^3) is the density of the fluid, y (m) is the actual distance from the wall and μ (Pa.s) is the dynamic viscosity and u^* is the dimensionless friction velocityis, given as:

$$u^* = \sqrt{\frac{\tau_w}{\rho}} = \bar{u}\sqrt{\frac{f}{8}} \tag{10.7}$$

where τ_w (Pa) is the wall shear stress, $\bar{u}$ (m/s) is the average flow velocity and f is the friction factor. The dimensionless wall temperature is then found as:

$${T_w}^+ = T\left(\frac{\rho C_p u^*}{Q/A}\right) \tag{10.8}$$

where T (°C) is the temperature of interest, ρ (kg/m^3) is the fluid density, C_p (J/K) is the heat capacity of the fluid, u^* is the friction velocity and the heat flow Q (W)

divided by the heat transfer area A (m^2) equals the heat flux, q (W/m^2). Finally, the temperature in the viscous sublayer is then determined:

$$T_{sub} = T^+ \frac{q}{\rho C_p u^*} \tag{10.9}$$

where T^+ is the dimensionless wall temperature, q (W/m^2) is the radial heat flux, ρ (kg/m^3) is the fluid density, C_p (J/K) is the heat capacity of the fluid and u^* is the friction velocity.

10.3.3 Interface Temperatures

The temperatures at the inner pipe wall, the outer pipe wall and at the deposit surface are calculated by Equation (9.10)-(9.13). When there is no deposit in the pipeline, the inner wall represents the interface are at which deposition occurs and the temperature of interest. When first deposition has occurred, the deposit surface is the area at which wax deposits and the temperature at the oil/deposit interface is the one sought for.

10.4 Wax Deposit Calculations

Based on the assumptions presented Fick's law is applied to determine the mass transfer rate in a binary mixture of wax and oil (Burger et al., 1981; Azevedo and Teixeira, 2003; Sarica and Volk, 2004; Lee, 2008; Benall et al., 2008; Aiyejina, 2011; Mirazizi et al., 2012) :

$$\frac{dm}{dt} = -\rho_w D_{wo} A_i \frac{dC}{dr}\Big|_i \tag{10.10}$$

where $\frac{dm}{dt}$ (kg/s) is the mass rate of wax transfer in oil, ρ_w (kg/m^3) is the density of solid wax, D_{wo} (m^2/s) is the diffusion coefficient of wax in oil, A_i (m^2) is the surface area at which the deposition occurs, C (volume fraction) is the concentration of wax in oil, and r (m) is the radial coordinate at the point of interest measured from the centerline of the pipe. The radial concentration gradient, $\frac{dC}{dr}$ is evaluated at the solid/liquid interface.

Since the density of wax is assumed equal to the density of oil, the weight percent of wax in solution corresponds to the volume percent of wax in solution. As a result, the solubility functions in Appendix E can be used directly in the calculations.

The interface area available for deposition, A_i, can be calculated as:

$$A_i = 2\pi r L \tag{10.11}$$

where r (m) is the radial coordinate of interest and L (m) is the length of the pipe. If there is no wax deposit at the place of interest, the solid/liquid interface radius equals the inner pipe radius, r(t) = r_i. If deposition has occurred, the solid/liquid interface equals the inner pipe radius minus the deposit thickness, r(t) = r_i - δ(t).

The deposit thickness, δ (m), is found by integration of Equation (10.10):

$$\delta(t) = -D_{wo} \frac{dC}{dr}\Big|_i t \tag{10.12}$$

where δ(t) (m) is the deposit thickness at the time of interest, D_{wo} (m^2/s) is the binary diffusion coefficient of wax in oil and $\frac{dC}{dr}$ (unit) is the radial concentration gradient at the solid/liquid interface.

As the driving force for deposition is found to change with time, the deposit thickness will be calculated as:

$$\delta(t + \Delta t) = \delta(t) + \left(-D_{wo} \frac{dC}{dr}\Big|_i \Delta t \right) \tag{10.13}$$

where δ(t) (m) is the deposit thickness in the previous time step and Δt (s) is the time step.

10.5 Simulations

The conducted simulations are performed on the Norne crude oil with subsea pipelines under realistic field condition. For determination of the viscous sub-layer thickness, the outer limit ($y^+ = 5$) has been applied. The outer limit is chosen to obtain the maximum value of wax transfer across the sub-layer; as the temperature difference over a thicker sub-layer is greater than over a thinner sub-layer, the driving force for deposition will be at its maximum when the maximum sub-layer thickness is applied. The resulting wax transfer represents an upper limit for wax deposition and, hence, a worst case scenario to be applied in planning and design. In the analytical model, a pipelenght of 10000 meter is chosen simulated, however no limitations regarding pipe sizing exists. The remaining input values are found attached in Appendix F.

10.5.1 Results

The thickness of the wax deposit is found to increase with time. With the applied conditions, the temperature in the viscous sub-layer reaches the WAT after 1284 meter. The maximum deposit thickness is observed at the point where the WAT is reached, and from this point on the thickness of the deposit gradually decreases throughout the pipeline.

The wax deposit profiles after one, two and seven days are plotted in Figure 10.1, graphically displaying the findings commented upon above. In Table 11, the

maximum deposit thicknesses (encountered at 1284 meter) and the thickness at the outlet of the simulated pipeline are given.

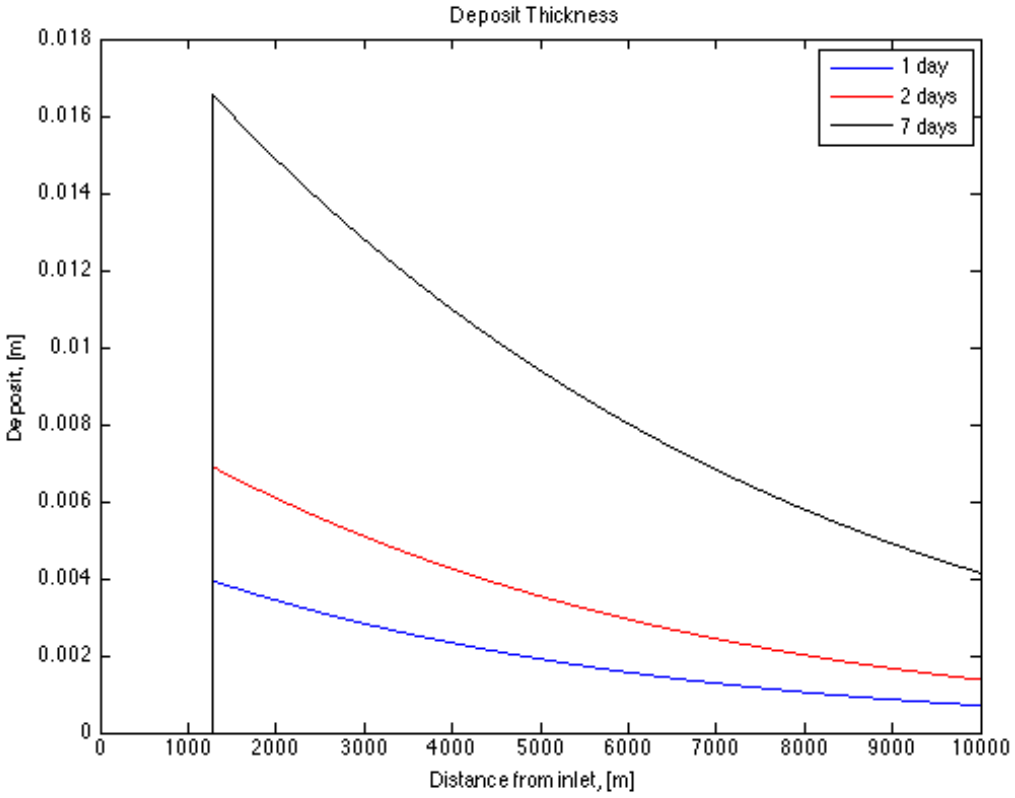

Figure 10.1: Deposit thickness profiles after one day, two days and seven days obtained by the analytical model. The maximum deposit thickness is obtained at 1284 meter, where the WAT is reached in the near-wall region.

The maximum deposit thickness is found to increase from 3.9 mm to 16.6 mm from the first to the seventh day, hence, the growth rate of the deposit is found to decrease with time. The findings are in correspondence with the results in Chapter 9, indicating a correct implementation of the model.

Table 11: Deposit thickness values obtained by the analytical model. The thickness at 1284 meter is the maximum deposit thickness and the values at 10000 meter is at the end of the simulated pipeline.

	Deposit Thickness [mm]	
Time	1284 m	10000 m
1 day	3.9	0.7
2 days	6.9	1.3
7 days	16.6	4.1

The results of the analytical simulations will be compared to the numerical simulations and results obtained by commercial software in Chapter 12.

11 Numerical Modeling

In the numerical model, the Finite Difference Method (FDM) is applied on a coupled set of heat and mass equations. By including a precipitation rate constant, the precipitation of wax molecules is accounted for and the correlation that exists between heat and mass transfer in the turbulent flow regime is accounted for.

11.1 Application and Assumptions

The numerical model is applicable for oil transporting pipelines where the flow is non-reacting and there is no thermal energy generation in the fluid. The fluid is assumed to be incompressible, it is treated as a Newtonian fluid and the density of wax is assumed equal to the density of oil.

The maximum amount of wax dissolved in solution is determined by the WAT and the solubility function. Above the WAT the flow is single-phase and below it is a two phase mixture of liquid oil and solid wax. Zero water content and zero gas rate in the pipeline is assumed, and the surrounding seawater is assumed to hold a constant temperature of 5 °C.

The fluid flow is treated as one dimensional and the fluid velocity assumed constant. No shear removal is accounted for and there is no thermal isolation of the pipeline. To calculate the effective thermal conductivity of the deposit, the EMT has been applied. To calculate the inner convective heat transfer coefficient, the Dittus-Boelter correlation is used.

The growth rate of the paraffin wax deposit is calculated as the difference in radial flux from the bulk to the oil/deposit interface and the flux from the interface into the deposit. The solid wax content in the deposit is assumed to increase with time. The precipitation kinetics of wax is accounted for by a precipitation rate constant, correlating the heat and has transfer phenomena.

11.2 Mathematical Approach

A numerical solution enables the determination of a variable at discrete points only. To perform such a calculation, the medium will have to be subdivided into a number of smaller regions. In the center of each region, a reference point called a nodal point, or node, is assigned. At each nodal point the value of the variable is a measure of the average value of the region or surrounding area, and together the nodes form a nodal network.

11.2.1 Continuity Equations

A continuity equation is a mathematical description of transport of conserved quantities and can be regarded as a local form of conservation laws. The continuity equations for heat and mass transfer, or the heat and mass balance equations, will be used to obtain the temperature and concentration gradients in the fluid.

Given in radial coordinates, the governing equation for heat transfer is written as (Lee, 2008):

$$u_z \frac{\partial T}{\partial z} = \frac{1}{r}\frac{\partial}{\partial r}\left[r(\varepsilon_h + \alpha_T)\frac{\partial T}{\partial r}\right] - \beta(T - T_{wo}) \tag{11.1}$$

where u_z (m/s) is the fluid velocity in lateral direction, T (K) is the temperature, z (m) is the axial distance, r (m) is the radial position, ε_h (m^2/s) is the turbulent heat diffusivity, α_T (m^2/s) is the thermal diffusivity, and β (s^{-1}) a crystallization constant for heat of fusion. For mass transfer, the corresponding equation is (Lee, 2008):

$$u_z \frac{\partial C}{\partial z} = \frac{1}{r}\frac{\partial}{\partial r}\left[r(\varepsilon_m + D_{wo})\frac{\partial C}{\partial r}\right] - k_r(C - C_{wo}) \tag{11.2}$$

where u_z (m/s) is the fluid velocity in lateral direction, C (kg/m^3) is the concentration of wax dissolved in oil, z (m) is the axial distance, r (m) is the radial position, ε_m (m^2/s) is the turbulent mass diffusivity, D_{wo} (m^2/s) is the binary diffusion coefficient of wax in oil, and k_r (s^{-1}) is the precipitation rate constant.

The terms β(C-C_{wo}) and k_r(C-C_{wo}) are generation terms resulting from possible crystallization of wax in the bulk. In the heat balance equation, the contribution from the precipitation term, β(C-C_{wo}), is reported to be less than 0.1 percent (Lee, 2008). The contribution of heat from bulk precipitation is therefore considered insignificant and the precipitation term in Equation (11.1) negligible. Thus, the appropriate form of the heat equation to be worked with in the current thesis is written as:

$$u_z \frac{\partial T}{\partial z} = \frac{1}{r}\frac{\partial}{\partial r}\left[r(\varepsilon_h + \alpha_T)\frac{\partial T}{\partial r}\right] \tag{11.3}$$

The generation term in the mass transfer equation, k_r(C-C_{wo}),, accounts for the kinetics of wax precipitation and should on the other hand not be neglected in the computations. Thus, Equation (11.2) should will be utilized in the concentration profile calculations.

11.2.2 Continuity Equations on a Finite-Difference Form

The first step when solving a continuity equation is to write the equation on a discrete form. The continuous model is then transferred into a discrete set of equations. To solve the heat and mass balance equations, the finite-difference method (FDM) will be used. The FDM is a numerical technique suitable for the interior nodes of a two-dimensional network found. It is found applicable for the current work with the boundary conditions given in Chapter 11.4. As it is less computational expensive than the finite-element method (FEM), the FDM is chosen implemented.

The FDM requires an approximated equation to be written for each nodal point, resulting in a set of equations to be solved simultaneously. The approximated equation is known as *the finite-difference form* of the continuity equation, giving name to the method. The general expressions of the first derivatives are written as (Incropera et al., 2011):

$$\frac{\partial \psi}{\partial z}\Big|_{m+1/2,n} \approx \frac{\psi_{m+1,n} - \psi_{m,n}}{\Delta z} \tag{11.4}$$

$$\frac{\partial \psi}{\partial z}\Big|_{m-1/2,n} \approx \frac{\psi_{m,n} - \psi_{m-1,n}}{\Delta z} \tag{11.5}$$

where ψ is the transport property in question and z is the direction of flow. The subscripts, m and n, represents the nodal position in the network. The expression in Equation (11.4) is known as forwards discretization and the expression in Equation (11.5) as backwards discretization. The second derivate can further be written as (Incropera et al., 2011):

$$\frac{\partial^2 \psi}{\partial z^2}\Big|_{m,n} \approx \frac{\frac{\partial \psi}{\partial z}|_{m+1/2,n} - \frac{\partial \psi}{\partial z}|_{m-1/2,n}}{\Delta z} \tag{11.6}$$

where the variables are as above. Substituting Equation (11.4) and Equation (11.5) into Equation (11.6) a central difference discretization is performed and the expression to be worked with is obtained:

$$\frac{\partial^2 \psi}{\partial z^2}\Big|_{m,n} \approx \frac{\psi_{m+1,n} - 2\psi_{m,n} + \psi_{m-1,n}}{(\Delta z)^2} \tag{11.7}$$

For a further elaboration of the FDM, the reader is referred to a mathematical textbook.

11.2.3 Finite-Difference Solution

To solve the network of finite-difference equations, a matrix system of N equations corresponding to N unknown variables will have to be constructed with one equation

to be solved at each node. The nodal points are identified with integer subscripts as above. The procedure begins by writing the set of equations as (Incropera and Dewitt, 2008):

$$\begin{array}{ccccccccccc} a_{11}\psi_1 & + & a_{12}\psi_2 & + & a_{13}\psi_3 & + & \cdots & + & a_{1N}\psi_N & = & C_1 \\ a_{21}\psi_1 & + & a_{22}\psi_2 & + & a_{23}\psi_3 & + & \cdots & + & a_{2N}\psi_N & = & C_2 \\ \vdots & + & \vdots & + & \vdots & + & \vdots & + & \vdots & = & \vdots \\ a_{N1}\psi_1 & + & a_{N2}\psi_2 & + & a_{N3}\psi_3 & + & \cdots & + & a_{NN}\psi_N & = & C_N \end{array}$$

where a_{11}, a_{12}, ..., a_{NN} and C_1, C_2, , C_N are known coefficients and constants and ψ is the variable to be found. Using matrix notation, the set of equations can be written as a square coefficient matrix [A] and two column vectors [ψ] and [C]. In such a notation, the system is expressed as:

$$[A][\psi] = [C] \tag{11.8}$$

where

$$A = \begin{pmatrix} A_1 1 & A_1 2 & \cdots & A_1 N \\ A_2 1 & A_2 2 & \cdots & A_2 N \\ \vdots & \vdots & \vdots & \vdots \\ A_N 1 & A_N 2 & \cdots & A_N N \end{pmatrix}, \quad \psi = \begin{pmatrix} \psi_1 \\ \psi_2 \\ \vdots \\ \psi_N \end{pmatrix}, \quad \text{and} \quad C = \begin{pmatrix} C_1 \\ C_2 \\ \vdots \\ C_N \end{pmatrix}. \tag{11.9}$$

Performing the matrix multiplication implied on the left-hand side of Equation (11.8), the set of equations listed above is obtained. By inverting the matrices, the solution vector ψ is found.

11.3 Numerical Calculations

In the current sub-chapter, the continuity equations of heat and mass will be applied on the situation in the pipeline, discretized and written in a matrix form. The final matrices are the ones to be implemented in the computer code in order to obtain the temperature and concentration profiles.

11.3.1 Heat Transfer Calculations

Initially, the derivatives of the heat balance equation are written out and a collective expression for the thermal diffusivity and turbulent heat diffusivity, $\alpha_{tot} = \alpha_T + \varepsilon_h$, is introduced to simplify the notation. Equation 11.3 can then be expressed as:

$$u_z \frac{\partial T}{\partial z} = \alpha_{tot} \frac{\partial^2 T}{\partial r^2} + \frac{\alpha_{tot}}{r} \frac{\partial T}{\partial r} \tag{11.10}$$

where u_z (m/s) is the fluid velocity in lateral direction, T (K) is the temperature, z (m) is the axial distance, r (m) is the radial position and α_{tot} is the collective expression for the thermal and turbulent heat diffusivity.

Using backward discretization on the convection term on the left hand side of Equation 11.10, central discretization on the second order radial diffusion term and forward discretization on the first order radial diffusion term of yields (Siljuberg, 2012):

$$u_z \frac{T_{i,j} - T_{i-1,j}}{\Delta z} = \alpha_{tot} \left(\frac{T_{i,j+1} - 2T_{i,j} + T_{i,j-1}}{\Delta r_j^2} \right) + \frac{\alpha_{tot}}{r_{j-1}} \left(\frac{T_{i,j+1} - T_{i,j}}{\Delta r_{j+1}} \right) \tag{11.11}$$

Rearranging the equation, the system can be written as (Lee, 2008):

$$A_j^T T_{i,j} + B_j^T T_{i,j+1} + C_j^T T_{i,j-1} = D_j^T \tag{11.12}$$

where:

$$A_j^T = \frac{v_{z,j}}{\Delta z_j} + \frac{1}{r_j} \frac{2}{\Delta r_{j+1} + \Delta r_j} \left\{ \left[\frac{r_{j+1}\alpha_{tot,j+1} + r_j \alpha_{tot,j}}{2} \right] \left(\frac{1}{\Delta r_{j+1}} \right) + \left[\frac{r_j \alpha_{tot,j} + r_{j-1}\alpha_{tot,j-1}}{2} \right] \left(\frac{1}{\Delta r_j} \right) \right\} \tag{11.13}$$

$$B_j^T = -\frac{1}{r_j} \frac{2}{\Delta r_{j+1} + \Delta r_j} \left\{ \left[\frac{r_{j+1}\alpha_{tot,j+1} + r_j \alpha_{tot,j}}{2} \right] \left(\frac{1}{\Delta r_{j+1}} \right) \right\} \tag{11.14}$$

$$C_j^T = -\frac{1}{r_j} \frac{2}{\Delta r_{j+1} + \Delta r_j} \left\{ \left[\frac{r_j \alpha_{tot,j} + r_{j-1}\alpha_{tot,j-1}}{2} \right] \left(\frac{1}{\Delta r_j} \right) \right\} \tag{11.15}$$

$$D_j^T = \frac{v_z T_{i-1,j}}{\Delta z} \tag{11.16}$$

For a uniform grid, that is, a grid where the differentials are of equal size throughout the entire nodal network ($\Delta r_i = \Delta r_{i+1}$), the coefficients are reduced to:

$$A_j^T = \frac{v_{z,j}}{\Delta z_j} + \frac{1}{2 r_j \Delta r^2} (2 r_j \alpha_{tot,j} + r_{j+1}\alpha_{tot,j+1} + r_{j-1}\alpha_{tot,j-1}) \tag{11.17}$$

$$B_j^T = -\frac{1}{2 r_j \Delta r^2} (r_{j+1}\alpha_{tot,j+1} + r_j \alpha_{tot,j}) \tag{11.18}$$

$$C_j^T = -\frac{1}{2r_j\Delta r^2}(r_j\alpha_{tot,j} + r_{j-1}\alpha_{tot,j-1}) \tag{11.19}$$

with D_j^T remaining the same.

With the nodal network established, the problem is reduced to solving a system of linear, algebraic equations. The final matrices are expressed as (Lee, 2008):

$$\begin{pmatrix} 1 & -1 & 0 & 0 & 0 & \cdots & 0 & 0 & 0 \\ C_2 & A_2 & B_2 & 0 & 0 & \cdots & 0 & 0 & 0 \\ 0 & C_3 & A_3 & B_3 & 0 & \cdots & 0 & 0 & 0 \\ 0 & 0 & C_4 & A_4 & B_4 & \cdots & 0 & 0 & 0 \\ \vdots & \vdots & \vdots & \vdots & \vdots & \ddots & \vdots & \vdots & \vdots \\ 0 & 0 & 0 & 0 & 0 & \cdots & C_{N-1} & A_{N-1} & B_{N-1} \\ 0 & 0 & 0 & 0 & 0 & \cdots & 0 & 0 & 1 \end{pmatrix} \begin{pmatrix} T_{i,1} \\ T_{i,2} \\ T_{i,3} \\ T_{i,4} \\ \vdots \\ T_{i,N-1} \\ T_{i,N} \end{pmatrix} = \begin{pmatrix} D_1 \\ D_2 \\ D_3 \\ D_4 \\ \vdots \\ D_{i,N-1} \\ T_{wall} \end{pmatrix}$$

By inverting the system, the radial temperature distribution in the pipeline is obtained. Marching numerically from the inlet to the outlet of the pipe, the complete temperature profile with respect to radial and lateral position is produced as desired.

11.3.2 Mass Transfer Calculations

Numerical solution of the mass transfer equation follows the same procedure as the heat transfer calculations. The differentials of the mass balance equation is written out, and $D_{wo,tot} = D_{wo} + \varepsilon_m$ is introduced as a common expression for the binary diffusion coefficient and turbulent mass diffusivity. Equation 11.2 can then be expressed as (Siljuberg, 2012):

$$u_z\frac{\partial C}{\partial z} = D_{wo,tot}\frac{\partial^2 C}{\partial r^2} + \frac{D_{wo,tot}}{r}\frac{\partial C}{\partial r} + k_r(C - C_{wo}) \tag{11.20}$$

Discretizing the equation:

$$v_z\frac{C_{i,j} - C_{i-1,j}}{\Delta z} = D_{wo,tot}\left(\frac{C_{i,j+1} - 2C_{i,j} + C_{i,j-1}}{\Delta r_j}\right) + \frac{D_{wo,tot}}{r_{j-1}}\left(\frac{C_{i,j+1} - C_{i,j}}{\Delta r_{j+1}}\right) + k_r(C - C_{wo}) \tag{11.21}$$

and rearranging the concentration variable yields:

$$A_jC_{i,j} + B_jC_{i,j+1} + C_jC_{i,j-1} = D_j \tag{11.22}$$

where

$$A_j^C = \frac{v_{z,j}}{\Delta z_j} + \frac{1}{r_j}\frac{2}{\Delta r_{j+1} + \Delta r_j}$$

$$\left\{\left[\frac{r_{j+1}D_{wo,tot,j+1} + r_j D_{wo,tot,j}}{2}\right]\left(\frac{1}{\Delta r_{j+1}}\right) + \left[\frac{r_j D_{wo,tot,j} + r_{j-1}D_{wo,tot,j-1}}{2}\right]\left(\frac{1}{\Delta r_j}\right)\right\} + k_r \tag{11.23}$$

$$B_j^C = -\frac{1}{r_j}\frac{2}{\Delta r_{j+1} + \Delta r_j}\left\{\left[\frac{r_{j+1}D_{wo,tot,j+1} + r_j D_{wo,tot,j}}{2}\right]\left(\frac{1}{\Delta r_{j+1}}\right)\right\} \tag{11.24}$$

$$C_j^C = -\frac{1}{r_j}\frac{2}{\Delta r_{j+1} + \Delta r_j}\left\{\left[\frac{r_j D_{wo,tot,j} + r_{j-1}D_{wo,tot,j-1}}{2}\right]\left(\frac{1}{\Delta r_j}\right)\right\} \tag{11.25}$$

$$D_j^C = \frac{v_z C_{i-1,j}}{\Delta z} + k_r C_{wo}(T_{i,j}) \tag{11.26}$$

For a uniform grid, the equations reduces to:

$$A_j^C = \frac{v_{z,j}}{\Delta z_j} + \frac{1}{2r_j\Delta r^2}(2r_j D_{wo,tot,j} + r_{j+1}D_{wo,tot,j+1} + r_{j-1}D_{wo,tot,j-1}) \tag{11.27}$$

$$B_j^C = -\frac{1}{2r_j\Delta r^2}(r_{j+1}D_{wo,tot,j+1} + r_j D_{wo,tot,j}) \tag{11.28}$$

$$C_j^C = -\frac{1}{2r_j\Delta r^2}(r_j D_{wo,tot,j} + r_{j-1}D_{wo,tot,j-1}) \tag{11.29}$$

with $D^C{}_j$ remaining the same.

The final linear system then looks like (Lee, 2008):

$$\begin{pmatrix} 1 & -1 & 0 & 0 & 0 & \cdots & 0 & 0 & 0 \\ C_2 & A_2 & B_2 & 0 & 0 & \cdots & 0 & 0 & 0 \\ 0 & C_3 & A_3 & B_3 & 0 & \cdots & 0 & 0 & 0 \\ 0 & 0 & C_4 & A_4 & B_4 & \cdots & 0 & 0 & 0 \\ \vdots & \vdots & \vdots & \vdots & \vdots & \ddots & \vdots & \vdots & \vdots \\ 0 & 0 & 0 & 0 & 0 & \cdots & C_{N-1} & A_{N-1} & B_{N-1} \\ 0 & 0 & 0 & 0 & 0 & \cdots & 0 & 0 & 1 \end{pmatrix} \begin{pmatrix} C_{i,1} \\ C_{i,2} \\ C_{i,3} \\ C_{i,4} \\ \vdots \\ C_{i,N-1} \\ C_{i,N} \end{pmatrix} = \begin{pmatrix} D_1 \\ D_2 \\ D_3 \\ D_4 \\ \vdots \\ D_{i,N-1} \\ C_{wo}(T_{interface}) \end{pmatrix}$$

ready to be implemented into the computer program.

11.4 Boundary Conditions

The boundary conditions for heat transfer are as follows:

$$\mathrm{T} = \begin{cases} \mathrm{T_{inlet}} & \text{at z} = 0 \text{ (inlet)} \\ \mathrm{T_b} & \text{at r} = \mathrm{R} \text{ (radial position of interest)} \\ \mathrm{T_{dep}} & \text{at r} = \mathrm{r_{dep}} \text{ (oil/deposit interface)} \\ \mathrm{T_{wall}} & \text{at r} = \mathrm{r_i} \text{ (inner pipe wall)} \end{cases}$$

$$\frac{\partial T}{\partial r} = 0 \quad \text{at r} = 0 \text{ (axial centerline)}$$

where T (K) is the temperature of interest, $\mathrm{T_{inlet}}$ (K) is the inlet temperature, $\mathrm{T_b}$ (K) is the average bulk flow temperature, $\mathrm{T_{dep}}$ (K) is the temperature at the oil/deposit interface, $\mathrm{T_{wall}}$ (K) is the temperature at the wall, $\mathrm{T_{dep}}$ (K) is the temperature at the solid/liquid interface, z (m) is the distance in the axial direction, r (m) is the radial distance, R (m) is the radial position at point of interest, r_i (m) is the inner pipe radius and $\frac{\partial T}{\partial r}$ (K/m) is the radial temperature gradient.

For mass transfer, the boundary conditions are given as a function of temperature:

$$\begin{cases} \mathrm{C_{inlet}} = f(\mathrm{T_{inlet}}) & \text{at z} = 0 \\ \mathrm{C_b} = f(\mathrm{T_b}) & \text{at r} = \mathrm{R} \\ \mathrm{C_{dep}} = f(\mathrm{T_{dep}}) & \text{at r} = \mathrm{R} \\ \mathrm{C_{wall}} = f(\mathrm{T_{wall}}) & \text{at r} = \mathrm{r_i} \\ \mathrm{C_{max}} = f(\mathrm{WAT}) & \text{at r} = \mathrm{R} \end{cases}$$

$$\frac{\partial C}{\partial r} = 0 \quad \text{at r} = 0$$

where $\mathrm{C_{inlet}}$ (wt-%) is the concentration of wax dissolved in oil at the inlet, $\mathrm{C_b}$ (wt-%) is the concentration of wax dissolved in the bulk, $\mathrm{C_{dep}}$ (wt-%) is the concentration at the solid/liquid interface, $\mathrm{C_{wall}}$ (wt-%) is the concentration at the inner pipe wall and $\mathrm{C_{max}}$ (wt-%) is the maximum amount of wax dissolved in oil and $\frac{\partial C}{\partial r}$ (wt-%/m) is the radial concentration gradient. The applied solubility equation is presented in Appendix E.

11.5 Wax Deposit Calculations

As explained in Chapter 6.3, the growth rate and aging of the wax deposit are both a result of the convective flux of wax molecules from the bulk to the oil/deposit

interface (Lee, 2008). The growth rate equals the difference between the convective flux to the gel deposit surface and the internal diffusion away from the interface, and is calculated as (Singh, 2000):

$$(-2\pi r_{dep})\rho_{gel}F_w\frac{dr_{dep}}{dt} = (2\pi r_{dep})k_M(C_b - C_{ws}(T_i)) - (2\pi r_{dep})\left(-D_e\frac{dC_{ws}}{dr}\Big|_{int}\right) \tag{11.30}$$

where r_{sep} (m) is the effective flow radius, F_w (-) is the weight fraction of wax in the deposit, ρ_{gel} (kg/m^3) is the density of the gel, k_M (m/s) is the inner convective mass transfer coefficient, C_b (wt-%) is the bulk concentration of wax, C_{ws} (wt-%) is the wax content at the solid/liquid interface, $\frac{dC_{ws}}{dr}$ is the radial concentration gradient evaluated at the solid/liquid interface and D_e (unit) is the effective diffusivity in the deposit given by Equation (C.3) in Appendix C.

$$\frac{dr_{dep}}{dt} = \frac{1}{(-2\pi r_{dep})\rho_{gel}F_w}\left\{(2\pi r_{dep})k_M(C_b - C_{ws}(T_i)) - (2\pi r_{dep})\left(-D_e\frac{dC_{ws}}{dr}\Big|_{int}\right)\right\} \tag{11.31}$$

The effective flow radius is found as:

$$r_{dep}(t) = r_i - \frac{dr_{dep}}{dt}\Delta t \tag{11.32}$$

where r_{sep} (m) is the effective flow radius, r_i (m) is the inner pipe radius and Δt (s) is the time of interest, and the deposit thickness given by:

$$\delta(t) = r_i - r_{dep}(t) \tag{11.33}$$

where δ (m) is the thickness of the deposit layer, r_i (m) is the inner pipe radius and r_{sep}(t) (m) is the effective flow radius at the time of interest.

The aging of the deposit is calculated as follows (Lee, 2008):

$$\pi\rho_{gel}(r_i^2 - {r_{dep}}^2)\frac{dF_w}{dt} = -2\pi r_{dep}\left(-D_e\frac{dC_{ws}}{dr}\Big|_{int}\right) \tag{11.34}$$

where ρ_{gel} (kg/m^3) is the density of the deposit, r_i (m) is the inner pipe radius, r_{dep} (m) is the effective flow radius, F_w (-) is the wax fraction in deposit,$\frac{dF_w}{dt}$ (s^{-1}) is the change of wax fraction in deposit with time (aging), D_e (m^2/s) is the effective diffusivity in the deposit, C_{ws} (wt-%) is the wax content at the solid/liquid interface and $\frac{dC_{ws}}{dr}$ (wt-%/K) is the concentration difference at the solid/liquid interface.

Integrating and rearranging Equation (11.34), the weight fraction of wax to be used in Equation (11.31) is given as:

$$F_w(t) = \frac{2r_{dep} D_e \frac{dC_{ws}}{dr}\Big|_{int}}{\rho_{gel}(r_i^2 - {r_i}^2)} \tag{11.35}$$

with the variables as presented above.

The numerical model requires the convective mass transfer coefficient, k_M (m/s), when calculating the mass transfer rate of wax. This is obtained by the Sherwood number (Lee, 2008):

$$Sh = \frac{(-2r_{dep})\frac{dC_{ws}}{dr}\Big|_{int}}{C_b - C_{dep}} = \frac{(2r_{dep})k_M}{D_{wo}} \tag{11.36}$$

where Sh is the Sherwood number and the variables are as above.

Rearranging Equation (11.36) yields the Equation for the calculation of the mass transfer coefficient by the MWP:

$$k_M = D_{wo}\frac{(-2r_{dep})\frac{dC}{dr}\Big|_{int}}{C_b - C_{dep}} \tag{11.37}$$

11.6 Numerical Simulations

The flow conditions and fluid properties applied in the numerical simulations corresponds to the input used in the analytical model, allowing for a direct comparison of results, as will be done in the subsequent chapter. Because of its complexity, the numerical model is found to be computational expensive. In the current work, a pipeline of 1500 meter is chosen simulated. This ensures that the distance at which the temperature in the viscous sub-layer in the analytical model reaches the WAT is covered. It should be noted that the numerical model is applicable for any length and pipeline dimensions and that computer capacity is the only limiting source.

11.6.1 Results

The wax deposit thickness is found to increase with time. The WAT is reached after 49 meter and the maximum deposit thickness is located where the WAT is reached. From this point on in the pipeline, the deposit thickness is found to decrease. The deposit thickness profiles obtained by the numerical model are given in Figure 11.1, where the situation in the pipeline after one, two and seven days are plotted.

The shape of the deposit profiles are again a result of the temperature difference in the near-wall region being at its maximum where the WAT is reached then decreasing along the pipeline. The growth rate of the layer decrease with time, in correspondence with the findings in Chapter 9,

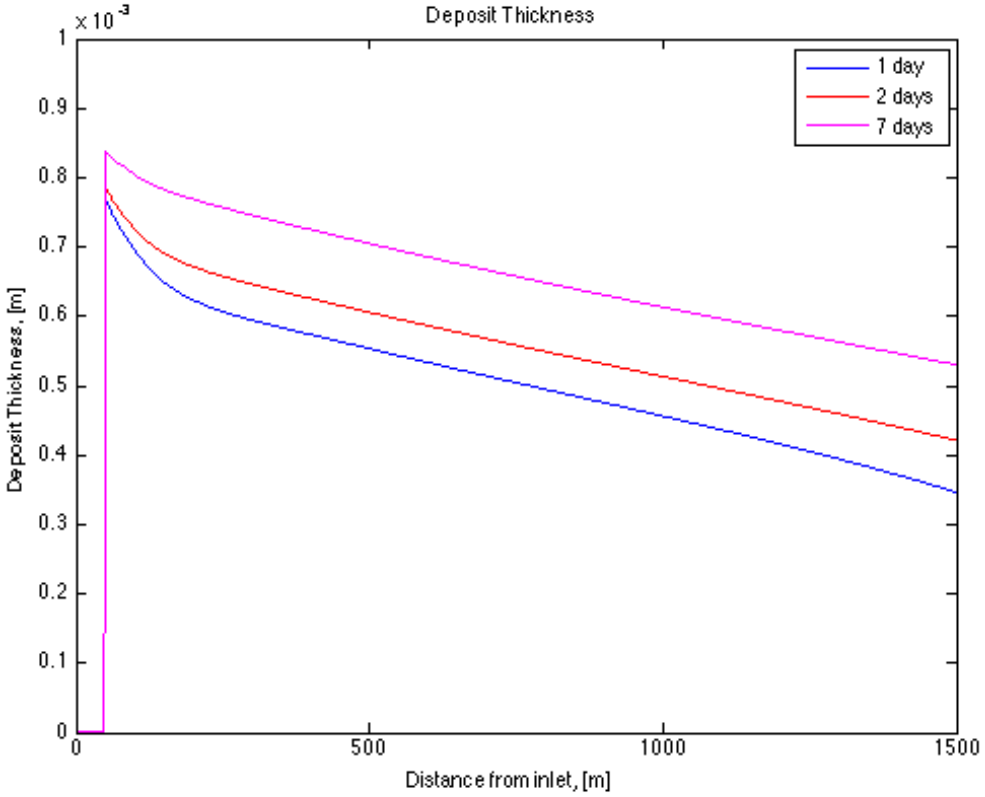

Figure 11.1: Deposit thickness profiles after 1 day, 2 days and 7 days obtained by the numerical model. The maximum deposit thickness is found at 49 meter, where the WAT is reached in the near-wall region

The deposit thicknesses at 49 meter at the end of the simulated pipeline are reported in Table 12. The results shows the decreased thickness with axial distance and a slow growth of the deposit thickness with time. The results will be compared to the analytical predictions and further commented upon in the subsequent chapter. In Appendix K, the temperature and concentration profiles in the pipeline after 24 hours are found attached.

Table 12: Deposit thickness values obtained by the analytical model. The thickness at 49 meter is the maximum deposit thickness and the values at 1500 meter is at the end of the simulated pipeline..

	Deposit Thickness [mm]	
Time	49 m	1500 m
1 day	0.77	0.35
2 days	0.78	0.42
7 days	0.84	0.53

12 Model Comparison

The wax deposit profiles obtained by the analytical and the numerical models will in the current chapter be compared to external results and to each other. The numerical results will first be compared to simulations conducted with the same mathematical model at a different university. The analytical results will then be compared to wax deposit profiles obtained by a commercial software built upon the same principles as the analytical model. Finally, the results from the analytical and the numerical simulations will be compared to each other.

12.1 External Material for Comparison

The wax deposit predictions compared to the simulations conducted in the current work, are acquired at the University of Michigan (UiM) and at the Norwegian University of Science and Technolgoy (NTNU) (Lee, 2008; Kjøraas, 2012). The results from the UiM are calculated by the mathematical model termed the numerical model in the current thesis, however, with a different crude oil and under different flow conditions. Consequently, the deposit thickness predictions from the UiM are suitable for a qualitative comparison with the numerical results only.

The deposit thickness predictions performed at the NTNU are obtained with the commercial software HYSYS. HYSYS assumes molecular diffusion as the sole mechanism for wax deposition using Fick's law to calculate the mass transfer rate of wax (Kjøraas, 2012). The concentration gradient is evaluated with the assumption of thermodynamic equilibrium between the solubility of wax and the actual concentration of wax in solution, hence, the simulations performed in HYSYS are based upon the same principles as the implemented analytical model.

One distinction between HYSYS and the numerical model, is that HYSYS requires a detailed oil composition as input, whilst a solubility equation considering the paraffin wax as a pseudo component is applied in the analytical model. The same oil has been applied in the analytical and in HYSYS, and except from an assumed oil density of 800 kg/m^3 and an inlet temperature of 50 °C in the HYSYS simulations[4], the applied fluid properties and flow conditions are identical in the three simulators (Kjøraas, 2012). The HYSYS results are hence found suitable for quantitative comparison with the wax deposit predictions obtained in the current work.

[4]The oil density is assumed to be 750 kg/m^3 and the inlet temperature set to 43°C in the current work. It should be noted that the inlet temperature only affects where the temperature of the fluid reaches the WAT in the pipeline and not the deposit thickness used for comparison.

12.2 Comparison of Results

Comparing the results from the UiM with the wax deposit profiles obtained by the numerical model in the current work, it is observed how the results are in the same order of magnitude. The deposit thicknesses obtained with the Norne crude oil is slightly higher than the results reported from the UiM, a deviation that can be accredited to the differences in flow conditions and applied fluid. The finding is considered an implication of a correct implementation of the numerical model in the presented work. The values and differences of the maximum deposit thicknesses obtained at UiM and with the numerical model are given in Table 13.

Table 13: Maximum deposit thickness in the pipeline calculated by the analytical model at the UiM (Lee, 2008) and NTNU. The results are in the same order of magnitude, indicating a correct implementation of the numerical model in the current work.

	Maximum Deposit Thickness [mm]		
Time	**UiM**	**Numerical**	**Difference**
1 day	0.1	0.77	0.67
2 days	-	0.78	-
7 days	0.3	0.84	0.54

Comparing the results obtained by the analytical model with the deposit thicknesses acquired in HYSYS, the values of the analytical simulations are found to be well above the results from HYSYS. As the models are based upon the same principles and the same oil are applied under identical flow conditions, the results were expected to be more congruent. The deviation may be accredited to the way the fluid composition is given as input in the models. Kjøraas (2012) reports to have included only the components up to C45 in the HYSYS simulations, whilst the solubility equation applied in the analytical model is based on the total composition of the Norne crude oil covering components up to C100. Since the deviation after only one day is 3.0 mm and after a week has increased to 11.3 mm, the correctness of the analytical model is not considered verified by the HYSYS comparison. The compared results from the analytical simulations and HYSYS are found in Table 14.

The wax deposit thicknesses obtained by the analytical model are found to be greater than the results obtained by the numerical model. The findings applies to all three time steps and is in correspondence with the expectations based on the literature study; the assumption of thermal equilibrium at every point in the pipeline was expected to result in too high an amount of wax transfer in the viscous sub-layer and, consequently, a deposit thickness over predicting the situation.

Table 14: Maximum deposit thickness in the pipeline calculated by HYSYS and the analytical model. The results shows a higher amount of wax to be expected by the analytical simulations than with the commercial simulator.

	Maximum Deposit Thickness [mm]		
Time	**HYSYS**	**Analytical**	**Difference**
1 day	0.9	3.9	3.0
2 days	1.8	6.9	5.1
7 days	5.3	16.6	11.3

The differences between the maximum deposit thicknesses predicted by the analytical and numerical models are found to deviate significantly, as can be seen from the model comparison in Table 15. After one day, the analytical model predicts a layer of deposit being 3.1 mm thicker than the numerical model, and after a week the difference is at 15.8 mm. The result quantifies the deviation that occurs when Fick's law is being applied without any modifications on oil field conditions, as were one of the aims of the thesis.

Table 15: Maximum deposit thickness in the pipeline calculated by the analytical and the numerical model. The results shows a significant higher amount of wax to be expected by the analytical simulations than with the numerical solution.

	Maximum Deposit Thickness [mm]		
Time	**Numerical**	**Analytical**	**Difference**
1 day	0.77	3.9	3.1
2 days	0.78	6.9	6.1
7 days	0.84	16.6	15.8

Because of the deviation found between the analytical solution and the results obtained in HYSYS, raising questions about the correctness of the implemented analytical model, the numerical results will be compared to the HYSYS simulations. In Table 16, it is seen how the numerical model yields less predicted wax deposits at each time step. After the first day, the difference is only at 0.13 mm, but as the growth rate of the layer decreases more rapidly in the numerical model than in HYSYS, the difference after seven days is at 4.46 mm. The comparison of the numerical simulations to the commercial software confirms how the inclusion of a precipitation constant to account for the correlation between heat and mass transfer will yield noticeably less wax predicted compared to models based upon an assumption of thermodynamic equilibrium in the pipeline.

Table 16: Maximum deposit thickness in the pipeline calculated by the numerical model and HYSYS. The results shows a higher amount of wax to be expected by the HYSYS simulations than with the numerical solution.

	Maximum Deposit Thickness [mm]		
Time	**Numerical**	**HYSYS**	**Difference**
1 day	0.77	0.9	0.13
2 days	0.78	1.8	1.02
7 days	0.84	5.3	4.46

The wax deposit profiles for the Norne crude oil obtained in HYSYS are found in Figure 12.1, showing the deposit thicknesses after 1, 2, 7 and 10 days (Kjøraas, 2012).

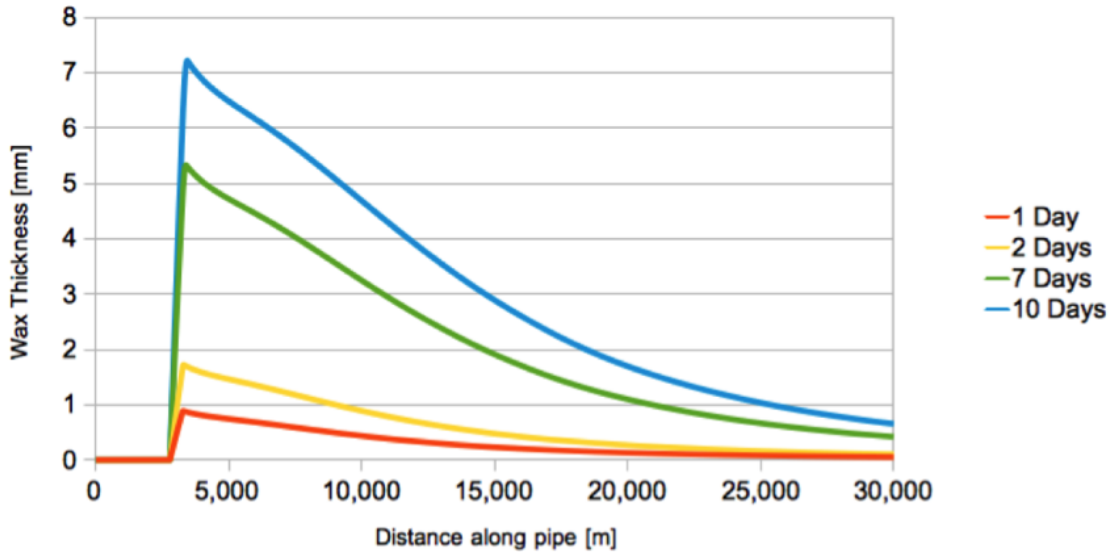

Figure 12.1: Wax deposit thickness for the Norne crude oil predicted by the commercial software HYSYS (Kjøraas, 2012). The deposit thicknesses are found to be higher than the results from the numerical simulations, but lower than the analytical results.

13 Shortcomings

The evaluation of the shortcomings in the thesis is divided into shortcomings associated with the wax deposit models and shortcomings in the conducted work.

13.1 Shortcomings in the Implemented Models

Neither in the presented models nor in HYSYS is the effect of shear-removal, or the balance between the deposit layer build up and erosion by the shear effect of the fluid, included in the wax deposit predictions. Due to high shear at the oil/deposit interface, the paraffin deposited on the pipeline wall may be sloughed of when the flow is turbulent (Lee, 2008). Shear-removal is considered a random event and no model based on first principles are available. If the effect is accounted for i modeling, empirical tuning parameters are applied (Rønningsen, 2012).

Since the effect of shear-removal is not included in either of the presented models, the comparative basis of the wax deposit profiles are correct. However, the physical processes are not correctly described and modeled, representing a severe shortcoming in the models. The result of including the effect of shear-removal would be a thinner layer of deposit predicted. The reported deposit thicknesses should therefore be considered an upper estimate of the actual situation in the pipeline.

Although being a model applied in literature and commercial software, a known limitation with the analytical model is the area of validity being restricted to laminar flow conditions. A direct application of the model to normal operative oil field conditions will, per definition, yield incorrect results, an incorrectness being quantified in the current thesis.

A shortcoming present in both the models, is the applicability of the simulators being restricted to single phase flow. Oil flow in subsea pipelines is frequently accompanied by water and gas, however, neither of the models presented are applicable for multiphase flow systems (Huang, 2011).

13.2 Shortcomings in the Conducted Work

In the conducted work, the assumption of a constant fluid density and viscosity has been an applied simplification of the actual situation in the pipeline. In future studies, the impact of density and viscosity on the wax deposit profiles are recommended investigated and functions accounting for variations in conditions implemented if found necessary.

An original idea of the current work, was to compare the results of the analytical and numerical simulations with what was believed to be a wax deposit profile of the Norne crude oil applied for verification in previous work (Kjøraas, 2012). The

deposit thickness profile in question was acquired from a Statoil presentation held at NTNU (Aske, 2007). Analyzing the results from Statoil, the rate of deposition showed to increase with time, contradicting the findings in the current study. It was confirmed by Statoil that the graphs were not true values from the Norne field, but an example used for illustration only[5] (Stokkenes, 2013b; Stokkenes, 2013c). Hence, the results from Statoil could neither be used for verification nor falsification of the implemented work, and the comparison of results obtained with the Norne crude oil became restricted to three simulators instead of four.

Representing an impracticality just as much as a shortcoming, the numerical method has shown to be expensive in terms of computer capacity and time required for a single run. The written computer code is valid for all pipe dimensions, but for future application, the mathematical model is recommended implemented in a different language to reduce the runtime and requirement for computer capacity when performing simulations.

[5]The deposit thickness was not produced by a combination of the commercial software PVTSim and OLGA which Statoil uses for wax deposit prediction, but was merely a product of power point (Stokkenes, 2013b; Stokkenes, 2013c).

14 Summary

A full implementation of an analytical and a numerical model facilitating the prediction of paraffin wax deposits in oil flowing pipelines has been obtained. To account for temperature variations in the pipeline with position and time, conductive heat transfer equations have been included for calculation of the radial heat flux through the wall and the growing layer of wax deposit. As a result, the applicability of the models are not restricted to flow loops, but valid for real field conditions.

As part of the model construction, five effective thermal conductivity models for determination of the effective thermal conductivity of the wax deposit have been evaluated. Based on the structure of the deposit, being a random distribution of wax and oil, the Effective Medium Theory is found suitable for the wax deposit modeling.

To evaluate the need for dynamic simulations, the changes in thermal conditions occurring in the pipeline when wax deposits on the inner pipe wall has been investigated. The presence of deposits is found to add a layer of insulation to the system, increasing the resistance towards heat flow with an increasing thickness of the layer. A higher amount of wax in deposit is found to cause less resistance towards heat flow than a layer of corresponding thickness and a lesser amount of wax. The result is explained by the thermal conductivity of wax being higher than the thermal conductivity of oil. The influence of the deposit thickness on the temperature conditions is found to be greater than the influence of the composition.

As a consequence of the added layer of insulation, the temperature at the oil/deposit interface is found to increase with an increasing deposit thickness. With the temperature at the deposit surface brought closer the bulk flow temperature, the radial temperature gradient in the pipeline, or the thermal driving force for deposition, decreases. The decreasing driving force for deposition with an increasing thickness yields a non-linear growth rate of the layer of deposit, requiring dynamic simulations.

Dynamic wax deposition simulations on a field scale pipeline system under realistic flow conditions have been performed with the analytical and the numerical models. The results have been compared to external material and to each other. The numerical model is found to yield results in the same order of magnitude as what is obtained with the mathematical model at a different university. As different crude oils under different flow conditions have been applied at the two institutions, the results are valid for qualitative comparison only. The similarities in the deposit thickness predictions is taken as an implication of a correct implementation of the numerical model in the current work.

The analytical simulations have been compared to results obtained with a com-

mercial wax deposit predictor. The commercial software is built upon the same assumptions as the analytical model and simulations are conducted with the same fluid under identical flow conditions. The analytical model showed to predict a thicker layer of wax to be expected than was the case with the commercial software. A possible explanation is the difference in how the fluid composition are given as input in the two models.

Finally, the analytical and the numerical results were compared. Based on the literature study, the analytical model was expected to yield a higher amount of wax deposits than the numerical model. The expectations was found to be true. After only one day, the analytical model predicted a maximum wax deposit thickness being 3.1 mm higher than the numerical model and after a week the difference was increased to 15.8 mm. The results quantifies the differences arising when the numerical model, with its assumption of thermodynamic equilibrium at every point in the pipeline, is applied, compared to the numerical model which is taking the precipitation kinetics of wax into account. The comparison showed a significant discrepancy between the expected wax deposit thickness predicted by the two models.

15 Future Work

A possible continuation of the current work is to apply the implemented models as the tools they are meant to be. One option is to investigate the effect of thermal insulation on the situation in the pipeline. With sufficient knowledge about the prevailing conditions, the results can be used to evaluate if it will be economical beneficial to isolate the pipeline or not. On the basis of wax deposit simulations, pigging schedules for pipelines, with or without insulation, can be prepared, and costs related to stuck pipe incidents and chemical assistance can be sought for. The final product could be a report where recommendations for a field development project, based upon the collected information, is presented.

Before applying the analytical model in any field development project or planning of operational activity, the area of validity should be extended to the turbulent flow regime. As it is implemented today, the analytical model serves as the comparative basis it was supposed to be, but it is not recommended applied without any modifications. One possibility could be to include the turbulent mass diffusivity as given by Prandtl mixing length theory in the existing computer code and perform a new evaluation of the method.

An extension of the current work, could be to include the momentum equation in the implemented models, allowing for dynamic simulations of the axial pressure drop and the wall shear stress throughout the pipeline. A different direction of study could be to explore the combination of heat and mass transfer with hydrodynamics to extend the applicability of the models to multiphase oil/water flow.

A References

Aiyejina, A., a. C. D. P., Pilgrim, A., and Sastry, M. Wax formation in oil pipelines: A critical review. *International Journal of Multiphase Flow 37* (2011), 671–694.

Ajienka, J., and Ikoku, C. Criteria for the Design of Waxy Crude Oil Pipelines: Maximum Pump (Horsepower) Pressure Requirement. *Petroleum Science and Engineering 13* (1995), 87–94.

Armenante, P. M., and Kirwan, D. J. Mass Transfer to Microparticles in Agitated Systems. *Chemical Engineering Science 21* (2003), 393–408.

Aske, N. Wax - A flow assurance challenge. Guest lecture at NTNU, Statoil (2007).

Awad, M., and Muzychka, Y. Effective property models for homogeneous two-phase flow. *Experimental Thermal and Fluid Science 33* (2008), 106–113.

Azevedo, L., and Teixeira, A. A Critical Review of the Modeling of Wax Deposition Mechanisms. *Petroleum Science and Technology 21* (2003), 393–408.

Benall, A., Maurel, P., Agassant, J. F., Darbouret, M., Avril, G., and Peuriere, E. Wax Deposition in Pipelines: Flow-Loop Experiments and Investigations on a Novel Approach. SPE 115293, Society of Petroleum Engineers (2008).

Bunthebarth, G., and Jobmann, M. On Thermal Conductivity of 2-Component Systems. Presentation, Annual Meeting of the German Geophysical Society (2008).

Burger, E. D., Perkins, T. K., and Striegler, J. H. Studies of Wax Deposition in the Trans Alaska Pipeline. *Journal of Petroleum Technology 33(6)* (1981), 1075–1086.

Dirksen, J., and Ring, T. Fundamentals of Crystallization: Kinetic Effects on Particle Size Distribution and Morphology. *Chemical Engineering Science 46* (1991), 2389–2427.

Ekweribe, C., Civan, F., Lee, H., and Singh, P. Effect of System Pressure on Restart Conditions of Subsea Pipelines. SPE 115672, Society of Petroleum Engineers (2008).

Frigaard, I., Vinay, G., and Wachs, A. Compressible Displacement of Waxy Crude Oils in Long Pipeline Startup Flows. *Journal of Non-Newtonian Fluid Mechanics 147* (2007), 45–64.

Geankoplis, C. *Transport Processes and Separation Process Principles*, vol. 4. 2003.

Gudmundsson, J. Grunnleggende enhetsoperasjoner i produksjon av olje og gass. Compendium, NTNU Institutt for petroleumsteknologi og anvendt geofysikk (2009).

Gudmundsson, J. S. Unpublished Material. 2012.

Hayduk, W., and Minhas, B. S. Correlations for Prediction of Molecular Diffusivities in Liquids. *The Canadian Journal of Chemical Engineering 60(2)* (1982), 295–299.

Huang, Z. *Application of the Fundamentals of Heat and Mass Transfer to the Investigation of Wax Deposition in Subsea Pipelines*. PhD thesis, University of Michigan, 2011.

Incropera, F., Dewitt, D., Bergman, T. L., and Lavine, A. *Fundamentals of Heat and Mass Transfer*, vol. 7. 2011.

Kay, J., and Nedderman, R. *Fluid mechanics and transfer processes*, vol. 1. 1985.

Kennedy, M., and O'Hagan, A. Bayesian calibration of computer models. *Journal of the Royal Statistical Society 63* (2001), 425–464.

Kjøraas, M. Modeling of Wax Deposition in Subsea Pipelines. Project report, Norwegian University of Science and Technology, 2012.

Labes-Carrier, C., Rønningsen, H., Kolsnes, J., and Leporche., E. Wax Deposition in North Sea Gas Condensate and Oil Systems: Comparison Between Operational Experience and Model Prediction . SPE 77573, Society of Petroleum Engineers (2008).

Lee, H. S. *Computational and Rheological Study of Wax Deposit and Gelation in Subsea Pipelines*. PhD thesis, the University of Michigan, 2011.

Leontaritis, K., and Leontaritis, J. Cloud Point and Wax Deposition Measurements Techniques. SPE 80267, Society of Petroleum Engineers (2003).

MathWorks. MATLAB. http://www.mathworks.se/products/matlab/, June 2013.

Mirazizi, H. K., W., S., and Sarica, C. Paraffin Deposition Analysis for Crude Oils under Turbulent Flow Conditions. SPE 159385, Society of Petroleum Engineers (2012).

O'Hagan, A. Bayesian analysis of computer code inputs: A tutorial. *Reliability Engineering and System Safety 91* (2006), 1290–1300.

Rø nningsen, H. Rheological behavior of gelled, waxy North Sea crude oils. *Journal of Petroleum Science and Engineering 7* (1992), 177–213.

Rønningsen, H. P. Production of Waxy Oils on the Norwegian Continental Shelf: Experiences, Challenges, and Practices. *Energy and Fuels 26* (2012), 4124–4136.

Sarica, C., and Volk, M. Tulsa University Paraffin Deposition Projects. Tech. rep., University of Tulsa, 2004.

Sculkes, R. Flow Assurance - Why oil companies focus on multiphase transport. Guest lecture at NTNU, Statoil, 2013.

Serpil, S., and Servet, G. S. *Physical Properties of Food*, vol. 1. 2006.

Siljuberg, M. The Bulk Precipitation's Impact on Concentration Driving Force in Wax Depostion. Project report, Norwegian University of Science and Technology, 2011.

Siljuberg, M. Modelling of Paraffin Wax in Oil Pipelines. Master thesis, Norwegian University of Science and Technology, 2012.

Singh, A., Lee, H., Singh, P., and Sarica, C. SS: Flow Assurance: Validation of Wax Deposition Models Using Field Data from a Subsea Pipeline. OTC 21641, The Offshore Technology Conference (2011).

Singh, P., Venkatesan, R., and Fogler, H. S. Formation and Aging of Incipient Thin Film Wax-Oil Gels. *AIChE Journal 46*, 5 (2011), 1059–1074.

Stokkenes, A. Personal communication. E-mail, May, 2013b, Statoil.

Stokkenes, A. Personal communication. E-mail, June, 2013c, Statoil.

Stokkenes, A. Wax control. Guest lecture at NTNU, 2013a, Statoil.

Stubsjøen, M. Wax Modeling in Subsea Oil Pipelines. Project report, Norwegian University of Science and Technology, 2012.

Van Driest, E. R. On Turbulent Flow Near a Wall. *AIAA Journal Special Supplement: Centennial of Powered Flight 23* (1956).

Venkatesan, R., and Creek, J. Wax Deposition and Rheology: Progress and Problems From an Operator's View. OTC 20668, Offshore Technology Conference (2010).

Venkatesan, R., and Fogler, H. S. Comments on Analogies for Correlated Heat and Mass Transfer in Turbulent Flow. *AIChE Journal 47*, 1 (2001), 6–18.

Villazon, G. M., and Civan, F. Modeling Multiphase Wax Deposition in Submarine Pipelines After Shut-In, 5. SPE 124725, Society of Petroleum Engineers (2009).

Wang, J., Carson, J., North, M., and Cleland, D. A new approach to modeling the effective thermal conductivity of heterogeneous materials. *Heat and Mass Transfer 49* (2006), 3075–3083.

B Heat Transfer Coefficient

There are several empirical correlations available to determine the convective heat transfer coefficient, h (W/m.K), correlations expressing the Nusselt number as a function of the Reynolds number and the Prandtl number, Nu = f(Re,Pr). Combined with the definition of the Nusselt number, they allow for the calculation of the convective heat transfer coefficient. Which correlation found suitable for the situation is dependent upon flow conditions and geometry. Below, four correlations applicable for turbulent flow in a circular pipe are presented.

B.1 Chilton-Colburn Correlation

The Chilton-Colburn correlation, expressing the local Nusselt number as (Incropera et al., 2011):

$$Nu = 0.023 Re^{4/5} Pr^{1/3} \tag{B.1}$$

where Re is the Reynolds number and Pr is the Prandtl number. The equation is valid for turbulent flow in a smooth pipe where:

$$\begin{aligned} 0.7 \leq Pr \leq 160 \\ Re \geq 10000 \\ \frac{L}{d} \geq 10 \end{aligned}$$

L (m) is the length of the pipe and d (m) is the inner pipe diameter.

B.2 Dittus-Boelter Correlation

The Dittus-Boelter correlation is a slightly modified version of the Chilton-Colburn correlation, specifying whether the fluid is subject to cooling or heating (Incropera et al., 2011):

$$Nu = 0.023 Re^{4/5} Pr^{n} \tag{B.2}$$

where Re is the Reynolds number, Pr is the Prandtl number, n = 0.4 for heating and n = 0.3 for cooling. Beyond this, the criterions for using the Dittus-Boelter equation equals the criterions of the Chilton-Colburn correlation.

Because of their simplicity, the Chilton-Colburn and the Dittus-Boelter correlation are widely applied. However, the equations are found to yield errors as large

as 25 %, and sometimes more complex correlation are preferred (Incropera et al., 2011).

B.3 Pethukov Correlation

To reduce the uncertainty related to the value of the heat transfer coefficient calculation in the model, the Pethukov correlation can be applied (Incropera et al. 2011):

$$Nu = \frac{\frac{f}{8} RePr}{1.07 + 12.7 \left(\frac{f}{8}\right)^{\frac{1}{2}} (Pr^{\frac{2}{3}} - 1)} \tag{B.3}$$

where f is the friction factor, Re is the Reynolds number and Pr is the Prandtl number. The Pethukov correlation is valid when:

$$0.5 \leq Pr \leq 2000$$
$$10^4 < Re < 10^6$$

and the friction factor, f, can be obtained by a Moody chart or by (Incropera and Dewitt, aarstall):

$$f = 0.0790\, ln(Re - 1.64)^{-2} \tag{B.4}$$

for flow in the range of

$$3000 \geq Re \geq 5 \cdot 10^6$$

B.4 Gnielski Correlation

A modified version of the Pethukov equation is the Gnielski correlation, expressed as (Incropera and Dewitt, aarstall):

$$Nu = \frac{\frac{f}{8} (Re - 1000)Pr}{1 + 12.7 \left(\frac{f}{8}\right)^{\frac{1}{2}} (Pr^{\frac{2}{3}} - 1)} \tag{B.5}$$

where the friction factor can be found by a Moody chart or by Equation (B.4). The correlation is valid when:

$$0.5 \leq Pr \leq 2000$$
$$3000 < Re < 5 \cdot 10^6$$

Applying one of the more recent correlations, such as the Pethukov equation or the Gnielinski equation, can reduce the uncertainty of the heat transfer coefficient value to less than 10 % (Incropera and Dewitt, aarstall). Making use of a more complex correlation in the wax deposit model will result in a more computational demanding computer code.

In the wax deposit models, the Dittus-Boelter correlation is chosen applied, because of its validity under the simulated flow conditions and its simplicity. As part of a future sensitivity analysis, the influence of the heat transfer coefficient correlation on the wax deposit prediction is recommended addressed.

C Diffusion Coefficient

To predict the molecular diffusivity of wax in oil, the binary diffusivity coefficient, D_{wo} (m^2/s), is required in both the wax deposit models derived. To obtain the value, a correlation proposed by Hayduk and Minhas (1982) is used:

$$D_{wo} = 13.3 * 10^{-}12 * \frac{T^{1.47}\mu^{\gamma}}{V_a^{0.71}} \tag{C.1}$$

where T (K) is the temperature, μ (mPa.s) is the solvent viscosity, V_a (cm^3/mol) is the molar volume of wax, and γ is a dimensionless function of the molar volume, defined as:

$$\gamma = \frac{10.2}{V_a} - 0.791 \tag{C.2}$$

Since the wax deposit is a gel-like mixture and not a pure solid, an effective diffusivity constant is required to calculate the diffusion influx at the oil/deposit interface. To calculate the effective diffusivity of wax molecules within the layer of deposit, the following equation is applied (Lee, 2008):

$$D_e = \frac{D_{wo}}{1 + \frac{\alpha^2 F_w^2}{1 - Fw}} \tag{C.3}$$

where D_{wo} (m/s) is the binary diffusion coefficient given by Equation (C.1), α is the average aspect ratio (lenght-to-width) of the wax crystals and F_w the weight fraction of wax in deposit.

D Precipitation Rate Constant

During precipitation, new particles are created by nucleation events (Dirksen and Ring, 1991). To account for precipitation kinetics in the concentration profile calculations, a precipitation rate constant is included in the numerical model. The precipitation rate constant, or growth rate of wax nucleus in the supersaturated solution, is a function of temperature, varying in the pipeline with time and position.

With diffusion assumed to be the rate determining process for particle growth, the growth rate of precipitated wax particles is given by (Dirksen and Ring, 1991):

$$G = k_d A_p \rho_n (C - C_{ws}) = k_r (C - C_{ws}) \tag{D.1}$$

where G (m/s) is the growth rate of the precipitated particles, k_d (s^{-1}) is the mass transfer rate from bulk to individual nucleus surface, A_p (m^2) is the surface area of a nucleus, ρ_n (kg/m^3) the nuclei number density, C (kg/m^3) is the wax concentration at the point of interest C_{ws} (kg/m^3) is the solubility limit of wax molecules at a given temperature and k_r (s^{-1}) is the precipitation rate constant. The mass transfer rate from bulk to individual nucleus surface can be found as (Lee, 2008):

$$k_d = \frac{Sh_p D_{wo}}{d_p} \tag{D.2}$$

where Sh_p is the Sherwood number for micro particles, D_{wo} (m^2/s) is the binary diffusion coefficient of wax in oil found by the correlation of Hayduk and Minhas (1981), and d_p (m) i the diameter of the nucleus. Using a mass transfer coefficient correlation for micro particles (Armenante and Kirwan, 1989):

$$Sh_p = 2 + 0.52 Re^{0.52} Sc^{1/3} \tag{D.3}$$

.

where Re is the Reynolds number and Sc is the Schmidt number and combining Equation (D.1)-(D.3), an expression for the precipitation rate constant is obtained:

$$k_r = \frac{Sh_p A_p \rho_n}{d_p} D_{wo} \tag{D.4}$$

with the variables as above.

The viscosity is calculated from the Arrhenius equation (Lee, 2008):

$$\mu = \mu_{cloud} exp\Big[\frac{E_A}{r_i}\left(\frac{1}{T} - \frac{1}{T_{cloud}}\right)\Big] \tag{D.5}$$

where μ_{cloud} (Pa.s) is the dynamic viscosity at the cloud point temperature, E_A (J/mol) is the activation energy, r_i (m) is the inner pipe radius and T (K) is the

temperature at the point of interest.

Combining Equation (D.4)-(D.5) and taking the ratio between the precipitation rate constant at any given temperature and the precipitation rate constant at the cloud point temperature, the precipitation rate constant can be found as:

$$\frac{k_r}{k_{r,cloud}} = \left(\frac{T}{T_{cloud}}\right)^{1.47} exp\Big[\frac{\gamma E_A}{r_i}\left(\frac{1}{T} - \frac{1}{T_{cloud}}\right)\Big] \tag{D.6}$$

where k_r (s^{-1}) is the precipitate rate constant at any temperature of interest, $k_{r,cloud}$ is the precipitate rate constant at the wax appearance temperature, T (K) is the temperature of interest, T_{cloud} is the wax appearance temperature, γ is the dimensionless parameter found by Equation (C.2), E_A (J/mol) is the activation energy and r_i (m) is the inner pipe diameter.

The only adjustable parameter in Equation (D.7), is the precipitation rate constant at the wax appearance temperature. Based upon experiments conducted by Huang (2011), $k_{r,cloud} = 1.4\ s^{-1}$ is applied in the current thesis. Hence, the equation implemented in the numerical model is:

$$k_r = 1.4\left(\frac{T}{T_{cloud}}\right)^{1.47} exp\Big[\frac{\gamma E_A}{r_i}\left(\frac{1}{T} - \frac{1}{T_{cloud}}\right)\Big] \tag{D.7}$$

E Applied Solubility Function

To calculate the concentration profiles in both wax deposition models, a temperature dependent solubility equation is applied. The solubility equation is an empirical correlation estimating the fraction of wax forming components in the oil, considering the paraffin as a pseudo component. Since the equation is integrated in the models, no detailed input of the paraffin distribution is required in either of the models.

The oil applied in the simulations of the current thesis is acquired by Statoil at the Norne field in the North Sea. The solubility equations for the Norne Crude Oil is derived by Siljuberg (2012), and given as:

$$C(T) = 0.0007T^2 + 0.00989T + 1.7706 \tag{E.1}$$

where C (wt-%) is the concentration of wax and T (°C) is the temperature at the point of interest. The wax appearance temperature of the Norne crude oil is 39°C (Aske, 2007).

F Simulation Input

Table 17: Input values applied in the simulations.

Variable	**Symbol**	**Value**	**Unit**
Inner pipe diameter	d	0.3048	m
Wall Thickness	Δr_{wall}	0.012	m
Pipe length	L	2000	m
Ambient Temperature	T_{sea}	5	°C
Inlet Temperature	T_{inlet}	41	°C
Average Flow Velocity	u	2	m/s
Density of Oil	ρ_{oil}	750	kg/m^3
Density of Wax	ρ_{wax}	750	kg/m^3
Dynamic Viscosity of Oil	μ_{oil}	0.5	mPa.s
Activation Energy	E_A	37700	J/mol
Molecular Volume	V_a	430	cm^3/mol
Heat Capacity of Oil	C_p	2300	J/kg.K
Aspect Ratio of Wax Crystal	α	3	-
Thermal Conductivity of Oil	k_{oil}	0.1	W/m.K
Thermal Conducitivity of Wax	k_{wax}	0.25	W/m.K
Thermal Conductivity of Pipe	k_{pipe}	0.20	W/m.K
Precipitation Rate at WAT	$k_{r,cloud}$	1.4	s^{-1}
Overall Heat Transfer Coefficient	U	20	W/m^2K
Time step	Δt	60	min
Number of Steps in Radial direction	n_j	100	-
Number of Steps in Axial Direction	n_i	10000	-

Table 18: Variables calculated in the simulations.

Variable	**Symbol**	**Value**	**Unit**
Reynolds Number	Re	91440	-
Prandtl Number	Pr	11.5	-
Inner Heat Coefficient	h_i	922	W/m^2K
Outer Heat Coefficient	h_o	20.7	W/m^2K

G Effective Thermal Conductivity Models

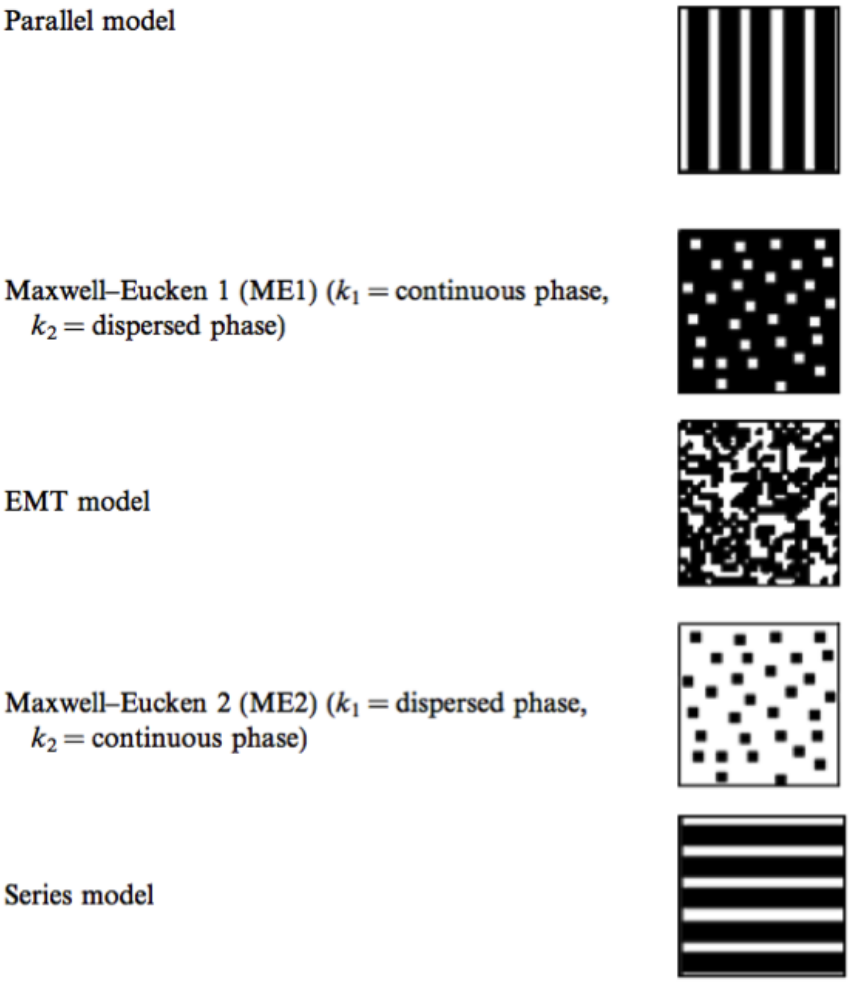

Figure G.1: Schematic representation of the structure of the five effective thermal conductivity models evaluated for application in the wax deposit models. The heat flow is assumed to be in the vertical direction (Wang et al., 2006).

H Heat Resistance Contribution

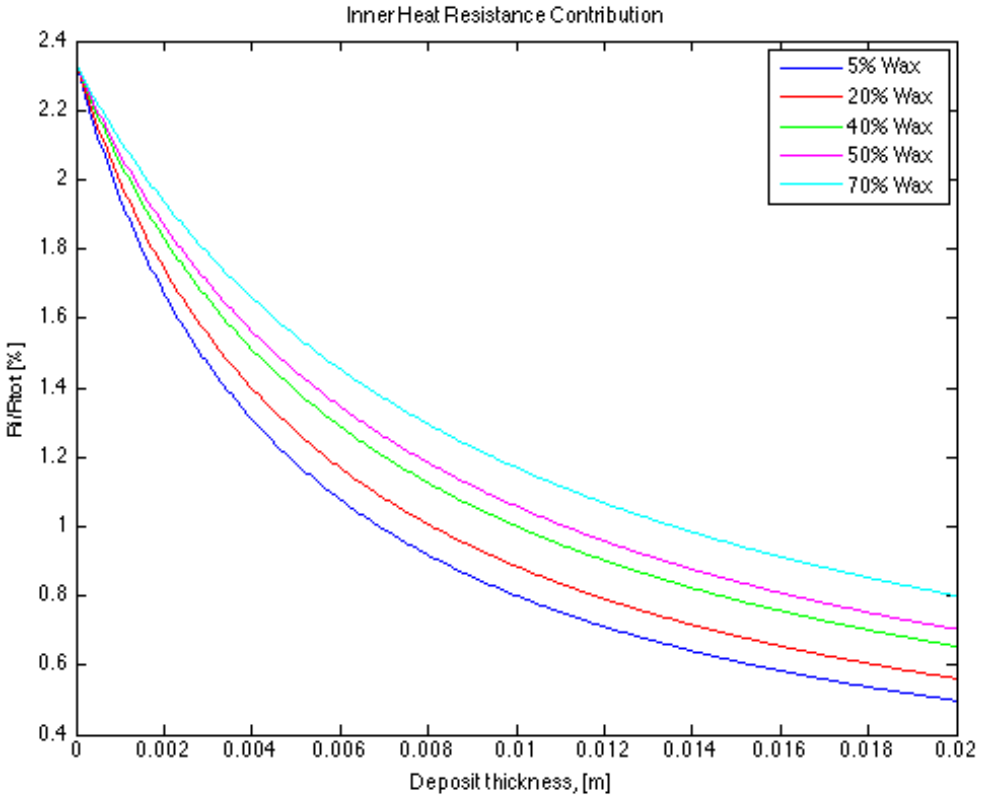

Figure H.1: The inner heat resistance contribution to the total thermal resistance is found to decrease with an increased deposit thickness. A higher wax content in deposit yields less reduction.

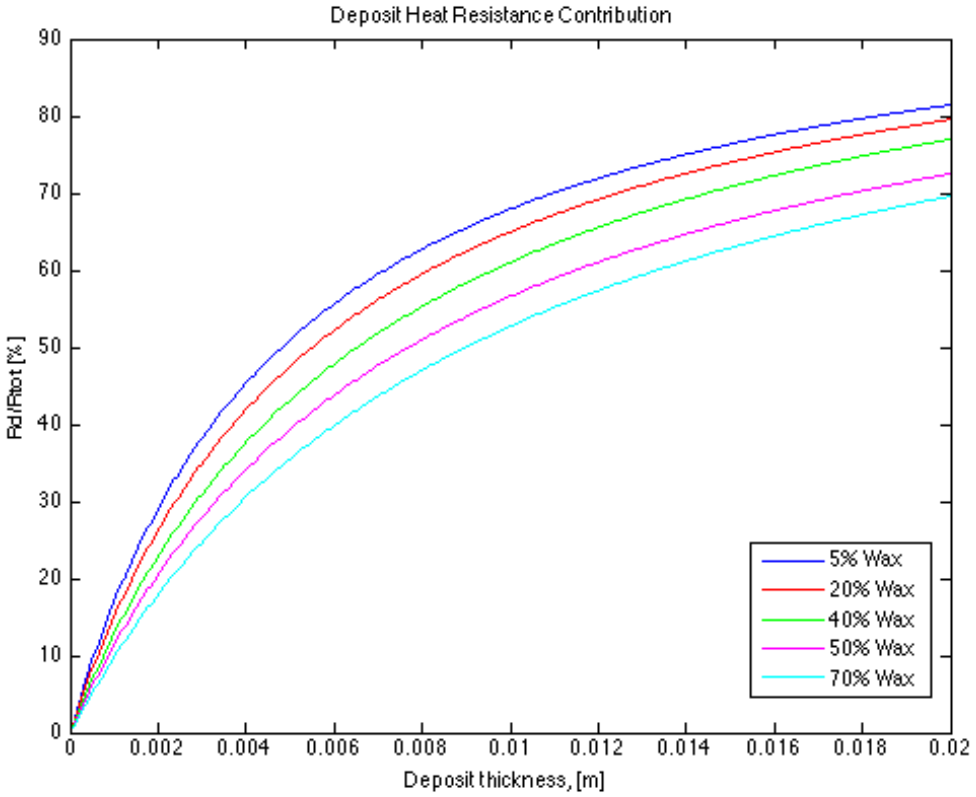

Figure H.2: The heat resistance contribution to the total thermal resistance of the layer of deposit is found to increase with an increased deposit thickness. A higher wax content in deposit causes a higher increase.

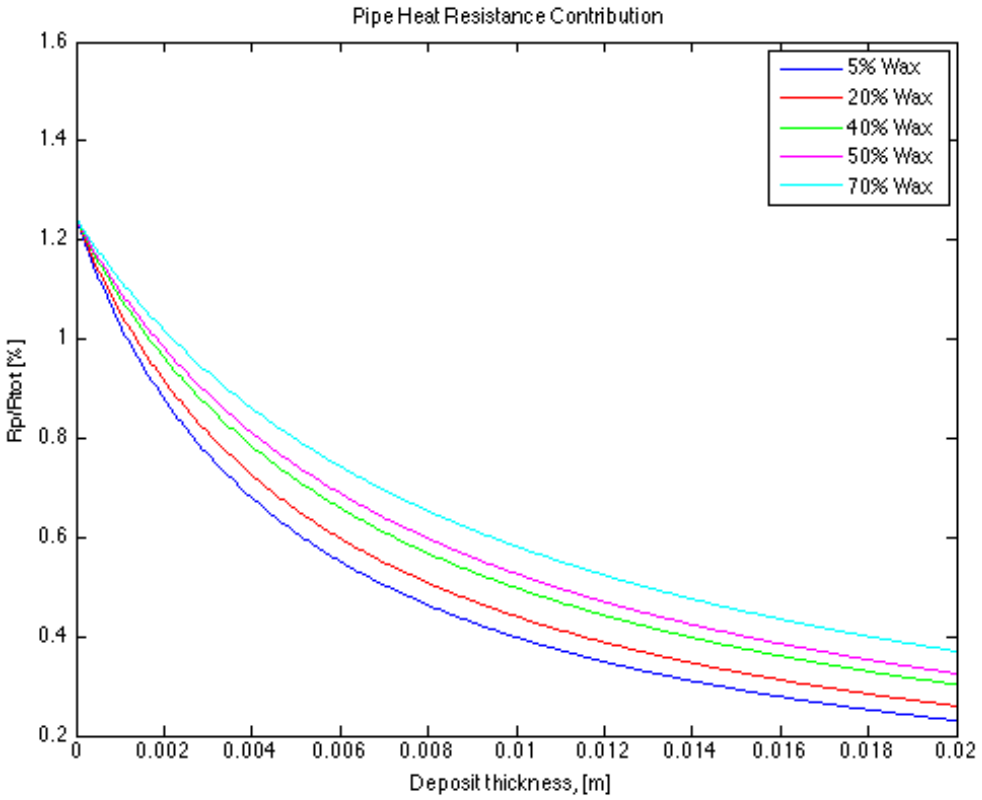

Figure H.3: The heat resistance contribution to the total thermal resistance from the pipe is found to decrease with an increased deposit thickness. A higher wax content in deposit yields less reduction.

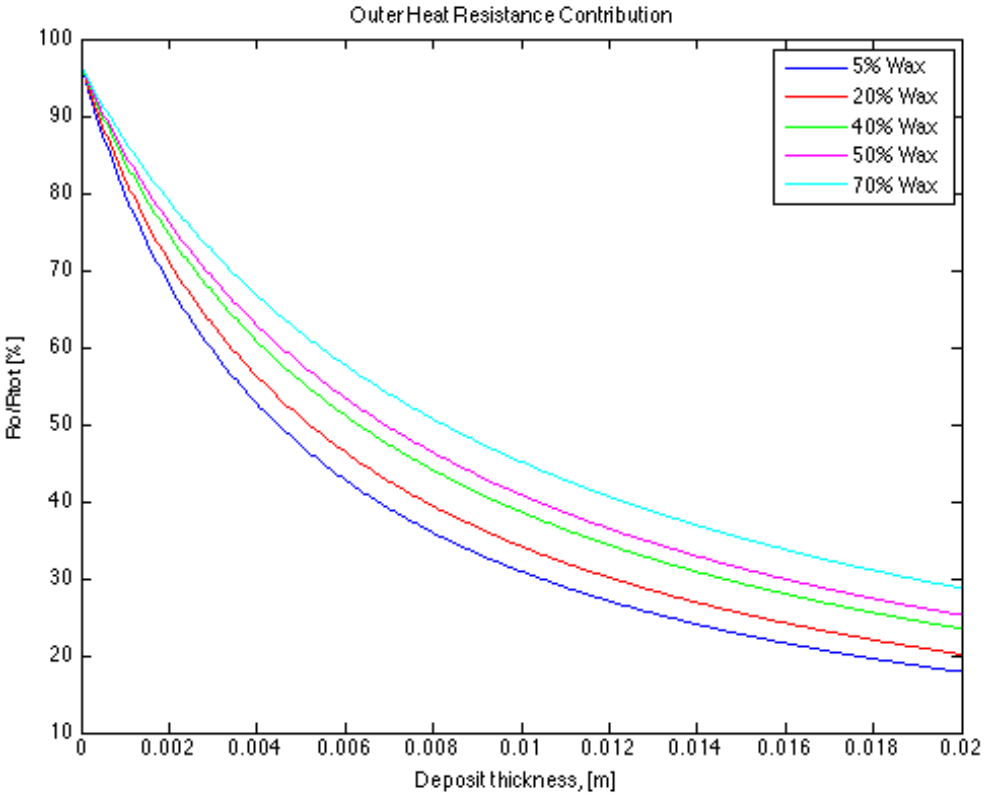

Figure H.4: The outer heat resistance contribution to the total thermal resistance is found to decrease with an increased deposit thickness. A higher wax content in deposit yields less reduction.

I Temperature Profiles

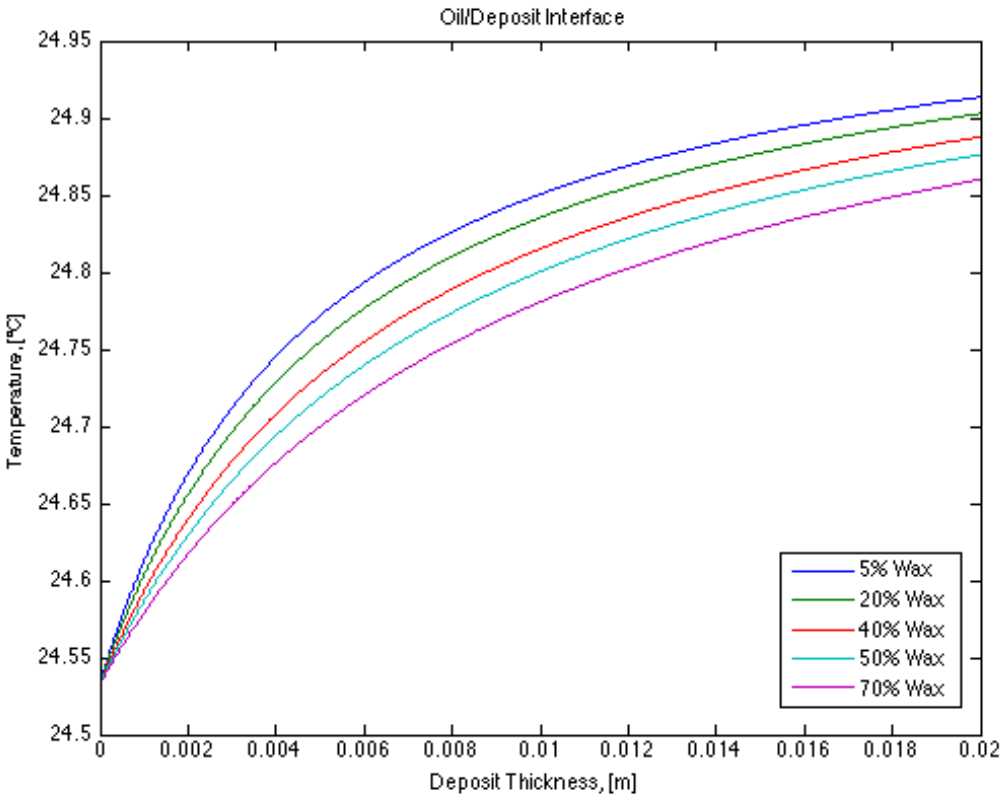

Figure I.1: The temperature at the oil/deposit interface is found to increase with an increased wax deposit thickness. The increase is higher with a higher wax content in deposit.

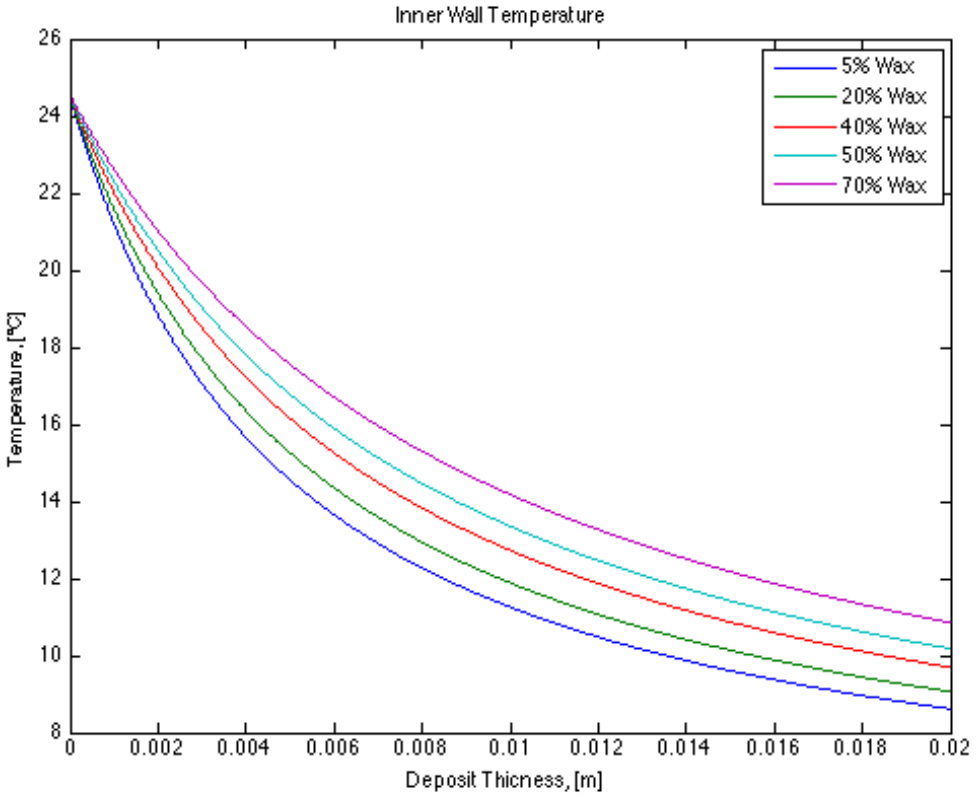

Figure I.2: The temperature at the inner pipe wall is found to decrease with an increased wax deposit thickness. The increase is less with a higher wax content in deposit.

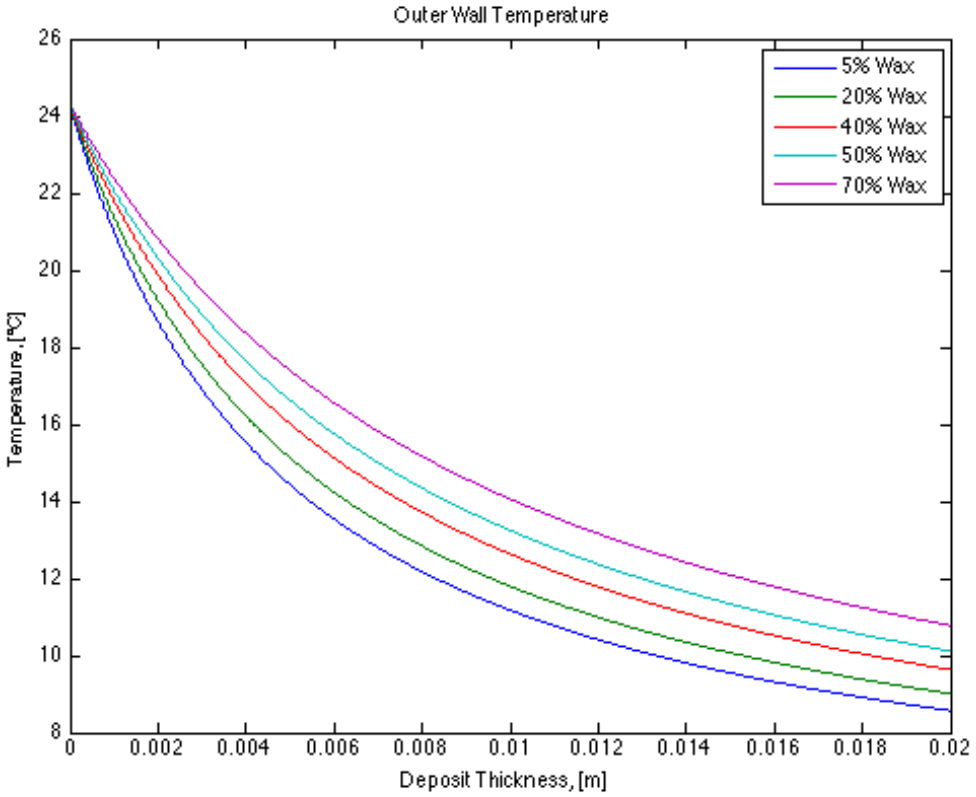

Figure I.3: The temperature at the outer pipe wall is found to decrease with an increased wax deposit thickness. The increase is less with a higher wax content in deposit.

J Analytical Solution

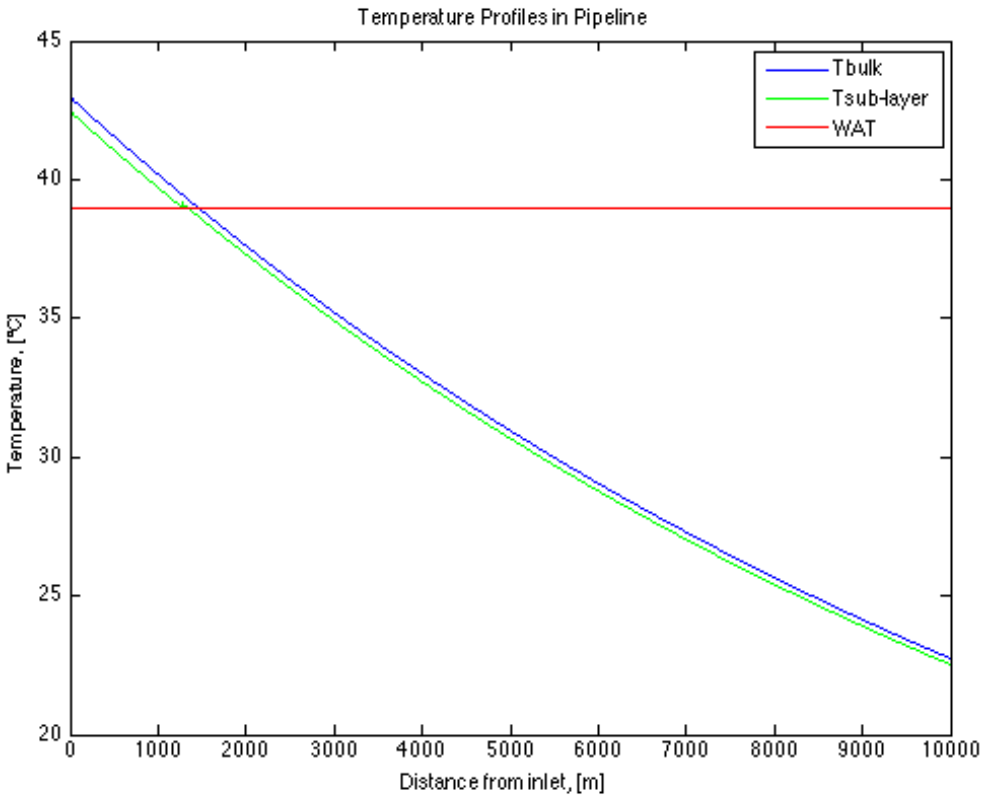

Figure J.1: Initial temperature situation with the average bulk flow temperature (blue) and the temperature in the viscous sub-layer (green). The temperature in the viscous sub-layer is found to reach the WAT (red) after 1284 meter and this is where first deposition will occur.

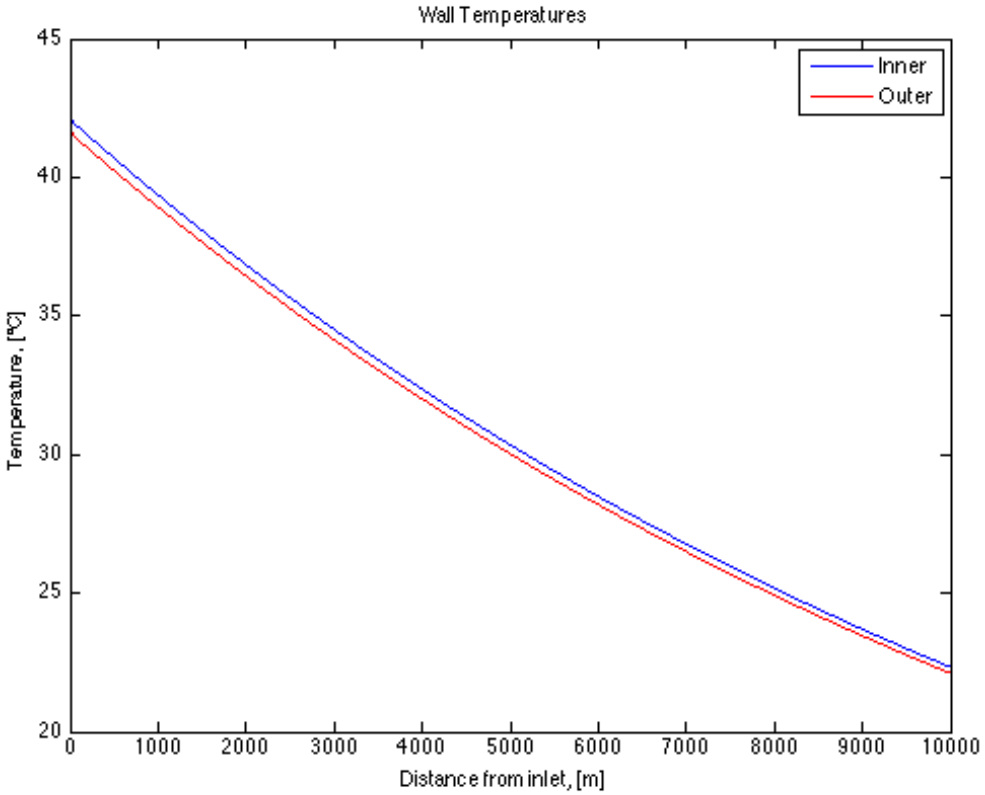

Figure J.2: Inner wall temperature (blue) and outer wall temperature (red) for a clean pipe, corresponding to the initial situation.

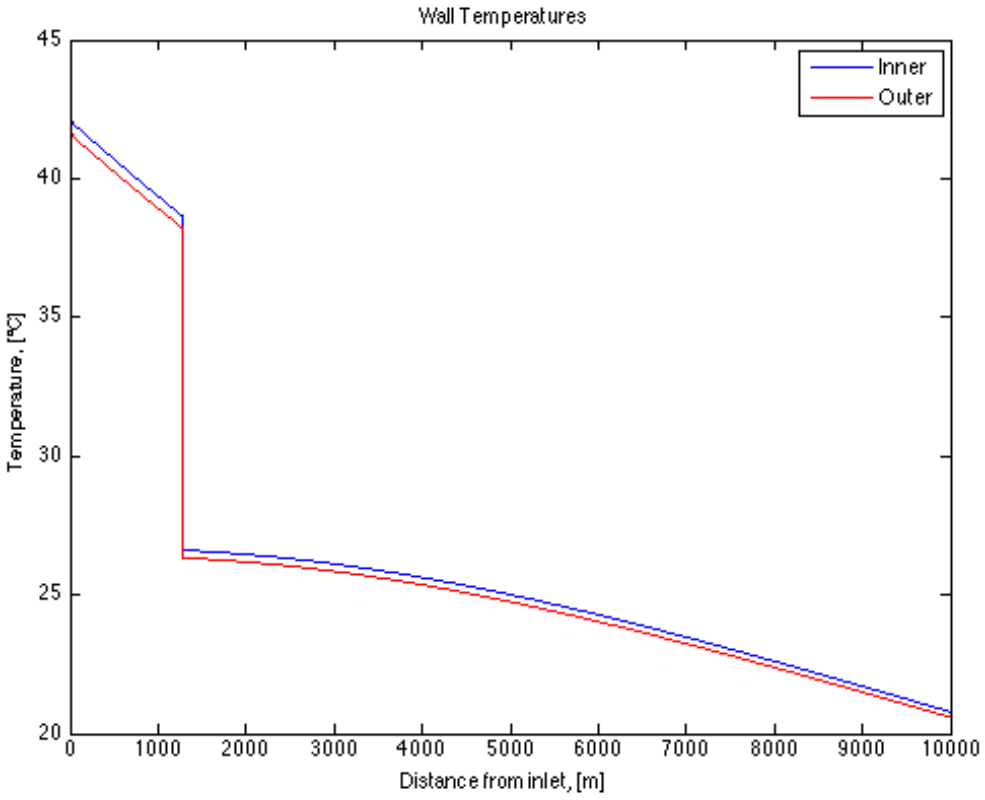

Figure J.3: Inner wall temperature (blue) and outer wall temperature (red) after 24 hours. The temperature reduction is caused by the layer of wax deposit that is formed.

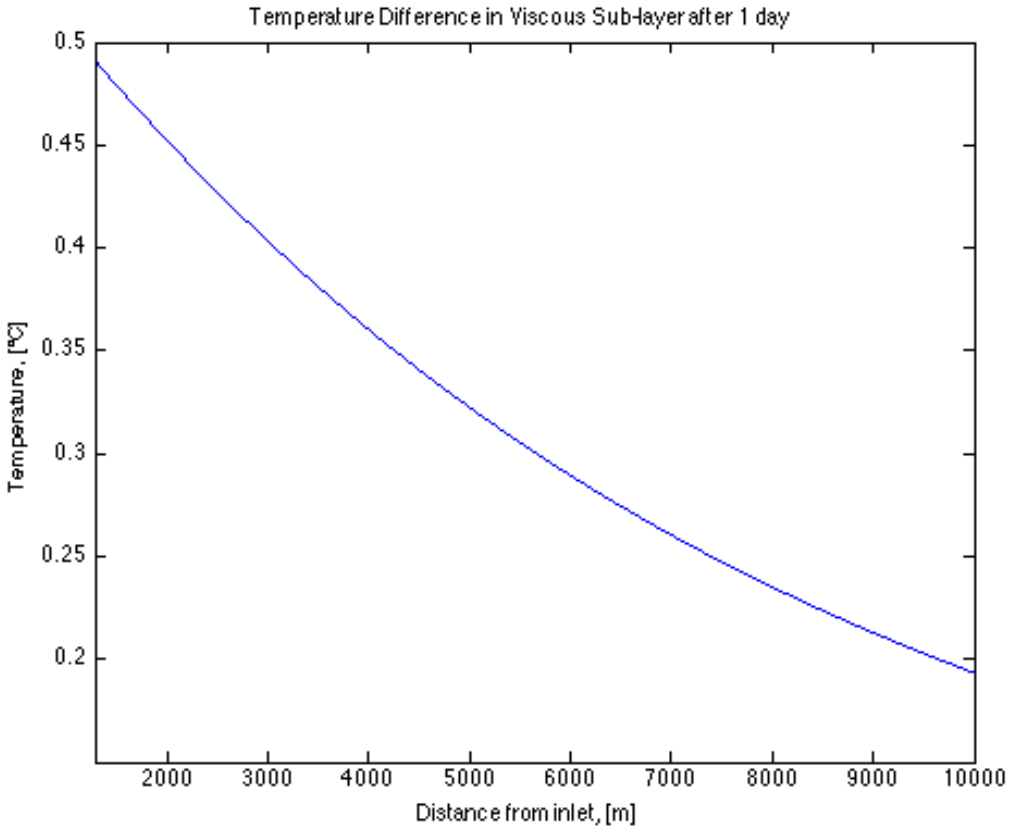

Figure J.4: Temperature difference across the viscous sub-layer after 24 hours. The maximum temperature difference is at 1284 meter, where the WAT is reached, explaining why the maximum deposit thickness is encountered here.

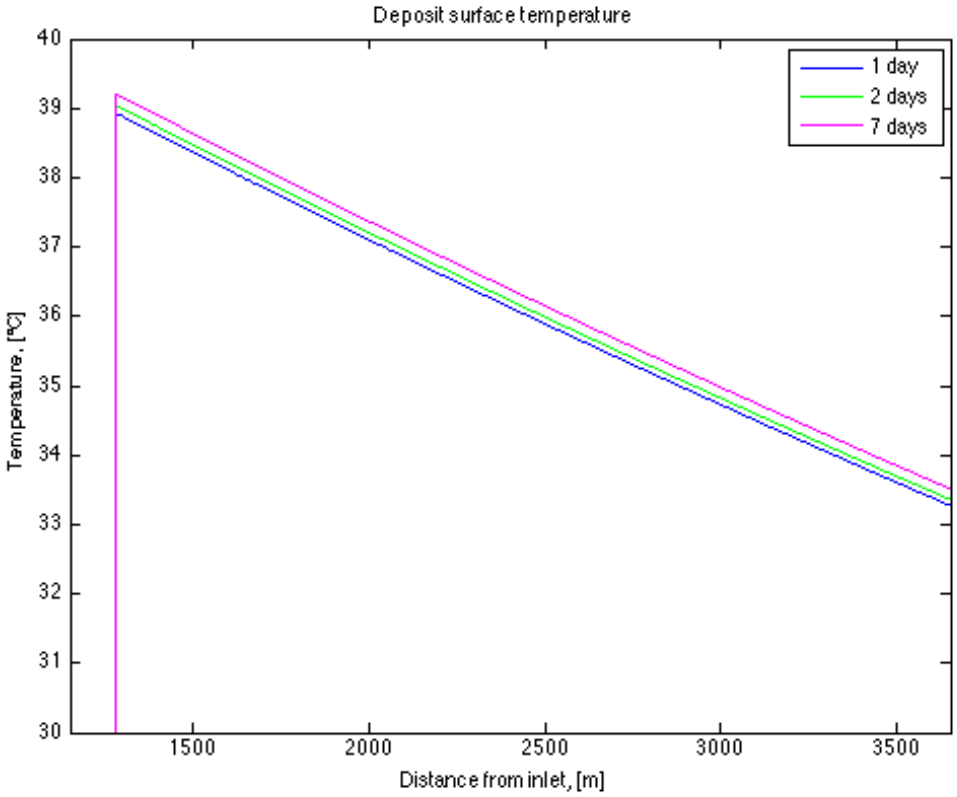

Figure J.5: Deposit surface temperature profiles after 1 day (blue), 2 days (green) and 7 days (pink) in a section of the pipe. The temperature at the deposit surface is found to increase with an increasing deposit thickness.

K Numerical Solution

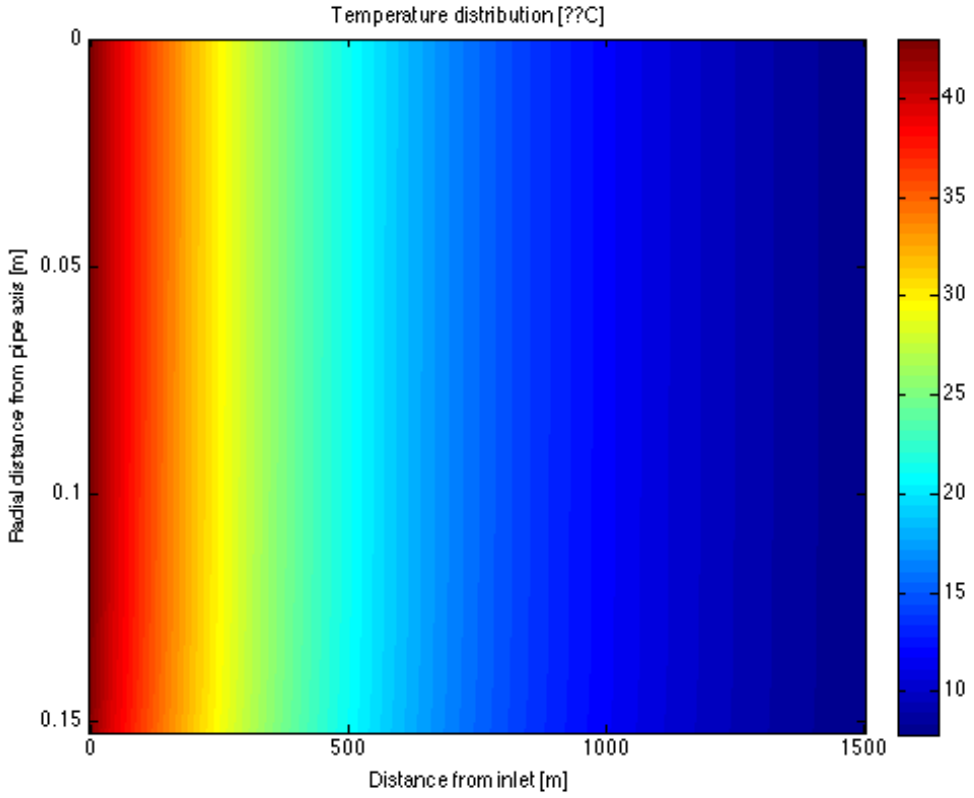

Figure K.1: Temperature profile in the pipeline after 24 hours obtained by the numerical model. The temperature in the near wall region is observed to be lower than the temperature in the bulk flow.

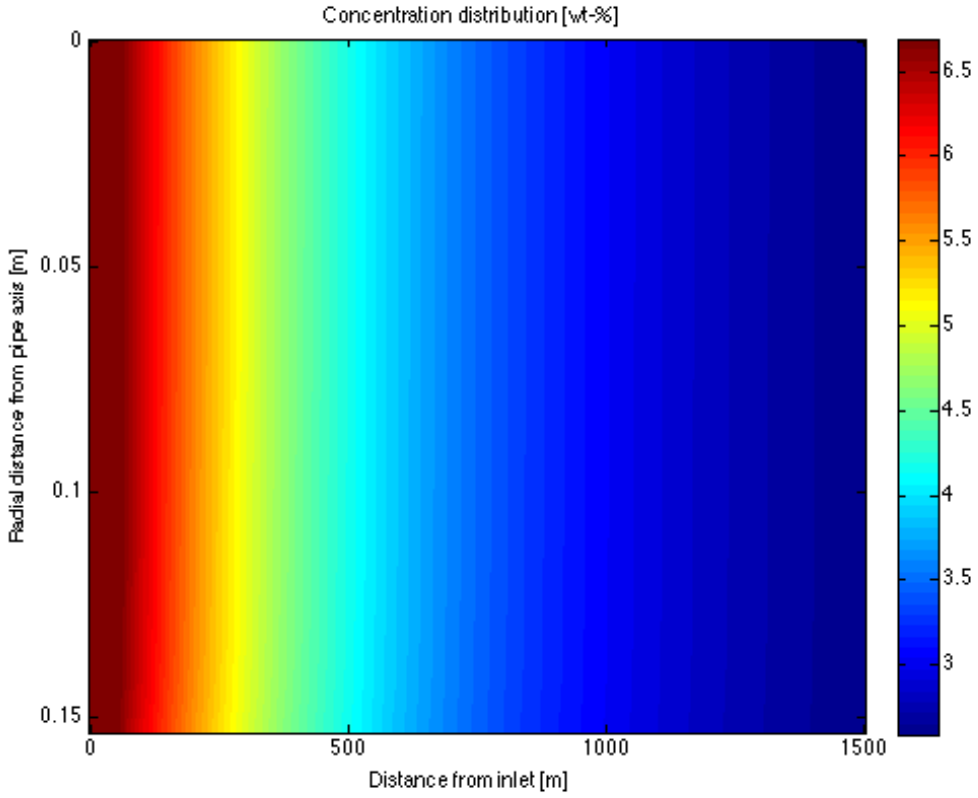

Figure K.2: Concentration profile in the pipeline after 24 hours obtained by the numerical model. The concentration profile is inferred from the temperature profile, and the concentration gradient in the near wall region is accordingly observed to be less than the concentration in the bulk flow.

L MATLAB I Effective Thermal Conductivity Calculations

Matlab Script 1 Program calculating the effective thermal conductivity of the wax deposit.

```
% Program computing the effective thermal conductivity of ...
    paraffin wax deposits by five different analytical methods

% Declaration of variables:
%   koil = thermal conductivity of oil,[W/(m.K)]
%   kwax = thermal conductivity of wax,[W/(m.K)]
%   kdep = effective thermal conductivity of paraffin wax ...
    deposit,[(W/m.K)]
%   Fw = weight fraction of wax in deposit
%
%   Effective thermal conductivity models:
%   kdep1 = the Parallel Model,[W/(m.K)]
%   kdep2 = the Series Model,[W/(m.K)]
%   kdep3 = Maxwell-Eucken 1,[W/(m.K)]
%   kdep4 = Maxwell-Eucken 2,[W/(m.K)]
%   kdep5 = EMT,[W/(m.K)]
%
%   Vwax = volume fraction of wax in deposit
%   Voil = volume fraction of oil in deposit
%
%   a,b,c,k1 and k2 = temporary variables for computation
%
%   Assumption: The average oil and wax molecules are of equal size.
% ***************************************************************
Fw = 0.05:0.0001:0.7;
number = length(Fw);
kwax = 0.25;
koil = 0.10;

% Initialization of matrices
kdep1 = zeros(number,1);
kdep2 = zeros(number,1);
kdep3 = zeros(number,1);
kdep4 = zeros(number,1);
kdep5 = zeros(number,1);

for i = 1:number
    Vwax(i) = Fw(i);
    Voil(i) = (1-Fw(i)) ;
end

% Parallel Model
for i = 1:number
    kdep1(i) = kwax*Fw(i) + koil*(1-Fw(i));
end
```

```
% Series Model
for i = 1:number
    kdep2(i)=1/((Fw(i)./kwax)+((1-Fw(i))./koil));
end

% Maxwell-Eucken 1 (ME1) with oil as the continuous phase and ...
    wax as the dispersed phase
    for i = 1:number
        kdep3(i) = ...
            (koil*Voil(i)+kwax*Vwax(i)*(3*koil/(2*koil+kwax)))./...
                (Voil(i)+Vwax(i)*((3*koil)/(2*koil+kwax)));
    end

% Maxwell-Eucken 2 (ME2) with wax as the continuous phase and ...
    oil as the dispersed phase
    for i = 1:number
        kdep4(i) = ...
            (kwax*Vwax(i)+koil*Voil(i)*(3*kwax/(2*kwax+koil)))./...
                    (Vwax(i)+Voil(i)*((3*kwax)/(2*kwax+koil)));
    end

% Effective Medium Theory (EMT) Model
 for i = 1:number

    a = -2*(Vwax(i)+Voil(i));
    b = 2*(Vwax(i)*kwax+Voil(i)*koil)-Voil(i)*kwax-Vwax(i)*koil;
    c = kwax*koil*(Vwax(i)+Voil(i));
    k1 = -b/(2*a) + sqrt(b^2-4*a*c)/(2*a);
    k2 = -b/(2*a) - sqrt(b^2-4*a*c)/(2*a);

        if k1 >= 0
            kdep5(i) = k1;
        else
            kdep5(i) = k2;
        end
 end
```

M MATLAB II Thermal Resistance

Matlab Script 2 Program calculating the thermal resistance in the pipeline.

```
% Program calculating the thermal resistance in the pipeline

% Declaration of variables:
%   d = inner pipe diameter, [m]
%   dr_wall = wall thickness, [m]
%   dz = differential in axial direction, [m]
%   rd = effective pipe radius, [m]
%   ri = inner pipe radius, [m]
%   ro = outer pipe radius, [m]
%
%   Ad = area of wax deposit (at solid/liquid interface), [m^2]
%   Ai = inside area of pipe, [m^2]
%   Ao = outside area of pipe, [m^2]
%
%   Alm_d = log mean area of deposit, [m^2]
%   Alm_p = log mean area of pipe, [m^2]
%
%   q = heat transfer rate (heat flux), [W]
%
%   hi = inner convective heat coefficient
%   ho = outer convective heat coefficient
%
%   Ri = inner resistance
%   Rd = resistance of deposit
%   Rp = resistance of pipe
%   Ro = outer resistance
%   Rtot = total resistance
%
%   u = flow velocity, [m/s]
%   mu = oil viscosity [mPs.s]
%   Utot_init = overall heat transfer coefficient, [W/m^2.K]
%   rho_oil = oil density, [kg/m^3]
%   Cp = heat capacaty of oil, [J/kg.K]
%
%   Fw = weight fraction of wax in deposit
%
%   koil = thermal conductivity of oil
%   kwax = thermal conductivity of wax
%   kpipe = thermal conductivity of pipe
%
%   kdep = effective thermal conductivity of deposit
%
%   Vwax = volume of wax in deposit
%   Voil = volume of oil in deposit
%
%   a,b,c,k1 and k2 = temporary variables for computation
%   Assumption: The oil and wax molecules are of equal size.
% ************************************************************
```

```
% Input variables:
d = 0.3048;
dr_wall = 0.012;
dz = 1;
ri = d/2;
ro = ri + dr_wall;
kwax = 0.25;
koil = 0.1;
kpipe = 20;
u = 2;
mu = 0.5*10^-3;
Utot_init = 20;
rho_oil = 750;
Cp = 2300;

Fw = [0.05,0.2,0.4,0.5,0.7];
number = length(Fw);

Δ = 0.00005:0.00005:0.02;
step = length(Δ);
rd = zeros(1,step);

Re = (rho_oil*u*d)/mu;
Pr = (Cp*mu)/koil;

% Inner convective heat transfer coefficient calculated by the ...
    Dittus-Boelter Correlation
Nu = 0.023*Re^0.8*Pr^0.3;
hi = (Nu*koil)/d;

% Initializing the matrices
kdep = zeros(number,1);

Vwax = zeros(number,1);
Voil = zeros(number,1);

for i = 1:number
    Vwax(i) = Fw(i);
    Voil(i) = (1-Fw(i));
end

Ad = zeros(number,step);
Alm_d = zeros(number,step);

Ri = zeros(number,step);
Rd = zeros(number,step);
Ri_contr = zeros(number,step);
Rd_contr = zeros(number,step);
Rp_contr = zeros(number,step);
Ro_contr = zeros(number,step);
Rtot = zeros(number,step);
Utot = zeros(number,step);
sum = zeros(number,step);
```

```
% Calculating the inner and outer area of the pipe
Ai = 2*pi()*ri*dz;
Ao = 2*pi()*ro*dz;
Alm_p = (Ao-Ai)/log(Ao/Ai);

% Calculating the heat resistance from the pipe
Rp = (ro-ri)/(kpipe*Alm_p);
hp = 1/Rp;

% Calculating the outer heat resistance
Rtot_init = 1/Utot_init;
ho = 1/(Rtot_init-1/hi-1/hp);
Ro = 1/(ho*Ao);

for i = 1:number

 % Effective Medium Theory (EMT)
    a = -2*(Vwax(i)+Voil(i));
    b = 2*(Vwax(i)*kwax+Voil(i)*koil)-Voil(i)*kwax-Vwax(i)*koil;
    c = kwax*koil*(Vwax(i)+Voil(i));
    k1 = -b/(2*a) + sqrt(b^2-4*a*c)/(2*a);
    k2 = -b/(2*a) - sqrt(b^2-4*a*c)/(2*a);

    if k1 ≥ 0
        kdep(i) = k1;
    else
        kdep(i) = k2;
    end

% Calculating the heat resistance contributions
    for j = 1:step

        % For each iteration, the effective flow radius is ...
           calculated
        rd(j) = ri - Δ(j);

        % The deposit area is calculated from the effective flow ...
           radius
        Ad(i,j) = 2*pi()*rd(j)*dz;
        Alm_d(i,j) = (Ai-Ad(i,j))./log(Ai./Ad(i,j));

        % Thermal resistance calculations
        Ri(i,j) = 1./(hi.*Ad(i,j));
        Rd(i,j) = (ri-rd(j))./(kdep(i).*Alm_d(i,j));
        Rtot(i,j) = Ri(i,j)+Rd(i,j)+Rp+Ro;
        Utot(i,j) = 1/(Rtot(i,j).*Ad(i,j));
        Ri_contr(i,j) = (Ri(i,j)./Rtot(i,j))*100;
        Rd_contr(i,j) = (Rd(i,j)./Rtot(i,j))*100;
        Rp_contr(i,j) = (Rp./Rtot(i,j))*100;
        Ro_contr(i,j) = (Ro./Rtot(i,j))*100;
        sum(i,j) = Ri_contr(i,j) + Rd_contr(i,j) + Rp_contr(i,j) ...
           + Ro_contr(i,j);
    end
```

N MATLAB III Interface Temperatures

Matlab Script 3 Program calculating the inner pipe wall temperature, the outer pipe wall temperature and the temperature at the deposit surface.

```
% Program calculating the temperatures at the different interfaces.

% Declaration of variables:
%   d = inner pipe diameter, [m]
%   dr_wall = pipe wall thickness, [m]
%   rd = effective pipe radius, [m]
%   ri = inner pipe radius, [m]
%   ro = outer pipe radius, [m]
%   mu = dynamic viscosity of oil or condensate, [Pa.s]
%   rho_oil = density of oil, [kg/m^3]
%   u = average flow velocity, [m/s]
%   Q = volumetric flow rate, [m^3/s]
%   m = mass flow, [kg/s]
%   Cp = heat capacity of oil, [J/kg.K]
%   Tb = bulk temperature, [ C ]
%   Td = temperature at solid/liquid interface, [ C ]
%   Twall_in = inner wall temperature, [ C ]
%   Two = outer wall temperature, [ C ]
%   Tsea = ambient temperature, [ C ]
%   Tcheck = control variable, [ C ]
%   Fw = wax fraction in deposit
%   ∆ = deposit thickness, [m]
%   Re = Reynolds number
%   Pr = Prandtl number
%   Nu = Nusselt number
%   Across = pipe cross section area, [m^2]
%   Ad = area of wax deposit (at solid/liquid interface), [m^2]
%   Ai = inside area of pipe, [m^2]
%   Ao = outside area of pipe, [m^2]
%   Alm_d = log mean area of deposit, [m^2]
%   Alm_p = log mean area of pipe, [m^2]
%   q = heat transfer rate (heat flux), [W]
%   hi = inner convective heat coefficient, [W/m^2.K]
%   ho = outer convective heat coefficient, [W/m^2.K]
%   koil = thermal conductivity of oil, [W/(m.K)]
%   kwax = thermal conductivity of wax, [W/(m.K)]
%   kdeposit = thermal conductivity of deposit, [W/(m.K)]
%   kpipe = thermal conductivity of pipe, [W/(m.K)]
%   Ri = inner resistance, [W/(m^2.K)]
%   Rd = resistance of deposit, [W/(m^2.K)]
%   Rp = resistance of pipe, [W/(m^2.K)]
%   Ro = outer resistance, [W/(m^2.K)]
%   Rtot = total resistance, [W/(m^2.K)]
%   frac, thick = loop counters (for iteration)
% ****************************************************************
```

```
% Assigning input values:
d = 0.3048;
dr_wall = 0.012;
dz = 1;
Tsea = 5;
Tb = 53;
u = 2;
U = 20;
rho_oil = 750;
Cp = 2300;
mu = 0.5*10^-3;

kwax = 0.25;
koil = 0.1;
kpipe = 20;

Δ = 0.00001:0.00001:0.02;
Fw = [0.05,0.2,0.4,0.5,0.7];
thick = length(Δ);
frac = length(Fw);
ri = d/2;
ro = ri + dr_wall;
Across = pi()*ri^2;
Q = u*Across;
m = Q*rho_oil;

Re = (rho_oil*u*d)/mu;
Pr = (Cp*mu)/koil;
Nu = 0.023*Re^0.8*Pr^0.3;
hi = (Nu*koil)/d;

% Initialization of matrices
kdeposit = zeros(1,frac);
diffTd = zeros(1,frac);
diffTwi = zeros(1,frac);
diffTwo = zeros(1,frac);
diffTch = zeros(1,frac);
rd = zeros(1,thick);
Ad = zeros(1,thick);
Alm_d = zeros(1,thick);
Rd = zeros(frac,thick);
Rtot = zeros(frac,thick);
q = zeros(frac,thick);
Td = zeros(frac,thick);
Twi = zeros(frac,thick);
Two = zeros(frac,thick);
Tcheck = zeros(frac,thick);
ΔTd = zeros(frac,thick);
ΔTp = zeros(frac,thick);
```

```
Ao = 2*pi()*ro*dz;
Alm_p = (Ao-Ai)/log(Ao/Ai);

R = 1/U;
Ri = 1/(hi*Ai);
Rp = (ro-ri)/(kpipe*Alm_p);
hp = 1/Rp;
ho = 1/(R-1/hi-1/hp);
Ro = 1/(ho*Ao);

for j = 1: frac
    for i = 1:thick
    rd(1,i) = ri - Δ(1,i);
    Ad(1,i) = 2*pi()*rd(1,i)*dz;
    Alm_d(1,i) = (Ai-Ad(1,i))./log(Ai./Ad(1,i));

    % Effective Medium Theory (EMT)
    a = -2*(Vwax(i)+Voil(i));
    b = 2*(Vwax(i)*kwax+Voil(i)*koil)-Voil(i)*kwax-Vwax(i)*koil;
    c = kwax*koil*(Vwax(i)+Voil(i));
    k1 = -b/(2*a) + sqrt(b^2-4*a*c)/(2*a);
    k2 = -b/(2*a) - sqrt(b^2-4*a*c)/(2*a);

        if k1 ≥ 0
            kdeposit(1,j) = k1;
        else
            kdeposit(1,j) = k2;
        end

    Rd(j,i) = (ri-rd(1,i))./(kdeposit(1,j).*Alm_d(1,i));
    Rtot(j,i) = Ri+Rd(j,i)+Rp+Ro;
    q(j,i) = (Tsea-Tb)./Rtot(j,i);

    Td(j,i) = Tb+(q(j,i).*Ri);
    Twi(j,i) = Td(j,i)+(q(j,i).*Rd(j,i));
    Two(j,i) = Twi(j,i)+(q(j,i).*Rp);
    Tcheck(j,i) = Two(j,i)+(q(j,i).*Ro);

    ΔTd(j,i) = Td(j,i)-Twi(j,i);
    ΔTp(j,i) = Twi(j,i)-Two(j,i);
    diffTd(1,j) = (1-Td(j,thick)./Td(j,1))*100;
    diffTwi(1,j) = (1-Twi(j,thick)./Twi(j,1))*100;
    diffTwo(1,j) = (1-Two(j,thick)./Two(j,1))*100;

    end
end
```

O MATLAB IV Analytical Wax Deposit Model

Matlab Script 4 Analytical wax deposit model.

```
%Program calculating the wax deposit thickness by calling ...
    associated functions.

% Declaration of variables:
%   ni = number of steps in radial direction
%   nj = number of steps in aksial direction
%   dr = differential in radial direction
%   dz = differential in lateral direction
%   d = inner pipe diameter, [m]
%   ri = inner pipe radius, [m]
%   dr_wall = pipe wall thickness, [m]
%   ro = outer pipe radius, [m]
%   L = pipe length, [m]
%   Across = pipe cross section area
%   Tsea = ambient temperature, [ C ]
%   Ti = inlet temperature, [ C ]
%   WAT = Wax Appearance Temperature, [ C ]
%   Tsection = temporary storage variabel for calculations, [ C ]
%   mu = dynamic viscosity of oil or condensate, [Pa.s]
%   nu = kinematic viscosity of oil or condensate, [m^2/s]
%   rho_oil = density of oil, [kg/m^3]
%   u = average flow velocity, [m/s]
%   Q = volumetric flow rate, [m^3/s]
%   m = mass flow, [kg/s]
%   Re = Reynolds number
%   Pr = Prandtl number
%   Cp = heat capacity of oil
%   hi = inner convective heat transfer coefficient
%   ho = outer convective heat transfer coefficient
%   U = overall heat transfer coefficient
%   koil = thermal conductivity of oil, [W/(m.K)]
%   kwax = thermal conductivity of wax, [W/(m.K)]
%   kpipe = thermal conductivity of pipe, [W/(m.K)]
%   kdeposit = thermal conductivity of deposit, [W/(m.K)]
%   Fw = wax fraction in deposit
%   Va = molecular volume of wax
%   Δ = initial deposit thickness
%   y = actual distance from pipe wall, [m]
%   f = friction factor
%   u_star = friction velocity
%   y_p = dimensionless wall distance
%   Tw = inner wall temperature [ C ]
%   qdivA = heat flux, [q/A]
% ****************************************************************

% Input values:
L = 10000;
d = 0.3048;
nj = L;
dz = L/nj;
```

```
Tsea = 5;
Ti = 43;
u = 2;
rho_oil = 750;
Cp = 2300;
Va = 430;
mu = 0.5*10^-3;
Δ = 10^-12;
Fw = 0.4;
y_p = 5;
U = 20;
WAT = 39;

kwax = 0.25;
koil = 0.1;
kpipe = 20;

Re = (rho_oil*u*d)/mu;
Pr = (Cp*mu)/koil;
Nu = 0.023*Re^0.8*Pr^0.3;
hi = (Nu*koil)/d;

gamma = 10.2/Va-0.791;

ri = d/2;
dr_wall = 0.012;
ro = ri + dr_wall;

Across = pi()*ri^2;
Q = u*Across;
m = Q*rho_oil;

dt = 3600;
t_final = dt*24*7;
t = 0:dt:t_final;
time = t_final/dt;

Vwax = Fw;
Voil = (1-Fw);

% Effective Medium Theory (EMT)
    a = -2*(Vwax+Voil);
    b = 2*(Vwax*kwax+Voil*koil)-Voil*kwax-Vwax*koil;
    c = kwax*koil*(Vwax+Voil);
    kdep1 = -b/(2*a) + sqrt(b^2-4*a*c)/(2*a);
    kdep2 = -b/(2*a) - sqrt(b^2-4*a*c)/(2*a);

    if kdep1 ≥ 0
        kdeposit = kdep1;
    else
        kdeposit = kdep2;
    end
```

```
temperatureL = tempL(Tsea,Ti,U,d,Cp,dz,nj,time,m);
[depThick,Tdep,Twin,Two,Tsub] = deposit(Δ,ri,ro,hi,kpipe,...
kdeposit,Tsea,temperatureL,dz,nj,time,mu,Va,gamma,WAT,dt,y_p,Cp,...
Re,U,rho_oil,Pr,u);
```

Matlab Script 5 Function calculating the average bulk flow temperature.

```
function temperatur = tempL(Tsea,Ti,U,d,Cp,dz,nj,time,m)

temperatur = zeros(time,nj);
temperatur(:,1) = Ti;

for i = 1:time
    Tsection = Ti;

    for j = 2:nj
        temperatur(i,j) = Tsea + ...
            (Tsection-Tsea)*exp((-U*pi()*d*dz)/(m*Cp));
        Tsection = temperatur(i,j);
    end
end

end
```

Matlab Script 6 Function calculating the temperature in viscous sub-layer.

```
function [Tsub,y] = tempSub(rho,Pr,mu,u,y_p,q,Tw,Cp,Re)

f = 0.305/Re^0.25;
u_star = u*sqrt(f/8);

Tw_p = Tw*(rho*Cp*u_star)/(-q);

if y_p ≤ 5
    T_p = Tw_p + Pr*y_p;
elseif y_p > 5 || y_p < 30
    T_p = Tw_p + (5*Pr + 5*log(0.2*Pr*y_p+(1-Pr)));
else
    T_p = Tw_p + (5*Pr + 5*log(1+5*Pr) + 2.5*log(y_p/30));
end

Tsub = T_p*(-q)/(rho*Cp*u_star);
y = (y_p*mu)/(rho*u_star);

end
```

Matlab Script 7 Function calculating the deposit thickness and the temperatures at the inner pipe wall, the outer pipe wall and at the deposit surface.

```
function [depThick,Tdep,Twin,Two,Tsub] = ...
          deposit(thickness,ri,ro,hi,kpipe,kdep,Tsea,tempBulk,dz,...
          nj,time,mu,Va,gamma,WAT,dt,y_p,Cp,Re,U,rho,Pr,u)

Tdep = zeros(time,nj);
Twin = zeros(time,nj);
Two = zeros(time,nj);
Tcheck = zeros(time,nj);
Tsub = zeros(time,nj);

Ain = 2*pi()*ri*dz;
Ao = 2*pi()*ro*dz;
Alm_p = (Ao-Ain)/log(Ao/Ain);

Rpipe = (ro-ri)/(kpipe*Alm_p);
hpipe = 1/Rpipe;
R = 1/U;
ho = 1/(R-1/hi-1/hpipe);
Rout = 1/(ho*Ao);

Ad = zeros(time,nj);
Alm_d = zeros(time,nj);

Roil = zeros(time,nj);
Rdep = zeros(time,nj);
Rtot = zeros(time,nj);

q = zeros(time,nj);

rdep = zeros(time,nj);
rdep(1,:) = ri - thickness;
dr = zeros(time,nj);

depThick = zeros(time,nj);
depThick(1,:) = thickness;

conc_dep = zeros(time,nj);
conc_sub = zeros(time,nj);

Roil(1,:) = 1/(hi*Ain);
Rtot(1,:) = Roil(1,1)+Rpipe+Rout;
```

```
for j = 1:nj
    q(1,j) = (Tsea - tempBulk(1,j))/Rtot(1,1);
    Twin(1,j) = tempBulk(1,j)+(q(1,j)*Roil(1,1));
    Two(1,j) = Twin(1,j)+(q(1,j)*Rpipe);
    Tcheck(1,j) = Two(1,j)+(q(1,j)*Rout);
    Tsub(1,j) = tempSub(rho,Pr,mu,u,y_p,q(1,j),Twin(1,j),Cp,Re);
end

for i = 2:time
    for j = 1:nj

    if depThick(i-1,j) ≤ thickness;

    Alm_d(i,j) = 0;

    Roil(i,j) = 1/(hi*Ain);
    Rtot(i,j) = Roil(i,j)+Rpipe+Rout;

    q(i,j) = (Tsea-tempBulk(i,j))./Rtot(i,j);

    Twin(i,j) = tempBulk(i,j)+(q(i,j).*Roil(i,j));
    Two(i,j) = Twin(i,j)+(q(i,j).*Rpipe);
    Tcheck(i,j) = Two(i,j)+(q(i,j).*Rout);
    [Tsub(i,j),dr(i,j)] = ...
        tempSub(rho,Pr,mu,u,y_p,q(i,j),Twin(i,j),Cp,Re);

    if Tsub(i,j) < WAT

        conc_dep(i,j) = 0.0007*Twin(i,j)^2 + 0.00989*Twin(i,j) + ...
            1.7706;
        conc_sub(i,j) = 0.0007*Tsub(i,j)^2 + 0.00989*Tsub(i,j) + ...
            1.7706;

        depThick(i,j) = (13.3*10^-12*(Twin(i,j)^1.47*mu^gamma)/...
        Va^.71.*(conc_sub(i,j)-conc_dep(i,j))/(dr(i,j)*100)).*dt;

if depThick(i,j) ≥ ri
    fprintf('The pipe is clogged after %d hours/days at %d ...
        meter\n', i,j);
    return
end

    rdep(i,j) = ri - depThick(i,j);
    Ad(i,j) = 2*pi()*rdep(i,j)*dz;
    end
```

```
    else
    Alm_d(i,j) = (Ain-Ad(i-1,j))./log(Ain/Ad(i-1,j));

    Roil(i,j) = 1./(hi.*Ad(i-1,j));
    Rdep(i,j) = (ri-rdep(i-1,j))./(kdep.*Alm_d(i,j));
    Rtot(i,j) = Roil(i,j)+Rdep(i,j)+Rpipe+Rout;

    q(i,j) = (Tsea-tempBulk(i,j))./Rtot(i,j);

    Tdep(i,j) = tempBulk(i,j)+(q(i,j).*Roil(i,j));
    Twin(i,j) = Tdep(i,j)+(q(i,j).*Rdep(i,j));
    Two(i,j) = Twin(i,j)+(q(i,j).*Rpipe);
    Tcheck(i,j) = Two(i,j)+(q(i,j).*Rout);
    [Tsub(i,j),dr(i,j)] = tempSub(rho,Pr,mu,u,y_p,q(i,j),...
                          Tdep(i,j),Cp,Re);

    conc_dep(i,j) = 0.0007*Tdep(i,j)^2 + 0.00989*Tdep(i,j) + 1.7706;
    conc_sub(i,j) = 0.0007*Tsub(i,j)^2 + 0.00989*Tsub(i,j) + 1.7706;

    depThick(i,j) = depThick(i-1,j) + (13.3*10^-12.*(Tdep(i,j).^...
    1.47.*mu.^gamma)./Va.^0.71.*(conc_sub(i,j)-conc_dep(i,j))./...
    (dr(i,j)*100)).*dt;
    rdep(i,j) = ri - depThick(i,j);
    Ad(i,j) = 2*pi()*rdep(i,j)*dz;

if depThick(i,j) ≥ ri
    fprintf('The pipe is clogged after %d hours/days at %d ...
       meter\n', i,j);
return
end

    end
    end
end
end
```

P MATLAB Numerical Wax Deposit Model

Matlab Script 8 Numerical Wax Deposition Model.

```
%Program calculating the wax deposit thickness by calling ...
    associated functions.

% Declaration of variables:
%   ni = number of steps in axial direction
%   nj = number of steps in radial direction
%   dr = differential in radial direction
%   dz = differential in lateral direction
%   d = inner pipe diameter, [m]
%   ΔWall = wall thickness, [m]
%   r = radius at point of interest, [m]
%   ri = inner pipe radius, [m]
%   ro = outer pipe radius, [m]
%   rd = effective flow radius, [m]
%   L = pipe length, [m]
%   Across = pipe cross section area
%   Ad = area of deposit surface, [m^2]
%   Ai = inside area of pipe, [m^2]
%   Ao = outside area of pipe, [m^2]
%   Alm_d = log mean area of deposit, [m^2]
%   Alm_p = log mean area of pipe, [m^2]
%   q = heat transfer rate (heat flux), [W]
%   Twi = inner wall temperature, [ C ]
%   Two = outer wall temperature, [ C ]
%   Ti = inlet temperature, [ C ]
%   Td = temperature at deposit surface, [ C ]
%   Tb = average bulk flow temperature, [ C ]
%   Tsea = ambient temperature, [ C ]
%   Tcheck = control variable, [ C ]
%   WAT = Wax Appearance Temperature, [ C ]
%   alpha = thermal diffusivity of wax in oil mixtures, [m^2/s]
%   Dwo = mass diffusivity of wax in oil mixtures, [m^2/s]
%   mu = dynamic viscosity of oil or condensate, [Pa.s]
%   nu = kinematic viscosity of oil or condensate, [m^2/s]
%   rho_oil = density of oil, [kg/m^3]
%   rho_gel = density of wax, [kg/m^3]
%   asp = wax crystal aspect ratio
%   Fw = weight fraction of wax in deposit
%   Va = molecular volume of wax, [cm^3/mol]
%   gamma = correlation coefficient
%   Cp = specific heat capacity of oil, [J/kg.K]
%   E = activation energy, [J/K.mol]
%   kr_c = precipitation rate constant at WAT, [1/s]
%   Q = volumetric flow rate, [m^3/s]
%   u = average flow velocity, [m/s]
%   Re = Reynolds number
%   Pr = Prandtl number
%   Nu = Nusselt number
%   U = overall convective heat transfer coefficient, [W/m^2.K]
%   hi = inner convective heat transfer coefficient, [W/m^2.K]
```

```
%   ho = outer convective heat transfer coefficient, [W/m^2.K]
%   Rtot = total thermal resistance, [m^2.K/W]
%   Ri = inner resistance, [m^2.K/W]
%   Rd = resistance of deposit, [m^2.K/W]
%   Rp = resistance of pipe, [m^2.K/W]
%   Ro = outer resistance, [m^2.K/W]
%   k = thermal conductivity,[W/(m.K)]
%   koil = thermal conductivity of oil, [W/(m.K)]
%   kwax = thermal conductivity of wax, [W/(m.K)]
%   kpipe = thermal conductivity of pipe, [W/(m.K)]
%   kdeposit = thermal conductivity of deposit, [W/(m.K)]
%   dt = time step
%   t = final simlation time, [s]
%   Cw = concentration of wax in solution at the wall, [wt-%]
%   Ci = concentration of wax in solution at the inlet, [wt-%]
%   kr = precipitation rate constant, [1/s]
%   Sc = Schmidt number
%   Sc_T = turbulent Schmidt number
%   C = concentration matrix
%   A_C = coefficient matrix
%   D_C = D-vector
%   gamma = diffusive constant
%   vz_p = dimensionless turbulent velocity, Vz+
%   f = friction factor
%   eddyDiffusivity = diffusion rate coefficient, [m^2/s]
%   C1 = correlation constant
%   C2 = correlation constant
%   y_p = dimensionless distance from wall, y+
%   y1 = dimensionless distance at radius r
%   y2 = dimensionless distance at radius (r+dr)
%   dy = difference between y1 and y2
%   dv = dimensionless velocity difference between y1 and y2
%   dvdy = derivative of dimensionless velocity to dimensionless ...
    distance
%   kr_c = precipitaion rate constant at the cloud point ...
    temperature, [1/s]
%   Tc = cloud point temperature, or WAT, [ C ]
%   T = temperature at position of interest, [ C ]
%   E = activation energy, [J/mol]

% Input values:
d = 0.3048;
ΔWall = 0.012;
L = 1500;
ni = L;
nj = 100;
Tsea = 5;
Ti = 43;
WAT = 39;
u = 2;
U = 20;
```

```
Δ = 10^-12;
ri = d/2;
rd = ri-Δ;
ro = ri+ΔWall;
kr_c = 1.4;
E = 37700;
Fw = 0.4;
Fwi = 0.05;
kwax = 0.25;
koil = 0.1;
kpipe = 20;
mu = 0.5*10^-3;
Va = 430;
rho_oil = 750;
rho_gel = 750;
Cp = 2300;
asp = 3;
gamma=10.2/Va-0.791;
nu = mu/rho_oil;
Re = u*d/nu;
alpha = koil/(rho_oil*Cp);
Pr=nu/alpha;
Nu = 0.023*Re^0.8*Pr^0.3;
hi = (Nu*koil)/d;
Across = pi()*ri^2;
Q = u*Across;
dr=ri/nj;
dz=L/ni;
Ai = 2*pi()*ri*dz;
Ao = 2*pi()*ro*dz;
Alm_p = (Ao-Ai)/log(Ao/Ai);
Rtotal = 1/U;
Rp = (ro-ri)/(kpipe*Alm_p);
hp = 1/Rp;
ho = 1/(Rtotal-1/hi-1/hp);
Ro = 1/(ho*Ao);
dt = 3600;
t_final = dt*24*7;
time = t_final/dt;
z=linspace(0,L,ni);
r=linspace(0,ri,nj);

if true % For folding and cell execution

rdnew = zeros(time+1,ni);
rdnew(1,:) = rd;
R=rdnew;
```

```
dmdt = zeros(time,ni);
Δ = zeros(time,ni);
Δ_in = 0;

Fwax = zeros(time+1,ni);

K = zeros(time,ni);
Dwo = zeros(time,ni);
dC = zeros(time,ni);
dCb = zeros(time,ni);

waxFrac = zeros(time,ni);
depThickness = zeros(time,ni);

T=zeros(nj,ni,time);
C=T;

% Calling functions and performing simulations:
for t = 1:time

    T(:,:,t) = ...
       temperature(ni,nj,ri,rdnew(t,:),ro,nu,Tsea,Ti,alpha,...
               dr,dz,Fwi,hi,ho,kwax,koil,kpipe,Pr,u,Re);
    kr = kr_generator(ni,nj,T(:,:,t),gamma,WAT,kr_c,E,Re);
    C(:,:,t) = ...
       concentration(ni,nj,rdnew(t,:),nu,Ti,T(:,:,t),mu,Va,...
               gamma,kr,dr,dz,u,Re);
    C(:,:,t) = wat_solubility(nj,ni,C(:,:,t),WAT);

    for i = 1:ni
        dC(t,i) = C(end,i,t)-C(end-1,i,t);
        dCb(t,i) = C(1,i,t)-C(end,i,t);

        if dC(1,i)<0
            Fwax(1,i) = Fwi;
        end

        if dC(t,i) == 0
            Dwo(t,i) = 0;
        else
            K(t,i) = T(end,i,t)+273.15;
            Dwo(t,i) = ...
                13.3*10^-12*(K(t,i)^1.47.*mu^gamma)./(Va^0.71);
        end

     [Fwax(t+1,i),depThick(t,i),rdnew(t+1,i),Sh(t,i),dFwdt(t,i),...
     drddtout(t,i),De(t,i),kM(t,i)] = FwdepThick(asp,ri,rho_gel,...
     dr,dt,rdnew(t,i),Fwax(t,i),Dwo(t,i),dC(t,i),dCb(t,i));
    end
end
```

Matlab Script 9 Function calculating the temperature profile in the pipeline.

```
function [T] = ...
    temperature(ni,nj,ri,rd,ro,nu,Tsea,Ti,alpha,dr,dz,Fw,hi,...
                ho,kwax,koil,kpipe,Pr,u,Re)

% Initializing the temperature grid
T = zeros(nj,ni);
T(:,1) = Ti;
T(nj,1) = Tw(Tsea,Ti,dz,Fw,hi,ho,kwax,koil,kpipe,rd(1,1),ri,ro);
Tb = zeros(1,ni);
Tb(1,1) = Ti;

% Initializing the coefficient matrix
A_T=zeros(nj,nj); A_T(nj,nj) = 1; A_T(1,1)=1; A_T(1,2)=-1;

for j=2:nj-1
% Calculating thermal diffusivities at different radial positions
    alpha1=alpha_tot(dr*(j-1));
    alpha2=alpha_tot(dr* (j) );
    alpha3=alpha_tot(dr*(j+1));

    vz=velocity(j*dr,ri,nu,u,Re);

% Writing the coefficient matrix
    A_T(j,j-1)=-1/(2*j*dr^3)*(j*dr*alpha2+(j-1)*dr*alpha1);
    A_T(j,j)=vz/dz+1/(2*j*dr^3)*(2*j*dr*alpha2+(j+1)*dr*alpha3+...
    (j-1)*dr*alpha1);
    A_T(j,j+1)=-1/(2*j*dr^3)*((j+1)*dr*alpha3+j*dr*alpha2);
end

% Initializing the D-vector
D_T=ones(nj,1); D_T(1)=0;

% Iterating along the pipe from inlet to outlet
for i=2:ni   % z-direction
    T(nj,i)=T(nj,i-1);
    T(nj-1,i)=T(nj,i-1);

% Producing the D-vector
    for j=2:nj-1
        vz=velocity(j*dr,ri,nu,u,Re);
        D_T(j)=T(j,i-1)*vz/dz;
    end

    D_T(nj) = Tw(Tsea,Tb(1,i-1),dz,Fw,hi,ho,kwax,koil,kpipe,...
    rd(1,i),ri,ro);

% Solving the linear system
    T(:,i)=A_T\D_T;
    T(1,i)=T(2,i);
    Tb(i)=T(1,i);
end
```

```
% Sub-function calculating the total thermal diffusivity
function alpha_t = alpha_tot(r)

    if Re > 4000
        Pr_T=0.85+0.015/Pr;
        alpha_t=alpha+eddyDiffusivity(r,ri,dr,Re)*Pr/Pr_T*alpha;
    else
        alpha_t = alpha;
    end
end

end
```

Matlab Script 10 Function calculating the temperature at the inner wall, the outer wall and at the deposit surface.

```
function Td = Tw(Tsea,Tb,dz,Fw,hi,ho,kwax,koil,kpipe,rd,ri,ro)

Vwax = Fw;
Voil = 1-Fw;

% Effective Medium Theory (EMT)
a = -2*(Vwax+Voil);
b = 2*(Vwax*kwax+Voil*koil)-Voil*kwax-Vwax*koil;
c = kwax*koil*(Vwax+Voil);
kdep1 = -b/(2*a) + sqrt(b^2-4*a*c)/(2*a);
kdep2 = -b/(2*a) - sqrt(b^2-4*a*c)/(2*a);

if kdep1 >= 0
    kdeposit = kdep1;
else
    kdeposit = kdep2;
end

Ad = 2*pi().*rd*dz;
Ai = 2*pi()*ri*dz;
Ao = 2*pi()*ro*dz;

Alm_d = (Ai-Ad)./log(Ai./Ad);
Alm_p = (Ao-Ai)./log(Ao./Ai);

Ri = 1/(hi*Ai);
Rd = (ri-rd)/(kdeposit.*Alm_d);
Rp = (ro-ri)/(kpipe*Alm_p);
Ro = 1/(ho*Ao);
Rtot = Ri+Rd+Rp+Ro;

q = (Tsea-Tb)./Rtot;

Td = Tb+(q.*Ri);
Twall_in = Td+(q*Rd);
Two = Twall_in+(q*Rp);
Tcheck = Two+(q*Ro);

end
```

Matlab Script 11 Function calculating the concentration profile in the pipeline.

```
function [C] = concentration(ni,nj,R,nu,Ti,T,mu,Va,gamma,kr,dr,...
               dz,u,Re)

% Initializing the concentration grid
    C = zeros(nj,ni);
    C(:,1) = solubility(Ti);
    C(nj,1)= solubility(T(nj,1));

% Initializing the coefficient matrix and D-vector
A_C=zeros(nj,nj-1); A_C(1,1)=1; A_C(1,2)=-1; A_C(nj,nj)=1;
D_C=ones(nj,1); D_C(1)=0; D_C(nj)=solubility(T(nj,1));

% Iterating over the pipe from inlet to outlet
for i=2:ni
    for j=2:nj-1
    % Calculating mass diffusivities at different radial positions
        Dwo1=Dwo_tot(dr,(j-1),i);
        Dwo2=Dwo_tot(dr, (j) ,i);
        Dwo3=Dwo_tot(dr,(j+1),i);
        vz=velocity(j*dr,R(i),nu,u,Re);
        %size(velocity(j*dr,R(i),nu,u,Re))

    % Computing a new coefficient matrix for each axial step
        A_C(j,j-1)=-1/(2*j*dr^3)*(j*dr*Dwo2+(j-1)*dr*Dwo1);
        A_C(j,j)=vz/dz+1/(2*j*dr^3)*(2*j*dr*Dwo2+(j+1)*dr*Dwo3+(j-1)...
            *dr*Dwo1)+kr(j,i);
        A_C(j,j+1)=-1/(2*j*dr^3)*((j+1)*dr*Dwo3+j*dr*Dwo2);

    % Computing a new D-vector for each axial step
        D_C(j)=C(j,i-1)*vz/dz+kr(j,i)*solubility(T(j,i));
    end

    D_C(nj) = solubility(T(nj,i));

    % Matrix inversion
    C(:,i)=A_C\D_C;
    C(1,i)=C(2,i);
end

% Sub-function calculating the total mass diffusivity
function Dwo_t = Dwo_tot(dr,j,i)
%
% Calculating the diffusion coefficient from the Hayduk Minhas ...
   correlation
    Dwo=13.3*10^-12*(T(j,i)+273.15)^1.47*mu^gamma/Va^0.71;
```

```
    if Re > 4000
        Sc=nu/Dwo;
        Sc_T=0.85+0.015/Sc;
        Dwo_t=Dwo+eddyDiffusivity(j*dr,R(i),dr,Re)*Sc/Sc_T*Dwo;
    else
        Dwo_t = Dwo;
    end
end

end
```

Matlab Script 12 Function calculating the solubility of wax in oil.

```
function [solubility] = solubility(T)
    solubility= 0.0007*T^2 + 0.0989*T + 1.7706;
end
```

Matlab Script 13 Function calculating the maximum solubility of wax in oil.

```
function [wat_sol] = wat_solubility(nj,ni,C,Tc)

wat_sol = zeros(nj,ni);
deposited = 0;

solubility_Tc= 0.0007*Tc^2 + 0.0989*Tc + 1.7706;

    for i=1:ni
        for j=1:nj
        if deposited
            wat_sol(j,i) = max(0, solubility_Tc - C(j,i));
        else
            wat_sol(j,i) = min(C(j,i), solubility_Tc);
        end
    end

end
```

Matlab Script 14 Function calculating the precipitation rate constant.

```
function [kr] = kr_generator(ni,nj,T,gamma,Tc,kr_c,E,Re)

    kr = zeros(size(T));
    for j=1:nj
        for i=1:ni
            if Re < 2300 || T(j,i) > Tc
                kr(j,i) = 0;
            else
                kr(j,i) = ...
                    kr_c*(T(j,i)/Tc)^1.47*exp(((gamma*E)/8.314)*...
                     ((1/T(j,i))-(1/Tc)));
        end
    end
end
```

Matlab Script 15 Function calculating the eddy diffusivity.

```
function eddyDiff = eddyDiffusivity(r,R,dr,Re)

C1=0.4;
C2=26;

f=0.305/Re^0.25;
y2=y_p(r+dr);
y1=y_p(r);
dv=vz_p(y2)-vz_p(y1);
dy=y2-y1;
dvdy=dv/dy;

% Calculating the eddy diffusivity by Van Driests equation
    eddyDiff=(C1.*y_p(r)).^2.*(1-exp(-y_p(r)/C2)).^2.*dvdy;

% Calculating the dimensionless turbulent velocity by the von Karman
% correlation
    function vz_p = vz_p( y_p )
        if (y_p≤5)
            vz_p=y_p;
        elseif (5≤y_p≤30)
            vz_p=5*log(y_p)-3.05;
        else
            vz_p=2.5*log(y_p)+5.5;
    end
end

% Calculating the dimensionless distance from the wall
    function y_p=y_p(r)
        y_p =(1-r/R)*Re/2*sqrt(f/8);
    end
end
```

Matlab Script 16 Function calculating the velocity profile.

```
function [velocity] = velocity(r,R,nu,u,Re)

    % Laminar flow, Re < 2300
    if Re<2300
        velocity = 2*u*(1-(r/R)^2);
        return;

    % Transition zone 2300 < Re < 4000
    elseif Re > 2300 && Re < 4000
        velocity = 2*u*(1-(r/R)^2);
        return;

    % Turbulent flow, Re > 4000
    else
        y=R-r;
        f=0.305/Re^0.25;
        y_p =(1-r/R)*Re/2*sqrt(f/8);

        if (y_p<=5)
            vz_p=y_p;
        elseif (5<=y_p<=30)
            vz_p=5*log(y_p)-3.05;
        else
            vz_p=2.5*log(y_p)+5.5;
        end

        velocity=vz_p*nu/y*(1-r/R)*Re/2*sqrt(f/8);
    end
end
```

Matlab Script 17 Function calculating the wax deposit thickness.

```
function [Fwax_new,depThick,rdnew,Sh,dFwdt,drddt,De,kM] = ...
    FwdepThick(asp,ri,rho_gel,dr,dt,rd,Fwax,Dwo,dC,dCb)

    if dC < 0
    De = Dwo./(1+((asp+Fwax.^2)./(1-Fwax)));
    Sh = (((-2*pi().*rd).*(dC)./dr))./dCb;
    kM = (Dwo.*Sh)./(2.*rd);
    drddt = -(1./(rho_gel.*Fwax)).*(kM.*dCb+De.*dC./dr);
    rdnew = rd + drddt.*dt;
    depThick = ri-rdnew;

        if rdnew <= 0
            disp('The pipe is clogged.')
            return
        end

     if abs(ri-rd)<1.1e-12
         dFwdt=0;
     else
        dFwdt = (2*rd./(rho_gel.*(ri.^2-rd.^2))).*(-De.*(dC)./dr);
     end

    Fwax_new = Fwax + dFwdt.*dt;

    else
        De = 0;
        Sh = 0;
        kM = 0;
        drddt = 0;
        rdnew = rd+drddt*dt;
        depThick = ri-rdnew;
        dFwdt = 0;
        Fwax_new = Fwax + dFwdt.*dt;
    end

end
```